

**OPTIMAL EXTRACTION OF SCATTERING MECHANISMS
FROM MEASURED DATA**

Thesis

Submitted to

**Graduate Engineering & Research
School of Engineering**

UNIVERSITY OF DAYTON

In Partial Fulfillment of the Requirements for

The Degree

Master of Science in Electrical Engineering

by

Hirsch Michael Chizever

Dayton, Ohio

August 1995

UNIVERSITY OF DAYTON ROESCH LIBRARY

OPTIMAL EXTRACTION OF SCATTERING MECHANISMS FROM MEASURED DATA

Approved by:

Krishna M. Pasala, Ph.D.
Professor of Electrical Engineering
Committee Chairperson

Gary A. Thiéle, Ph.D.
TAIT Professor
Committee Member

Theresa A. Tuthill, Ph.D.
Assistant Professor of Electrical Engineering
Committee Member

Donald L. Moon, Ph.D.
Associate Dean
Graduate Engineering Program & Research
School of Engineering

Joseph Lestingi, D. Eng., P.E.
Dean
School of Engineering

ABSTRACT

OPTIMAL EXTRACTION OF SCATTERING MECHANISMS FROM MEASURED DATA

**Name: Chizever, Hirsch Michael
University of Dayton, 1995**

Advisor: Dr. K. M. Pasala

The following thesis presents a method of decomposing a complex signal from a collection of spatially distributed scattering centers, each of which has a distinct frequency response. That is, from the observed frequency response data, it is required to estimate the locations of the scattering centers and their associated frequency responses. The method utilizes the MUSIC algorithm, a super-resolution technique, to determine the location of scattering centers from the maximum available bandwidth. Then, a generalized regression model is applied in sub-band increments to estimate the broadband complex frequency response of the scattering centers based on their derived locations.

The scattering from any target consists of contributions from several different scattering centers, each of which conceivably represents a different scattering mechanism. These scattering mechanisms may be specular reflections, edge diffractions, creeping waves, or a multi-mode resonance associated with a cavity. Signals from all these diverse mechanisms are buried in the composite signal. In addition, error sources such as scattering from support structures are also embedded in the measured data. It is required to delineate each of these different scattering centers, even when they are close together and further, to determine their frequency responses. Such a decomposition leads to a true understanding of the scattering from a target which is helpful in devising ways to control the same. Also, it becomes possible to

identify the error sources, eliminate them, and obtain better estimates of the true scattered fields, especially of low RCS targets.

The study presents a theoretical development followed by a parametric study to identify limits of the method in resolution and accuracy. The method is then applied to both synthetic and measured data scenarios. Processing of synthetic data revealed excellent agreement between extracted frequency responses and true responses in all cases. Analysis of measured data from canonical shapes such as a sphere, wire, and ogive is also included. Additional data is shown for dielectrics with weak and strong inhomogeneities.

TABLE OF CONTENTS

ABSTRACT	iii
TABLE OF CONTENTS.....	v
LIST OF FIGURES	vii
LIST OF TABLES.....	x
ACKNOWLEDGMENTS.....	xi
CHAPTER I.....	1
INTRODUCTION.....	1
1.1 Purpose.....	1
1.2 Background.....	2
1.3 Overview.....	3
CHAPTER II.....	4
THEORETICAL DEVELOPMENT	4
2.1 Signal Model	4
2.2 The MUSIC Algorithm	7
2.3 Regression Modeling.....	16
CHAPTER III.....	27
ANALYSIS OF SYNTHETIC AND MEASURED DATA	27
3.1 Synthetic Data.....	27
3.1.1 Parametric Study.....	28
3.2 Synthetic Data Analysis.....	41
3.2.1 Synthetic Case 1	41
3.2.2 Synthetic Case 2	48
3.2.3 Synthetic Case 3	54
3.2.4 Synthetic Case 4	60
3.2.5 Synthetic Case 5	67
3.3 Measured Data.....	73
3.3.1 Measured Case 1	75
3.3.2 Measured Case 2	83
3.3.3 Measured Case 3	90
3.3.4 Measured Case 4	93

3.3.5 Measured Case 5	96
CHAPTER IV	100
SUMMARY AND CONCLUSIONS	100
BIBLIOGRAPHY	104

LIST OF FIGURES

Figure 1. Scattering Centers Illuminated by a Plane Wave	5
Figure 2. Illustration of the Rayleigh Resolution Criterion.....	8
Figure 3 Two-Dimensional Averaging Applied to Correlation Matrix R_{φ}	10
Figure 4. MUSIC Spectrum as a Function of Noise Subspace Selection	14
Figure 5. Plot of Eigenvalue Magnitudes for Estimated Correlation Matrix R'_{φ}	15
Figure 6. Application of Regression Coefficients to Sub-Bands.....	19
Figure 7. RCOND as a Function of Regression Bandwidth (Order = 0)	23
Figure 8. RCOND as a Function of Regression Bandwidth (Order = 1)	24
Figure 9. Frequency Response of a Well-Conditioned System.....	25
Figure 10. Frequency Response of an Ill-Conditioned System	26
Figure 11. Histogram of MATLAB Noise Source	29
Figure 12. MUSIC Spectra Using 1 Aperture.....	31
Figure 13. MUSIC Spectra Using 2 Apertures.....	32
Figure 14. MUSIC Spectra Using 3 Apertures.....	33
Figure 15. MUSIC Spectra Using 6 Apertures.....	34
Figure 16. MUSIC and Fourier Spectra with .03 GHz Bandwidth and 2 Apertures	35
Figure 17. MUSIC Spectra Using 1 Aperture.....	37
Figure 18. MUSIC Spectra Using 2 Apertures.....	38
Figure 19. MUSIC Spectra Using 3 Apertures.....	39
Figure 20. MUSIC Spectra Using 6 Apertures.....	40
Figure 21. Exact Frequency Response for Synthetic Case 1.....	43
Figure 22. MUSIC Spectrum for Synthetic Case 1 ("Just Resolved")	44
Figure 23. Estimated Frequency Response for Synthetic Case 1 ("Just Resolved")	45
Figure 24. MUSIC and Fourier Spectra for Synthetic Case 1 ("Fully Resolved")	46
Figure 25. Estimated Frequency Response for Synthetic Case 1 ("Fully Resolved")	47
Figure 26. Exact Frequency Response for Synthetic Case 2.....	49
Figure 27 MUSIC and Fourier Spectra for Synthetic Case 2 ("Just Resolved").....	50
Figure 28. Estimated Frequency Response for Synthetic Case 2 ("Just Resolved")	51
Figure 29 MUSIC and Fourier Spectra for Synthetic Case 2 ("Fully Resolved")	52

Figure 30 Estimated Frequency Response for Synthetic Case 2 ("Fully Resolved")	53
Figure 31. Exact Frequency Response for Synthetic Case 3.....	55
Figure 32. MUSIC and Fourier Spectra for Synthetic Case 3 ("Just Resolved").....	56
Figure 33 Estimated Frequency Response for Synthetic Case 3 ("Just Resolved")	57
Figure 34. MUSIC and Fourier Spectra for Synthetic Case 3 ("Fully Resolved")	58
Figure 35. Estimated Frequency Response for Synthetic Case 3 ("Fully Resolved")	59
Figure 36. Exact Frequency Response for Synthetic Case 4.....	62
Figure 37. MUSIC and Fourier Spectra for Synthetic Case 4 ("Just Resolved").....	63
Figure 38. Estimated Frequency Response for Synthetic Case 4 ("Just Resolved")	64
Figure 39. MUSIC and Fourier Spectra for Synthetic Case 4 ("Fully Resolved")	65
Figure 40. Estimated Frequency Response for Synthetic Case 4 ("Fully Resolved")	66
Figure 41. Exact Frequency Response for Synthetic Case 5.....	68
Figure 42. MUSIC and Fourier Spectra for Synthetic Case 5 ("Just Resolved").....	69
Figure 43. Estimated Frequency Response for Synthetic Case 5 ("Just Resolved")	70
Figure 44. MUSIC and Fourier Spectra for Synthetic Case 5 ("Fully Resolved")	71
Figure 45. Estimated Frequency Response for Synthetic Case 5 ("Fully Resolved")	72
Figure 46. Side View of RCS Measurement Range at Wright-Patterson AFB.....	73
Figure 47. ARMR Radar Noise Histogram	74
Figure 48. Measured Case 1 Geometry	77
Figure 49. MUSIC and Fourier Spectra for Measured Case 1	78
Figure 50. Estimated Frequency Response for Measured Case 1	79
Figure 51. MUSIC Spectra for Measured Case 1	80
Figure 52 Estimated Frequency Response for Measured Case 1	81
Figure 53 Reconstructed Frequency Response for Measured Case 1	82
Figure 54. Measured Case 2 Geometry	84
Figure 55. MUSIC and Fourier Spectra for Measured Case 2	85
Figure 56. Estimated Frequency Response for Measured Case 2	86
Figure 57. MUSIC Spectra for Measured Case 2	87
Figure 58. Estimated Frequency Response for Measured Case 2.....	88
Figure 59. Reconstructed Frequency Response for Measured Case 2	89
Figure 60. Measured Case 3 Geometry	90
Figure 61. MUSIC and Fourier Spectra for Measured Case 3	91
Figure 62. Estimated Frequency Response for Measured Case 3.....	92
Figure 63. Measured Case 4 Geometry	93
Figure 64. MUSIC and Fourier Spectra for Measured Case 4	94
Figure 65. Estimated Frequency Response for Measured Case 4.....	95
Figure 66. Measured Case 5 Geometry	97

Figure 67. MUSIC and Fourier Spectra for Measured Case 598
Figure 68. Estimated Frequency Response for Measured Case 599

LIST OF TABLES

Table 1. Synthetic Data Parameters	41
Table 2. Location of Scattering Centers for Synthetic Case 1	42
Table 3. Location of Scattering Centers for Synthetic Case 2	48
Table 4. Location of Scattering Centers for Synthetic Case 3	54
Table 5. Location of Scattering Centers for Synthetic Case 4	60
Table 6. Location of Scattering Centers for Synthetic Case 5	67
Table 7. Measured Data Parameters	75

ACKNOWLEDGMENTS

The author would like to extend his sincere gratitude to Dr. Krishna M. Pasala for offering this research topic. His guidance and patience throughout this study was invaluable. A heartfelt thank you goes to Dr. Brian M. Kent of Wright-Patterson Air Force Base for use of the finest RCS measurement range in the world. The author extends his appreciation to Mr. Michael Menter of Mission Research Corporation for performing the RCS measurements in this study. The author is also grateful to committee members, Dr. Gary A. Thiele and Dr. Theresa A. Tuthill, for their critical reviews of this paper. Finally, to my wife, Tracy, and sons Eli and Micah, words are insufficient to express my heart for your sacrifice of a husband and daddy for far too long.

CHAPTER I

INTRODUCTION

1.1 Purpose

The objective of this study is to analyze the frequency response data obtained from measurements carried out in a radar cross section range and extract the maximum possible information from this data. The scattering from any target consists of contributions from several different scattering centers, each of which conceivably represents a different scattering mechanism. These scattering mechanisms may be specular reflections, edge diffractions, creeping waves, or a multi-mode resonance associated with a cavity. Signals from all these diverse mechanisms are buried in the composite signal. In addition, error sources such as scattering from support structures are also embedded in the measured data. It is required to delineate each of these different scattering centers, even when they are close together and further, to determine their frequency responses. Such a decomposition leads to a true understanding of the scattering from a target which is helpful in devising ways to control the same. Also, it becomes possible to identify the error sources, eliminate them and obtain better estimates of the true scattered fields, especially of low RCS targets.

Even though the objective of the present work is focused narrowly in the context of the range measurements, the underlying ideas and techniques are applicable in areas such as wideband radar. The signal received from a target illuminated by a wideband signal, if decomposed as indicated here, leads to a much better understanding of the target and its

possible identification. It may be possible to distinguish between a benign and cancerous tumor by virtue of their different frequency responses.

Some of the objectives outlined above may be attained using Fourier techniques with limited success. The resolution obtainable with Fourier techniques is limited. Even when scattering centers are resolvable, side lobes associated with the scattering center are a problem. When error sources are identifiable, it may be possible to "window" them out; but, edges of a window are a problem as well. Here, a super resolution method, viz., MUSIC, is coupled with regression analysis to overcome the problems with Fourier based techniques.

1.2 Background

Optimal extraction, a technique for modeling the frequency response of spatially distributed scattering centers, has received increased attention since the mid 1980's. However, it hasn't always been under this name. In 1978, Van Blaricum and Mitra¹ and Poggio et. al.² addressed optimal extraction under the heading of waveform parameterization. In their studies, Prony's method was used to model the transient electromagnetic pulse from nuclear explosions. Their rationale for a technique other than the Fourier transform is that it is limited in resolution and dynamic range. Pisarenko³ began the development of modern super resolution techniques with his "Harmonic decomposition" method which culminated in the MUSIC algorithm by Schmidt⁴. MUSIC was used by Delfeld and Delfeld⁵ in 1989 and Gupta⁶ in 1990 to isolate multi-path error sources in compact radar cross section ranges. In 1994, Moghaddar and Walton⁷ obtained the frequency response of scattering centers from a flat plate. This was done by first locating the scattering centers using a modified MUSIC algorithm. Then, by assuming a $(\frac{1}{f})^\alpha$ frequency dependence for each scattering center, the optimum α was obtained for each.

Recently, however, Moore and Ling⁸ have linked a "super-resolution" technique and waveform parameterization by using Prony's method and an averaging process to derive the complex frequency responses from both scattering centers and resonant targets. This technique, though, was not designed for use in the presence of noise. Moore et. al.⁹, responding to the

need for a noise resilient method, used ESPRIT¹⁰ in lieu of Prony's method but presented its use only with synthetic data.

1.3 Overview

The following investigation determines the frequency response of closely-spaced scattering centers from measured data using the MUSIC algorithm coupled with a regression technique. The theoretical approach is presented in Chapter 2. The investigation begins by developing a signal model for a collection of spatially distributed scattering centers illuminated by a plane wave. This model leads to a development of the MUSIC algorithm. A regression model is then formulated which utilizes the time delay estimates obtained from MUSIC to derive frequency response information.

Following the theoretical development, Chapter 3 applies the theory to a series of synthetic and measured data scenarios. The synthetic data sets comprise five different scattering types which include combinations of point, "linear" and resonant mechanisms - all in the presence of noise. A parametric study is performed to identify limits of the method in resolution and accuracy. Each synthetic data set is compared to the exact solution revealing the strengths and limitations of the method. The measured data include canonical shapes such as a sphere, wire, and ogive, with comparisons to exact solutions for the sphere and ogive. Additional data are shown for dielectrics with weak and strong inhomogeneities. Outputs are displayed for all data sets in a time and frequency domain format. The time domain shows the location of the scattering centers from MUSIC and is overlaid with the Fourier transform of the same data. The frequency domain plots identify the frequency response of individual sources found from MUSIC.

Finally, Chapter 4 summarizes the investigation and presents conclusions based on the parametric study and applied data results.

CHAPTER II

THEORETICAL DEVELOPMENT

The purpose of this study is to decompose a complex signal from a collection of spatially distributed scattering centers, each of which has a distinct frequency response. That is, from the observed frequency response data, it is required to estimate the locations of the scattering centers and their associated frequency responses. The approach, entitled optimal extraction, requires two parts. First, the MUSIC algorithm, an eigen-decomposition technique, is used to determine the location of scattering centers. Second, a regression technique estimates the complex frequency response of the scattering centers based on their derived locations. The theory behind both parts will be presented followed by a treatment of synthetic and measured data .

2.1 Signal Model

Consider a simple scenario where two scatterers are illuminated by a plane wave as shown in Figure 1. The back scattered signal is measured over a band of frequencies from f_1 to f_N at equal intervals. The range of the scatterers is such that their time delays, with respect to a reference, are t_1 and t_2 . Then, the received signal may be modeled as

$$v(f) = a_1(f)e^{-j2\pi ft_1} + a_2(f)e^{-j2\pi ft_2} + n(f) \quad (1)$$

In general, a_1 and a_2 are functions of frequency but will be considered to be constant initially. $n(f)$ represents measurement noise and modeling error. The more general case will be dealt with later. The measured signal at frequencies from f_1 to f_N may be expressed as

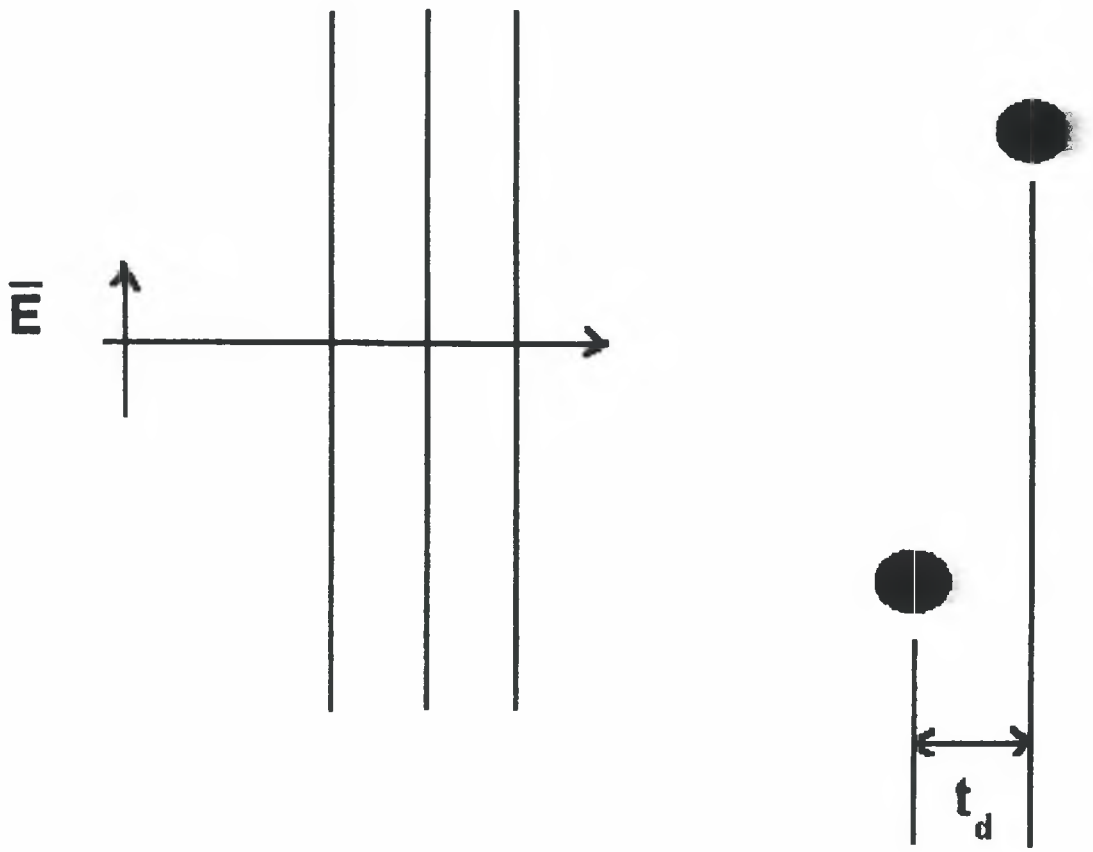


Figure 1. Scattering Centers Illuminated by a Plane Wave

$$\begin{aligned}
v_1 &= v(f_1) = a_1 e^{-j2\pi f_1 t_1} + a_2 e^{-j2\pi f_1 t_2} + n(f_1) \\
v_2 &= v(f_2) = a_1 e^{-j2\pi f_2 t_1} + a_2 e^{-j2\pi f_2 t_2} + n(f_2) \\
&\vdots \\
v_k &= v(f_k) = a_1 e^{-j2\pi f_k t_1} + a_2 e^{-j2\pi f_k t_2} + n(f_k) \\
&\vdots \\
v_N &= v(f_N) = a_1 e^{-j2\pi f_N t_1} + a_2 e^{-j2\pi f_N t_2} + n(f_N)
\end{aligned} \tag{2}$$

This may be stated compactly, as,

$$\vec{v} = \vec{w} \vec{a} + \vec{n} \tag{3}$$

where

$$\vec{v} = [v_1 \quad v_2 \quad \dots \quad v_N]^T$$

$$\vec{n} = [n_1 \quad n_2 \quad \dots \quad n_N]^T$$

$$\vec{a} = [a_1 \quad a_2]$$

$$\vec{w} = [\vec{w}_1 \quad \vec{w}_2]$$

$$\vec{w}_i = [e^{-j2\pi f_i t_1} \quad e^{-j2\pi f_i t_2} \quad \dots \quad e^{-j2\pi f_i t_N}]^T, \quad i = 1, 2.$$

Equation (3) continues to be valid for L sources with

$$\vec{w} = [\vec{w}_1 \quad \vec{w}_2 \quad \dots \quad \vec{w}_L] \tag{4}$$

and

$$\vec{a} = [a_1 \quad a_2 \quad \dots \quad a_L]^T \tag{5}$$

The correlation matrix is given by,

$$\mathbf{R}_{\vec{v}} = \mathbf{E}[\vec{v} \vec{v}^H] = \vec{w} \mathbf{R}_{\vec{a}} \vec{w}^H + \sigma^2 \mathbf{I} \tag{6}$$

where $R_x = E[\bar{a} \bar{a}^H]$ and σ^2 is the noise variance. The signals and noise are considered to be uncorrelated. The L -dimensional space spanned by $\bar{w}_1, \bar{w}_2, \dots, \bar{w}_L$ is defined to be the signal subspace which will be discussed later.

2.2 The MUSIC Algorithm

The MUSIC algorithm will be utilized to locate the L spatially distributed but distinct scattering centers instead of the classic Fourier approach. MUSIC, unlike the Fourier transform, is part of a larger class of "super-resolution" techniques which are not bound by the Rayleigh resolution criterion - a classic limitation of the Fourier transform. Haykin¹¹ states this criterion as, "... two components of equal intensity should be considered to be "just resolved" when the first maximum from one component sits at the first minimum from the other..." (see Figure 2). MUSIC is based on an eigen-decomposition of the correlation matrix R_v and is constructed from the measured signals v_k as

$$R_v = E[\bar{v}^H \bar{v}] = E \left[\begin{array}{c} v_1^* \\ v_2^* \\ \vdots \\ v_N^* \end{array} \begin{bmatrix} v_1 & v_2 & \dots & v_N \end{bmatrix} \right] \quad (7)$$

$$= E \left[\begin{array}{cccc} v_1^* v_1 & v_1^* v_2 & \dots & v_1^* v_N \\ v_2^* v_1 & v_2^* v_2 & \dots & v_2^* v_N \\ \vdots & \vdots & \ddots & \vdots \\ v_N^* v_1 & v_N^* v_2 & \dots & v_N^* v_N \end{array} \right] \quad (8)$$

MUSIC assumes that the observed signals are uncorrelated. That is,

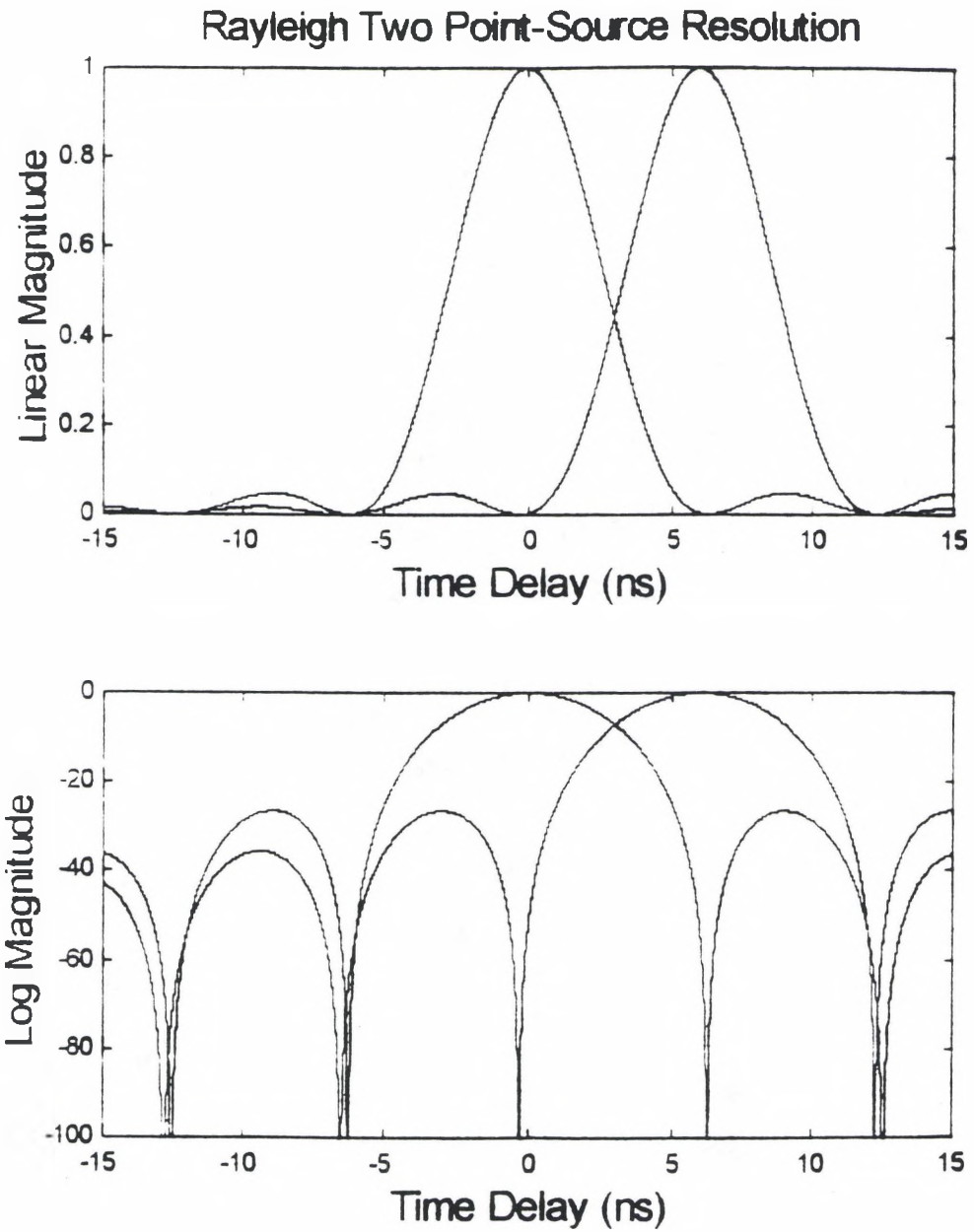


Figure 2. Illustration of the Rayleigh Resolution Criterion

$$E[v_k v_l^*] = \begin{cases} P_1, & k = l \\ 0, & k \neq l \end{cases} \quad (9)$$

where P_1 is the power in the 1st received signal. However, in actual measurements the scattering sources are illuminated by the same signal, thus making them coherent. One solution for this is to perform multiple measurements at each frequency and average them. Unfortunately, though, there is often only one "snap-shot" of the data, and ensemble averaging is not possible. As such, a form of post measurement averaging must be employed.

This procedure is implemented by creating a new correlation matrix R'_v which is an average of the correlation matrices associated with each of the vectors \bar{v}_{α_k} . That is,

$$R'_v = \frac{1}{n_A} \sum_{k=1}^{n_A} \bar{v}_{\alpha_k} \bar{v}_{\alpha_k}^H \quad (10)$$

where \bar{v}_{α_k} is a "sub-aperture" of the original signal vector \bar{v} and n_A is the number of "sub-apertures" used. This "sub-aperture" concept is illustrated in Figure 3 where three apertures are used for a correlation matrix of order five. The order of the original R_v matrix has been reduced to

$$\text{Order of } R'_v = \Theta = N_{\text{frequencies}} - n_A + 1 \quad (11)$$

which later will be shown to adversely affect resolution in certain cases.

The eigenvalues and associated eigenvectors of the matrix R'_v will now be computed.

The eigenvalue problem is formulated as

$$R'_v \bar{q} = \lambda \bar{q} \quad (12)$$

or stated another way,

3 Averaging Apertures Applied to Correlation Matrix of Order 5

$$R = \begin{bmatrix} \begin{bmatrix} R_{11} & R_{12} & R_{13} \end{bmatrix} & R_{14} & R_{15} \\ R_{21} & \begin{bmatrix} R_{22} & R_{23} & R_{24} \end{bmatrix} & R_{25} \\ \begin{bmatrix} R_{31} & R_{32} & \bar{R}_{33} \end{bmatrix} & R_{34} & R_{35} \\ R_{41} & \begin{bmatrix} R_{42} & R_{43} & R_{44} \end{bmatrix} & R_{45} \\ R_{51} & R_{52} & \begin{bmatrix} R_{53} & R_{54} & R_{55} \end{bmatrix} \end{bmatrix}$$

$$R' = \frac{\begin{bmatrix} \bar{R}_{11} & R_{12} & R_{13} \\ R_{21} & R_{22} & R_{23} \\ R_{31} & R_{32} & R_{33} \end{bmatrix} + \begin{bmatrix} \bar{R}_{22} & R_{23} & R_{24} \\ R_{32} & R_{33} & R_{34} \\ R_{42} & R_{43} & R_{44} \end{bmatrix} + \begin{bmatrix} \bar{R}_{33} & R_{34} & R_{35} \\ R_{43} & R_{44} & R_{45} \\ R_{53} & R_{54} & R_{55} \end{bmatrix}}{3}$$

Figure 3. Two-Dimensional Averaging Applied to Correlation Matrix R_v

$$(R'_v - \lambda I)\bar{q} = 0 \quad (13)$$

R'_v is the averaged correlation matrix with λ and \bar{q} the eigenvalues and eigenvectors respectively. For every eigenvalue there is a corresponding eigenvector which can be expressed as

$$R'_v q_k = \lambda_k q_k, \quad k = 1, 2, \dots, \Theta \quad (14)$$

The eigenvalues are sorted in descending order with their respective eigenvectors. A property of the correlation matrix R'_v is that the eigenvectors can be separated into two disjoint subspaces which are orthogonal to each other¹². The lowest $(M - L)$ eigenvectors are all equal and the corresponding eigenvectors define the noise subspace. The space spanned by the first L eigenvectors is called the signal plus noise subspace and is orthogonal to the noise subspace.

Let,

$$Q_S = [\bar{q}_1, \dots, \bar{q}_L] \quad (15)$$

and

$$Q_N = [\bar{q}_{L+1}, \dots, \bar{q}_M] \quad (16)$$

then

$$Q_N^H Q_S = 0 \quad (17)$$

where Q_S and Q_N represent the signal and noise spaces, respectively. Since the signal subspace spanned by $\bar{w}_1, \bar{w}_2, \dots, \bar{w}_L$ is also spanned by signal eigenvectors $\bar{q}_1, \bar{q}_2, \dots, \bar{q}_L$, equation (17) implies

$$\bar{w}_k^H \bar{q}_i = 0, \quad \begin{array}{l} k = 1, 2, \dots, L \\ i = L+1, L+2, \dots, \Theta \end{array} \quad (18)$$

The signal space is spanned by the eigenvectors corresponding to the L largest eigenvalues, and the noise space is spanned by the eigenvectors corresponding to the $\Theta - L$ smallest and equal eigenvalues. Theoretically, the L largest eigenvalues correspond to the number of sources at the receiver across the bandwidth of interest (i.e. two sources define the signal space as the first two eigenvectors, and the remaining eigenvectors define the noise space).

The ability to distinguish the two spaces is dependent on the signal-to-noise ratio (SNR). For example, two signals may be above the noise by 20 dB resulting in signal eigenvalues being well separated from the noise eigenvalues. On the other hand, two more sources may be weak, and the SNR may be only 0-5 dB. Then it is hard to distinguish between signal and noise eigenvalues. An improper boundary selection for the two subspaces will manifest itself in the MUSIC spectrum as shown in Figure 4. Figure 4 shows three MUSIC spectra for two point scatterers separated in time by 1 ns with a SNR of 20 dB. Each spectrum is obtained by defining the noise subspace from a different eigenvalue. According to (15), two distinct scattering centers will have a signal subspace spanned by the first two eigenvectors, corresponding to the first two largest eigenvalues. In this case, the averaged correlation matrix was of order 21. Thus, if the noise subspace begins with eigenvector two, then the signal subspace spans only one eigenvector while the noise spans 20. This choice leads to an ambiguous MUSIC spectrum, in which it becomes difficult to identify distinct scattering centers. A signal space defined by the first nine eigenvalues gives a number of false scattering centers. As the figure demonstrates, the best choice is a noise subspace corresponding to the third eigenvalue. To further illustrate which eigenvalues should mark the subspace boundary, Figure 5 plots the eigenvalue magnitudes for the two point scatterers. As the plot clearly shows, a marked fall-off is noticed after the second eigenvalue. This means that the first two eigenvalues mark the signal space and the remaining eigenvalues mark the noise space.

To compute the MUSIC spectrum (location of the scatterers) recall from (18) that

$$\begin{aligned} \bar{\mathbf{w}}_k^H \bar{\mathbf{q}}_i &= 0, & k &= 1, 2, \dots, L \\ & & i &= L + 1, L + 2, \dots, \Theta \end{aligned}$$

However, since the averaging procedure is an approximation, the eigenvectors of $\mathbf{R}'_{\bar{v}}$ are only estimates of the true eigenvectors. As such, one must search for a vector which is "... most closely orthogonal"¹³ to the noise space. Consider a scanning vector $\bar{\mathbf{w}}_m$ corresponding to time delay t_m defined below.

$$\bar{\mathbf{w}}_m = \left[e^{-j2\pi f_1 t_m} \quad e^{-j2\pi f_2 t_m} \quad \dots \quad e^{-j2\pi f_{\Theta} t_m} \right]^T \quad (19)$$

where Θ is the order of $\mathbf{R}'_{\bar{v}}$. This scanning vector will be approximately orthogonal to the noise space when a correct scattering center time delay has been achieved. This concept leads to the definition of the MUSIC spectrum

$$S_{\text{MUSIC}} = \frac{1}{\sum_{i=L+1}^{\Theta} |\bar{\mathbf{w}}_i^H \bar{\mathbf{v}}_i|^2} \quad (20)$$

$$= \frac{1}{\bar{\mathbf{w}}^H \mathbf{V}_N \mathbf{V}_N^H \bar{\mathbf{w}}} \quad (21)$$

S_{MUSIC} reaches a local maximum when the appropriate search vector is orthogonal to the noise space. It is important to note that the MUSIC spectrum is a "pseudo-spectrum" since it is not a true measure of power at the appropriate time delay as in Fourier techniques. The Fourier transform links the time and frequency domains via Parseval's identity. There is no such identity for MUSIC. However, the power from a particular source may be computed from (2) by solving for the \mathbf{a} 's via least squares.

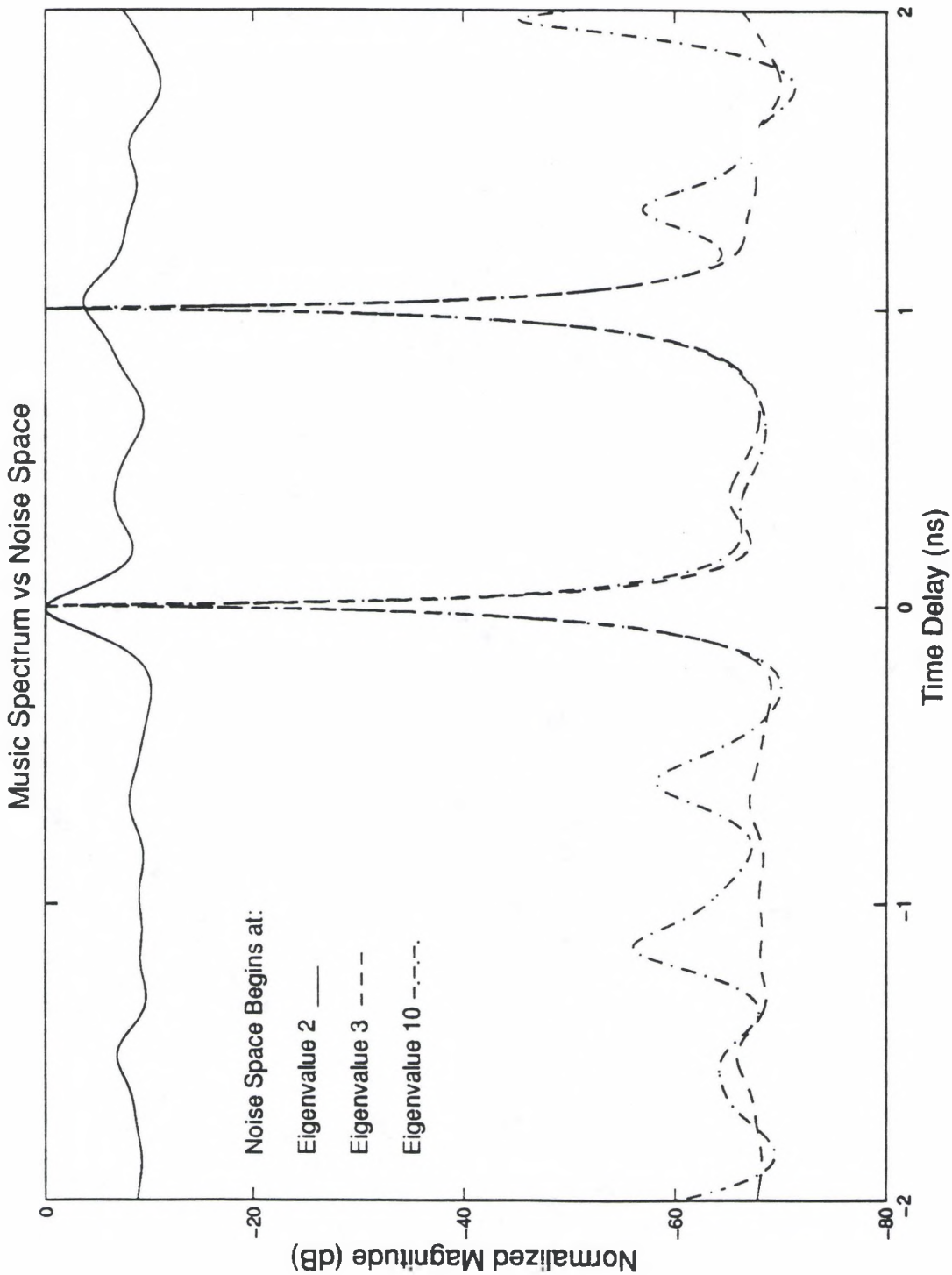


Figure 4. MUSIC Spectrum as a Function of Noise Subspace Selection

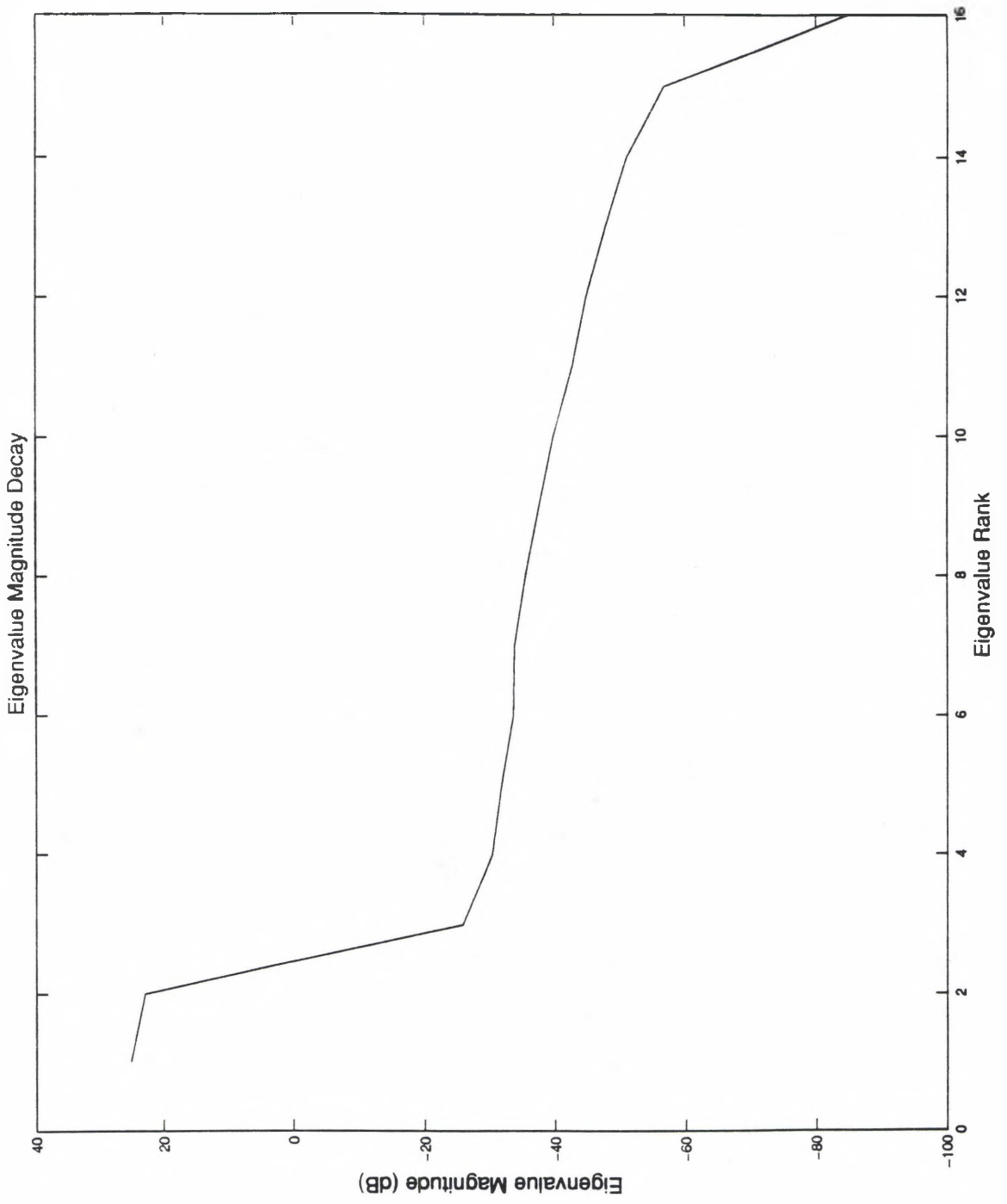


Figure 5. Plot of Eigenvalue Magnitudes for Estimated Correlation Matrix R'_v

2.3 Regression Modeling

Once the location of each scattering center is identified, then the task of estimating the associated frequency response for each may begin. This process of identifying \bar{a} in (3) begins with a restated, yet modified version of the signal model. This time, variation of the amplitudes with frequency is included. A regression model for L spatially distributed scattering centers whose measured signal ranges in frequency from f_1 to f_N at equal intervals, may be stated as,

$$\begin{aligned}
 v_1 &= v(f_1) = a_1(f_1)e^{-j2\pi f_1 t_1} + a_2(f_1)e^{-j2\pi f_1 t_2} + \dots + a_L(f_1)e^{-j2\pi f_1 t_L} + \varepsilon(f_1) \\
 v_2 &= v(f_2) = a_1(f_2)e^{-j2\pi f_2 t_1} + a_2(f_2)e^{-j2\pi f_2 t_2} + \dots + a_L(f_2)e^{-j2\pi f_2 t_L} + \varepsilon(f_2) \\
 &\vdots \\
 v_k &= v(f_k) = a_1(f_k)e^{-j2\pi f_k t_1} + a_2(f_k)e^{-j2\pi f_k t_2} + \dots + a_L(f_k)e^{-j2\pi f_k t_L} + \varepsilon(f_k) \\
 &\vdots \\
 v_N &= v(f_N) = a_1(f_N)e^{-j2\pi f_N t_1} + a_2(f_N)e^{-j2\pi f_N t_2} + \dots + a_L(f_N)e^{-j2\pi f_N t_L} + \varepsilon(f_N).
 \end{aligned} \tag{22}$$

Or stated in matrix form,

$$\bar{v} = \bar{w} \bar{a} + \bar{\varepsilon} \tag{23}$$

where

$$\begin{aligned}
 \bar{v} &= [v_1 \quad v_2 \quad \dots \quad v_N]^T \\
 \bar{w} &= [\bar{w}_1 \quad \bar{w}_2 \quad \dots \quad \bar{w}_L]
 \end{aligned}$$

$$\bar{w}_i = [e^{-j2\pi f_i t_1} \quad e^{-j2\pi f_i t_2} \quad \dots \quad e^{-j2\pi f_i t_L}]^T, \quad i = 1, 2, \dots, L.$$

$$\bar{a} = [a_1 \quad a_2 \quad \dots \quad a_L]^T$$

and

$$\bar{\varepsilon} = [\varepsilon_1 \quad \varepsilon_2 \quad \dots \quad \varepsilon_N]^T.$$

The two differences between the regression model just stated and the signal model described in (2) are that all elements are now considered frequency dependent and that the noise vector \bar{n} has been replaced by a new error vector $\bar{\varepsilon}$. In the previous section each

coefficient a_i was considered to be a constant over the frequency range f_1 to f_N . This implies that regardless of the bandwidth under study, the scattering centers had constant frequency responses. Over broad bandwidths such an assumption is invalid. In fact, most scattering mechanisms, although well behaved, are not constant. Some may be expressed as first, second, or even higher degree polynomials. Others might exhibit frequency responses whose magnitudes are inversely proportional to frequency. In either case, a regression model must be generic enough to account for a variety of scattering behaviors. This becomes more manageable if the bandwidth $f_N - f_1$ is divided into sub-bands of width B_r , where B_r is the regression bandwidth, or bandwidth where the coefficients a_i are valid. Figure 6 illustrates how the process is applied to each sub-band.

A polynomial assumption for each a_i may be stated as,

$$a_i = a_{i0} + a_{i1}f_k + a_{i2}f_k^2 + \dots + a_{i,M-1}f_k^M, \quad (23)$$

where f is the independent variable, frequency, and M is the order of the assumed polynomial. This approach allows each scattering center frequency response to be separately modeled as a different polynomial over B_r . To illustrate this concept consider the case of two scattering centers each having an assumed first order frequency response. The general case will be considered later. Substituting (23) into (22) yields the following set of equations:

$$\begin{aligned} v_1 &= (a_{10} + a_{11}f_1)e^{-j2\pi f_1 t_1} + (a_{20} + a_{21}f_1)e^{-j2\pi f_1 t_2} + \epsilon_1 \\ &\vdots \qquad \qquad \qquad \vdots \qquad \qquad \qquad \vdots \\ v_N &= (a_{10} + a_{11}f_N)e^{-j2\pi f_N t_1} + (a_{20} + a_{21}f_N)e^{-j2\pi f_N t_2} + \epsilon_N \end{aligned} \quad (24)$$

where N is now the number of measurement samples in B_r . The estimated frequency response at the first frequency may be written in matrix notation as,

$$v_1 = \begin{bmatrix} e^{-j2\pi f_1 t_1} & f_1 e^{-j2\pi f_1 t_1} & e^{-j2\pi f_1 t_2} & f_1 e^{-j2\pi f_1 t_2} \end{bmatrix} \begin{bmatrix} a_{10} \\ a_{11} \\ a_{20} \\ a_{21} \end{bmatrix} + \epsilon_1 \quad (25)$$

or in a more compact form,

$$v_1 = \bar{w}_1 \bar{a} + \epsilon_1 \quad (26)$$

where

$$\bar{w}_1 = \begin{bmatrix} \bar{w}_{11}^T & \bar{w}_{12}^T \end{bmatrix}$$

$$\bar{w}_{11} = \begin{bmatrix} e^{-j2\pi f_1 t_1} \\ f_1 e^{-j2\pi f_1 t_1} \end{bmatrix} \quad \text{and} \quad \bar{w}_{12} = \begin{bmatrix} e^{-j2\pi f_1 t_2} \\ f_1 e^{-j2\pi f_1 t_2} \end{bmatrix}$$

$$\bar{a} = \begin{bmatrix} a_{10} & a_{11} & a_{20} & a_{21} \end{bmatrix}^T$$

Now expanding (26) for N frequencies in B_r yields

$$\begin{bmatrix} v_1 \\ v_2 \\ \vdots \\ v_N \end{bmatrix} = \begin{bmatrix} \bar{w}_1 \\ \bar{w}_2 \\ \vdots \\ \bar{w}_N \end{bmatrix} \bar{a} + \begin{bmatrix} \epsilon_1 \\ \epsilon_2 \\ \vdots \\ \epsilon_N \end{bmatrix} \quad (27)$$

or in matrix notation as

$$\bar{v} = w \bar{a} + \bar{\epsilon} \quad (28)$$

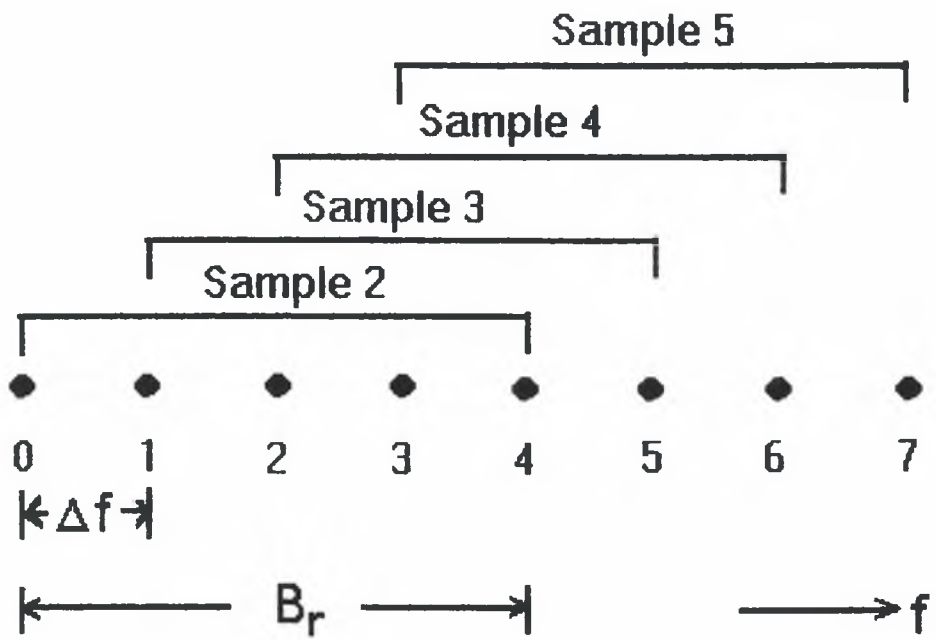


Figure 6. Application of Regression Coefficients to Sub-Bands

Now, consider the generalized polynomial case of (23) assuming L scattering centers and an M^{th} order polynomial. Equation 28 continues to be valid with

$$\bar{\mathbf{w}}_k = [\bar{\mathbf{w}}_{k1}^T \quad \dots \quad \bar{\mathbf{w}}_{kL}^T]$$

$$\bar{\mathbf{w}}_{kj} = \begin{bmatrix} e^{-j2\pi f_k t_j} \\ f e^{-j2\pi f_k t_j} \\ \vdots \\ f_k^{M-1} e^{-j2\pi f_k t_j} \end{bmatrix}$$

and
$$\bar{\mathbf{a}} = [[a_{10} \quad \dots \quad a_{1M}] [a_{20} \quad \dots \quad a_{2M}] \dots [a_{L0} \quad \dots \quad a_{LM}]]^T.$$

$\bar{\mathbf{w}}_k$ and $\bar{\mathbf{a}}$ may now be substituted into (27) and (28) without modification. This section assumes that the polynomial selected is applied to each scattering center equally. However, with only minor modifications to the model, one may extend the model to vary polynomial order for each scattering center. In addition, the model has been shown for only one B_x , assuming similar analysis for each sub band. An additional degree of freedom may be extended to applying different polynomials over different B_x 's without changing the model at all.

The coefficient vector $\bar{\mathbf{a}}$ is now computed by minimizing the mean squared error $\|\bar{\boldsymbol{\epsilon}}\|$.

Equation (21) may be rewritten as

$$\bar{\boldsymbol{\epsilon}} = \bar{\mathbf{v}} - \mathbf{w} \bar{\mathbf{a}} \tag{29}$$

Since the measurement data $\bar{\mathbf{v}}$ is complex, the coefficients $\bar{\mathbf{a}}$ will, in general, also be complex. Real valued minimization occurs when the derivative of a function is equal to zero. However, for complex minimization, one must ensure that the derivative with respect to both the real and imaginary parts of $\bar{\mathbf{a}}$ of the function are zero simultaneously¹⁴. Therefore, a real-valued function J is defined as,

$$J = \bar{\epsilon}^H \bar{\epsilon} = \|\bar{\epsilon}\|^2 \quad (30)$$

By minimizing J , the real power, or norm of the error vector is minimized. To minimize J , a gradient operator $\nabla_{\bar{a}}$ is defined as

$$\nabla_{\bar{a}} = \frac{\partial J}{\partial \bar{a}^*} \quad (31)$$

Substituting for $\bar{\epsilon}$ and expanding,

$$J = (\bar{v} - w\bar{a})^H (\bar{v} - w\bar{a}) = (\bar{v}^H - w^H \bar{a}^H) (\bar{v} - w\bar{a}) = \bar{v}^H \bar{v} - \bar{v}^H w\bar{a} - w^H \bar{a}^H \bar{v} + w^H \bar{a}^H w\bar{a} \quad (32)$$

Taking the gradient of J and setting the result equal to zero results in the following:

$$\nabla_{\bar{a}} J = -w^H \bar{v} + w^H w\bar{a} = 0 \quad \text{or} \quad \bar{a} = (w^H w)^{-1} w^H \bar{v} \quad (33)$$

The polynomial coefficients are now substituted into (29) to find the estimated value of \bar{v} and the error $\bar{\epsilon}$.

Deciding what polynomial to select for a given measurement may depend on a number of factors. A zero order function is recommended as a first-cut to observe the general shape of the estimated frequency responses. However, care must be taken to determine the proper B_r for a given polynomial set. An estimator for B_r is obtained by examining the condition number of the matrix $w^H w$. By plotting the MATLAB function $RCOND(w^H w)$ as a function of B_r , a peak in the condition number is found as the bandwidth increases. The first peak will best represent the physics of the problem. Figure 7 and Figure 8 show MATLAB $RCOND(x)$ as a function of B_r for a zero and first order polynomial equations, respectively. If B_r is too narrow, the system becomes ill-conditioned and degradation will occur in the estimated frequency responses. Figure 9 and Figure 10 show the estimated frequency response for a zero order polynomial with regression bandwidths of 1 GHz and 100 MHz respectively.

Each polynomial now represents the estimated frequency response of the individual scattering centers from f_1 to f_N . The method will now be applied to a series of synthetic and measured data.

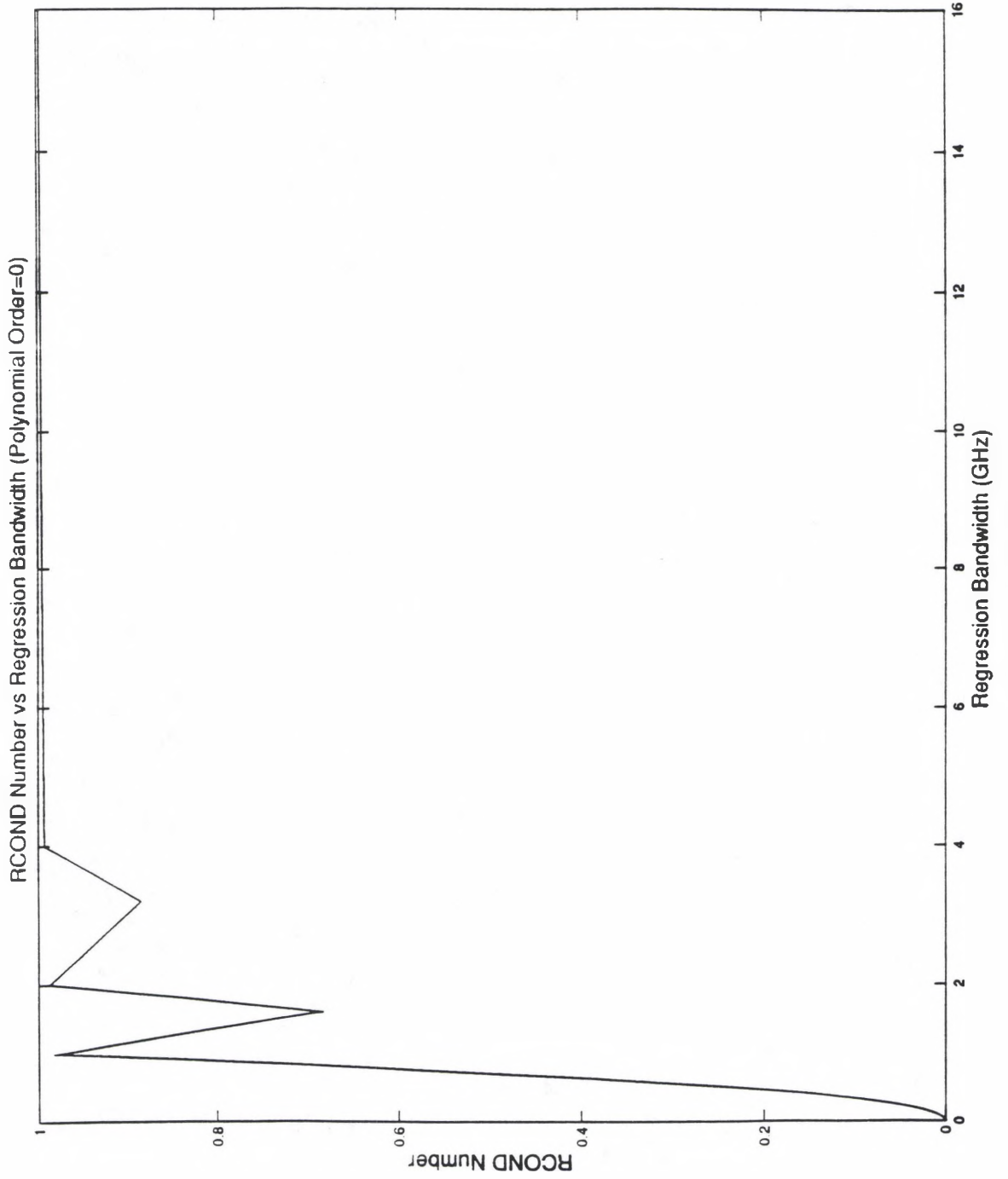


Figure 7. RCOND as a Function of Regression Bandwidth (Order = 0)

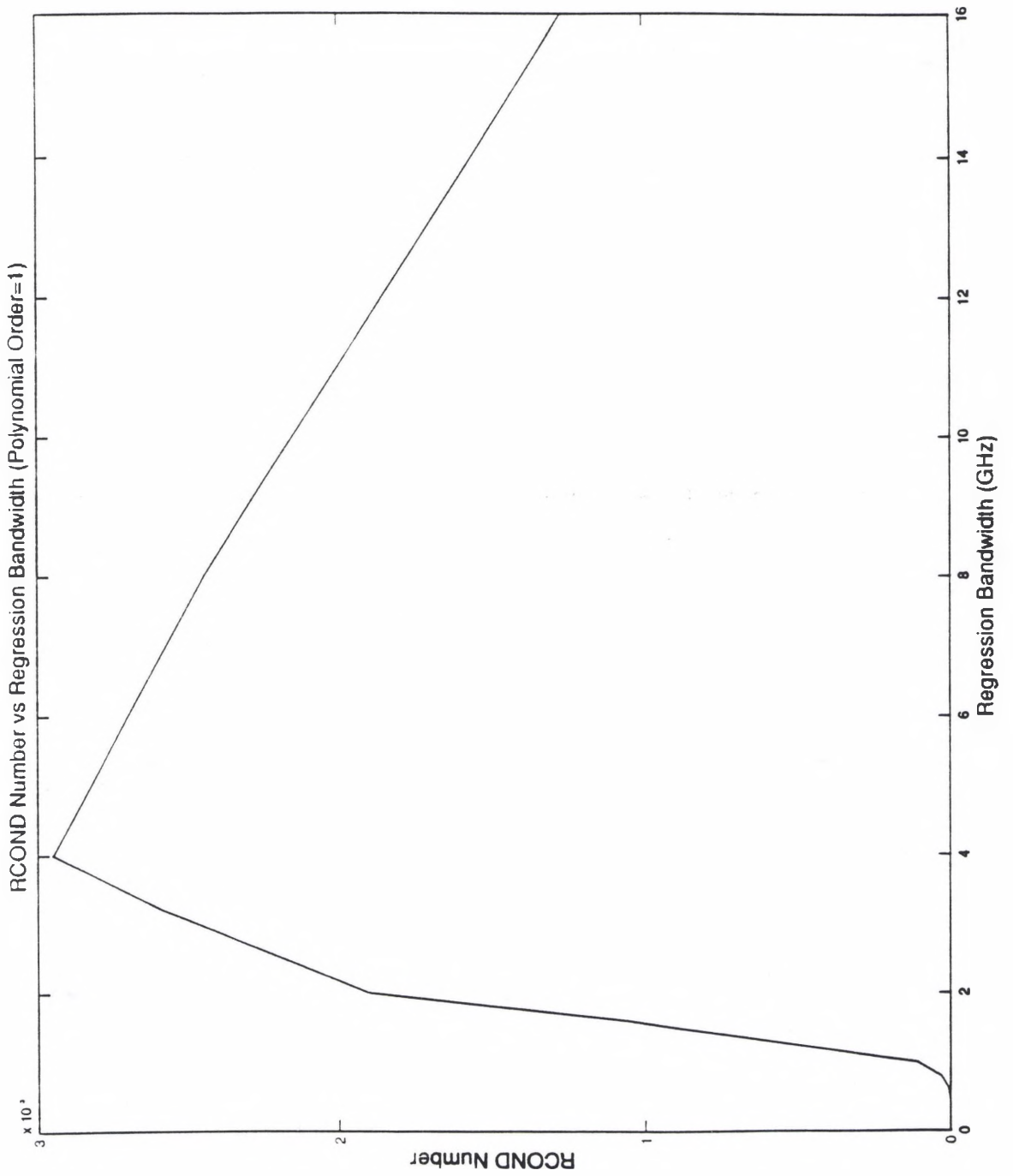


Figure 8. RCOND as a Function of Regression Bandwidth (Order = 1)

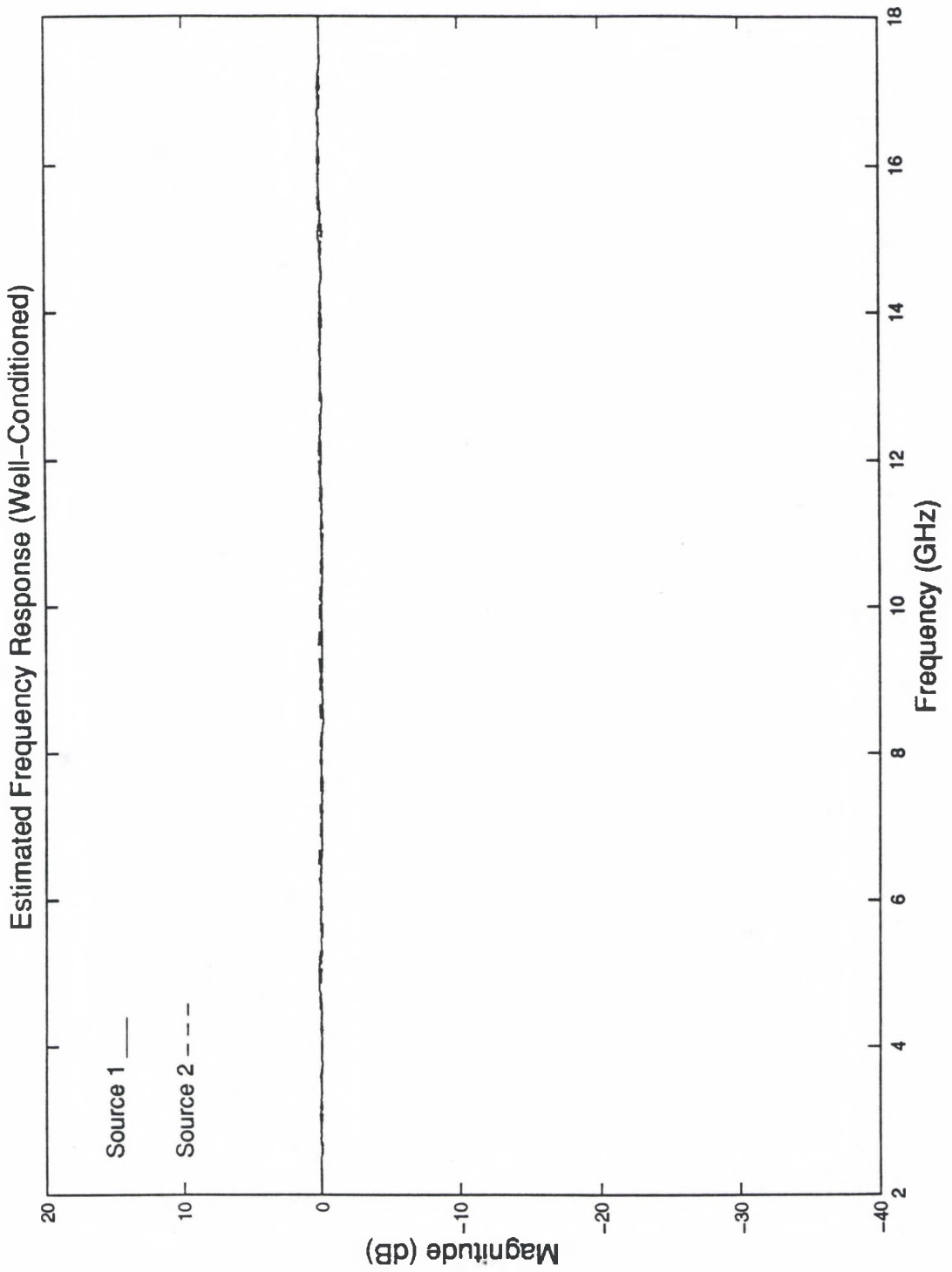


Figure 9. Frequency Response of a Well-Conditioned System

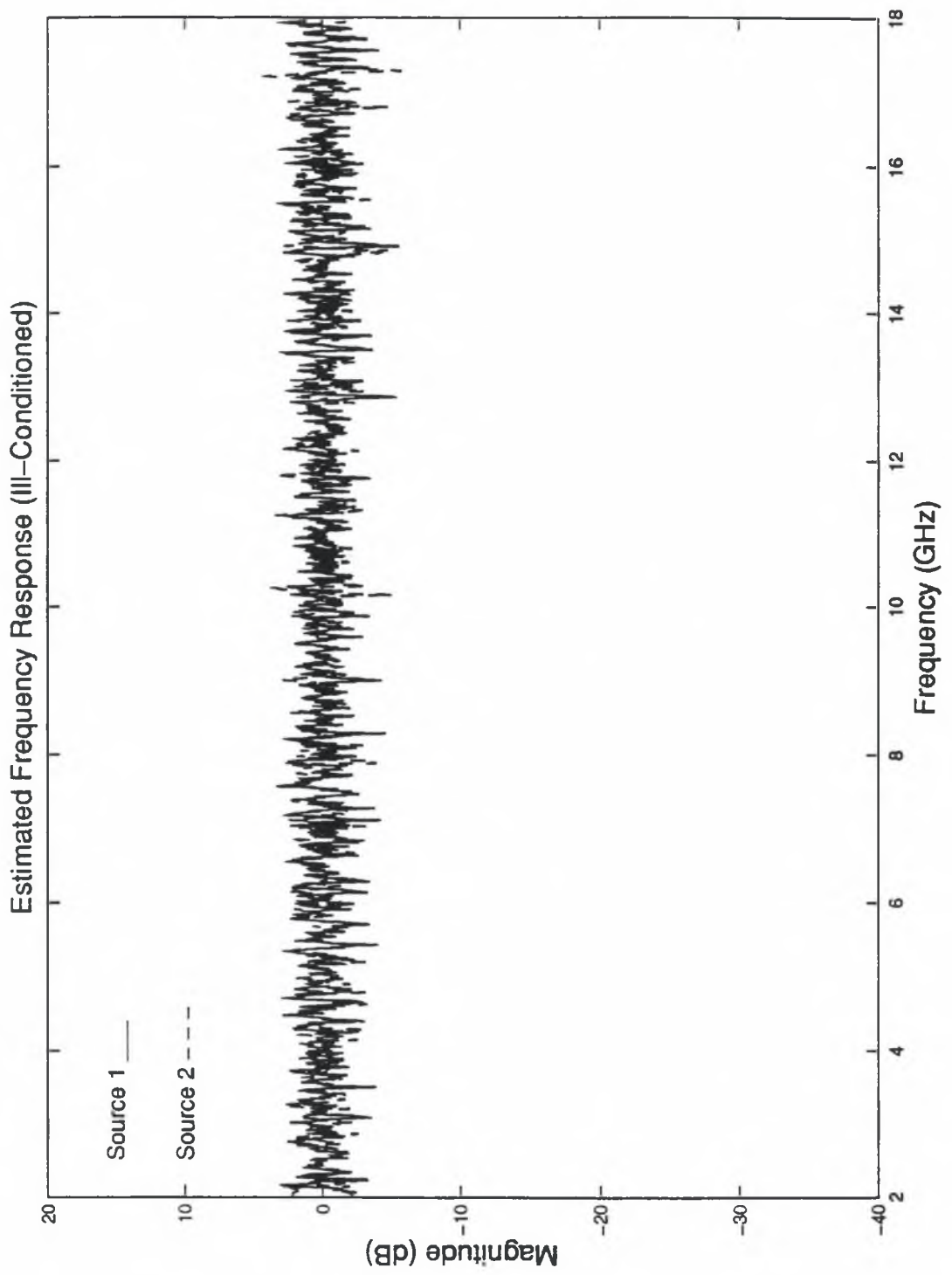


Figure 10. Frequency Response of an Ill-Conditioned System

CHAPTER III

ANALYSIS OF SYNTHETIC AND MEASURED DATA

Synthetic and measured data are presented here under various parametric conditions.

These parameters include:

- bandwidth
- dynamic range
- number of sources
- signal-to-noise ratio
- averaging apertures (apertures)
- size of correlation matrix
- various scattering types

3.1 Synthetic Data

The white Gaussian noise used in the signal model of (2) was generated by MATLAB.

The signal-to-noise ratio (SNR) is defined as

$$\text{SNR} = \frac{\sum_{k=1}^N |s_k|^2}{\sum_{k=1}^N |n_k|^2} \quad (34)$$

where s_k and n_k represent complex signal and noise components at the receiver for the k^{th} frequency. Since the data is complex, a separate noise spectrum is generated for both the real and imaginary components. Figure 11 shows a histogram of the Gaussian noise source used from MATLAB.

3.1.1 Parametric Study

The performance of the MUSIC algorithm depends on a number of variables. In order to decouple the effects one may have on another, a baseline test scenario of two point sources separated in time delay by 1 ns will be used to study the effects of bandwidth, apertures, and the order of the correlation matrix. In all cases the SNR is 20 dB.

The evaluation begins with analysis of parameters affecting resolution and accuracy. Resolution is the capability of detecting the presence of two closely-spaced sources and accuracy is the ability to determine their true time separation.

3.1.1.1 Resolution

Consider the two point source baseline time delay of 1 ns. This spacing dictates a resolution bandwidth of approximately 1 GHz for the Fourier transform. This bandwidth is calculated from what Bracewell calls the time bandwidth product¹⁵. The well known $\frac{c}{2B}$ criterion where c =speed of light and B =bandwidth, results in a bandwidth requirement of 1 GHz. Another parameter of interest is the number of apertures. In this analysis, the MUSIC algorithm's resolving capacity will be tested using 1,2,3 and 6 apertures each with bandwidths of 1, .8 and .5 GHz. In each of these cases, the frequency increment is adjusted so that the size of the correlation matrix remains constant for each case (e.g. a frequency increment Δf of .1 GHz for a bandwidth of 1 GHz corresponds to an averaged correlation matrix of order six if using six apertures). This means that a true comparison can be made for a specific aperture size without disputing the effect that the size of R_{φ} has on resolution.

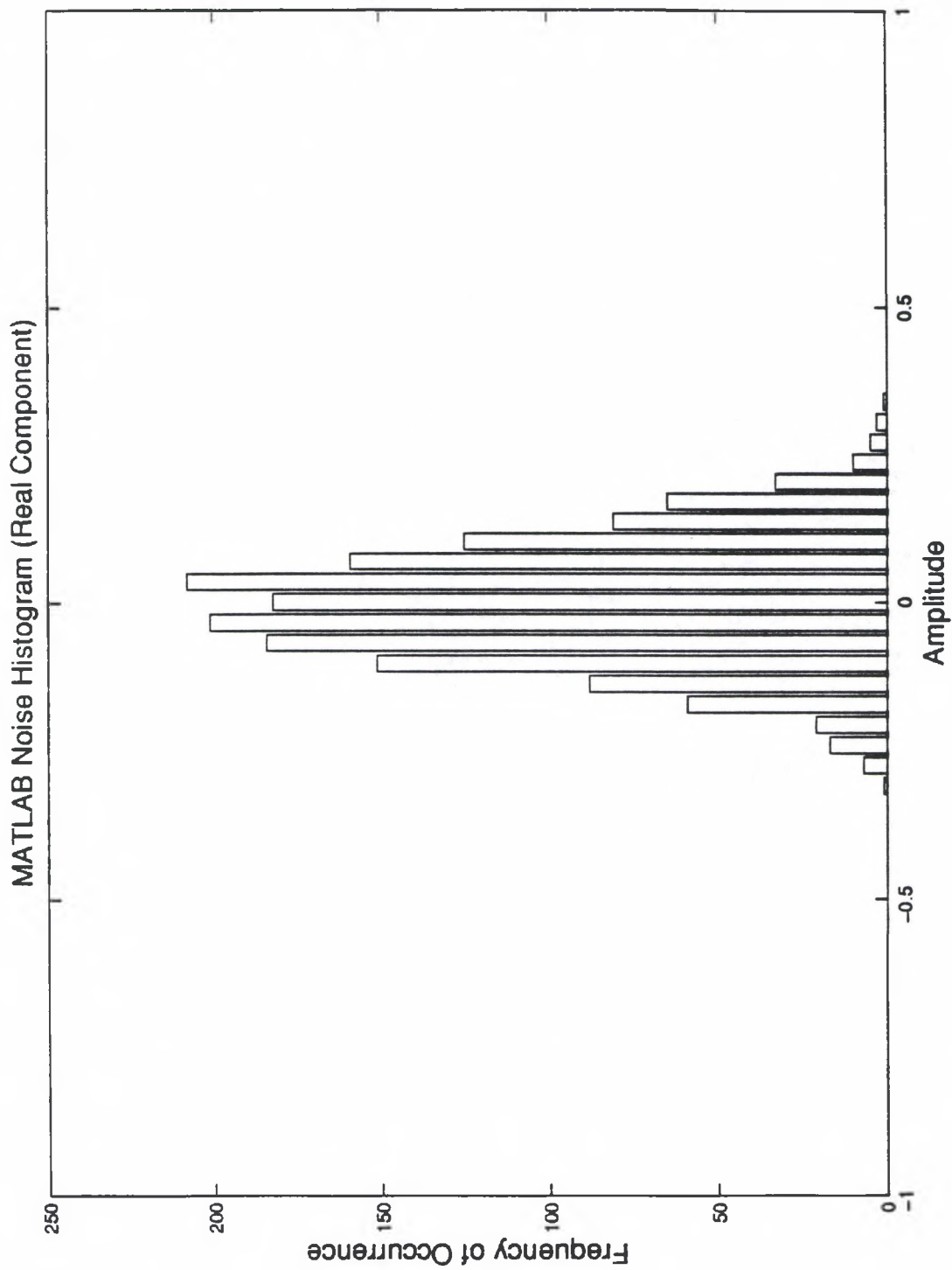


Figure 11. Histogram of MATLAB Noise Source

Figure 12 - Figure 15 plot the MUSIC spectrum as a function of bandwidth and number of apertures. In all four cases the resolution was enhanced by additional bandwidth. The resolution increases up to three apertures. However, no further improvement is seen from 3-6 apertures. The conclusion from these parametric studies is that once the data samples are sufficiently decorrelated, then no additional improvement in resolution is gained except from increased bandwidth. Figure 16 shows the MUSIC spectrum and Fourier transform overlaid in a "noiseless" (SNR=100 dB) scenario with only 2 apertures and 0.03 GHz bandwidth. In this case, the Fourier transform failed to resolve the two scattering centers but MUSIC resolved them very well.

MUSIC and the Fourier transform both give better resolution with increasing bandwidth. Often, in order to adequately view sources with the Fourier transform, a window is applied in the frequency domain to reduce the spectral contribution from the edges of the band. This window reduces the bandwidth according to the window's shape. In like manner, the MUSIC algorithm suffers reduced resolution as the number of apertures increases. This averaging procedure reduces the size of the correlation matrix, which, in turn, reduces resolution. As such there is a practical limit to the number of apertures that can be utilized and still resolve closely spaced sources.

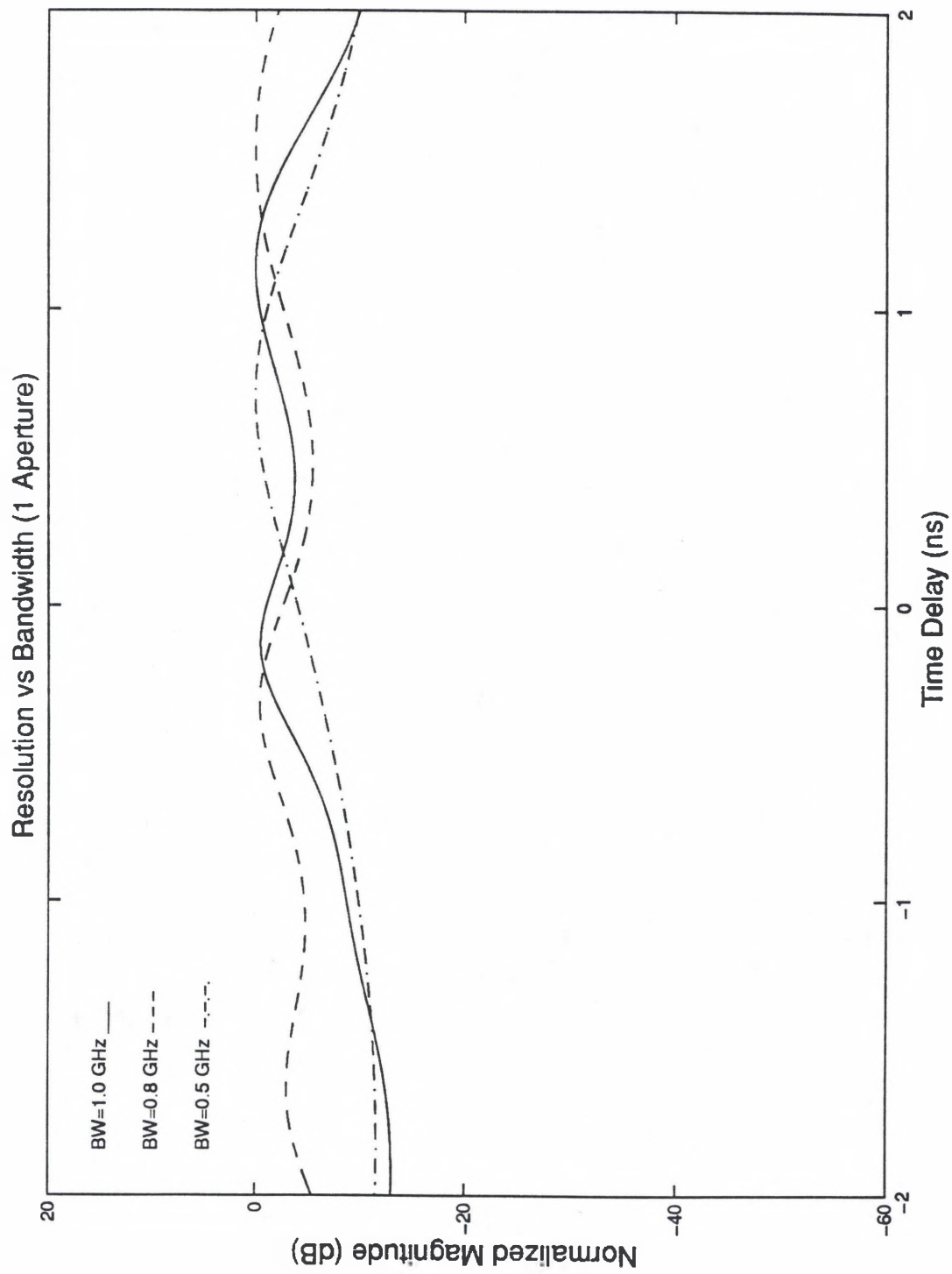


Figure 12. MUSIC Spectra Using 1 Aperture

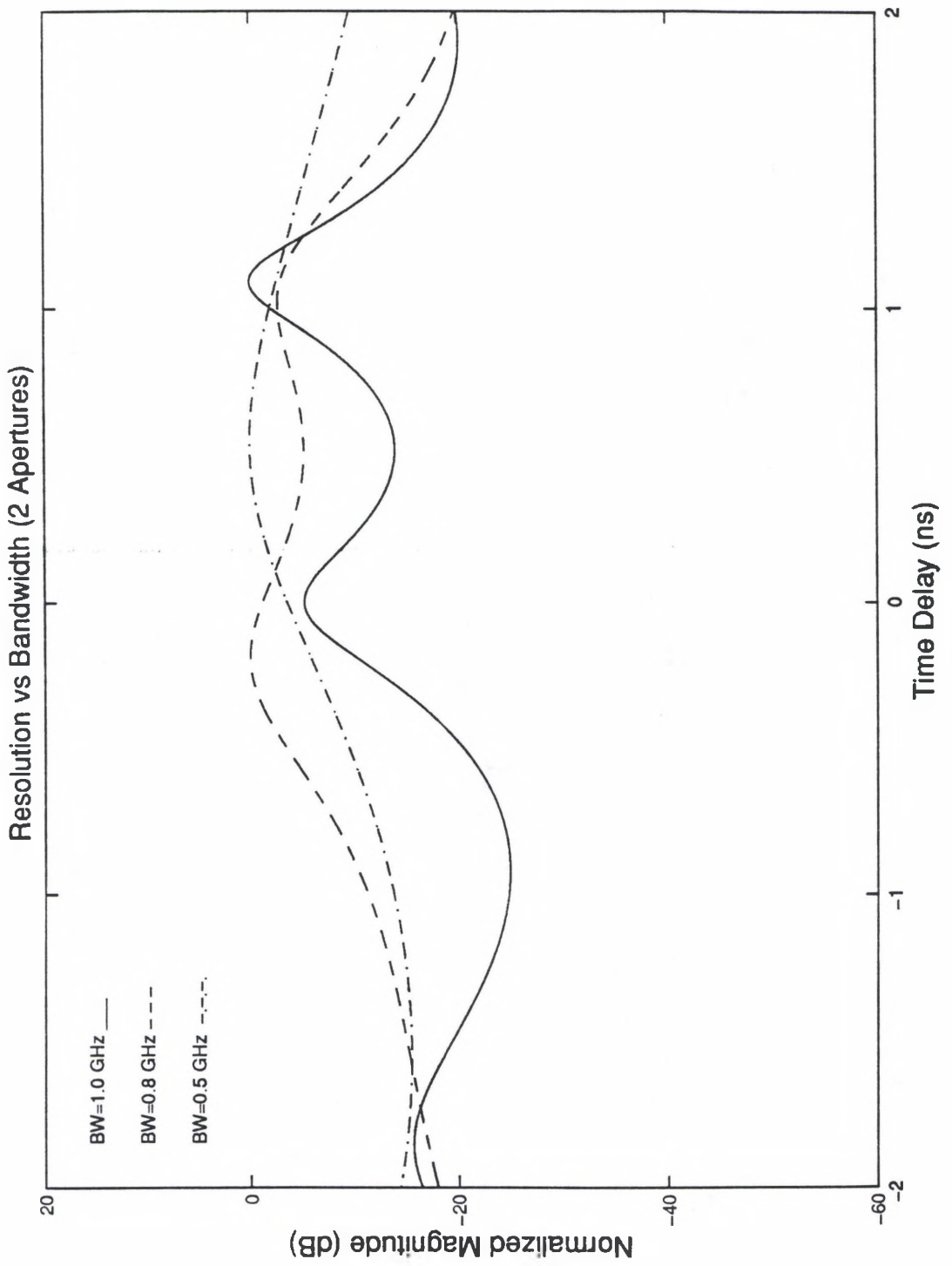


Figure 13. MUSIC Spectra Using 2 Apertures

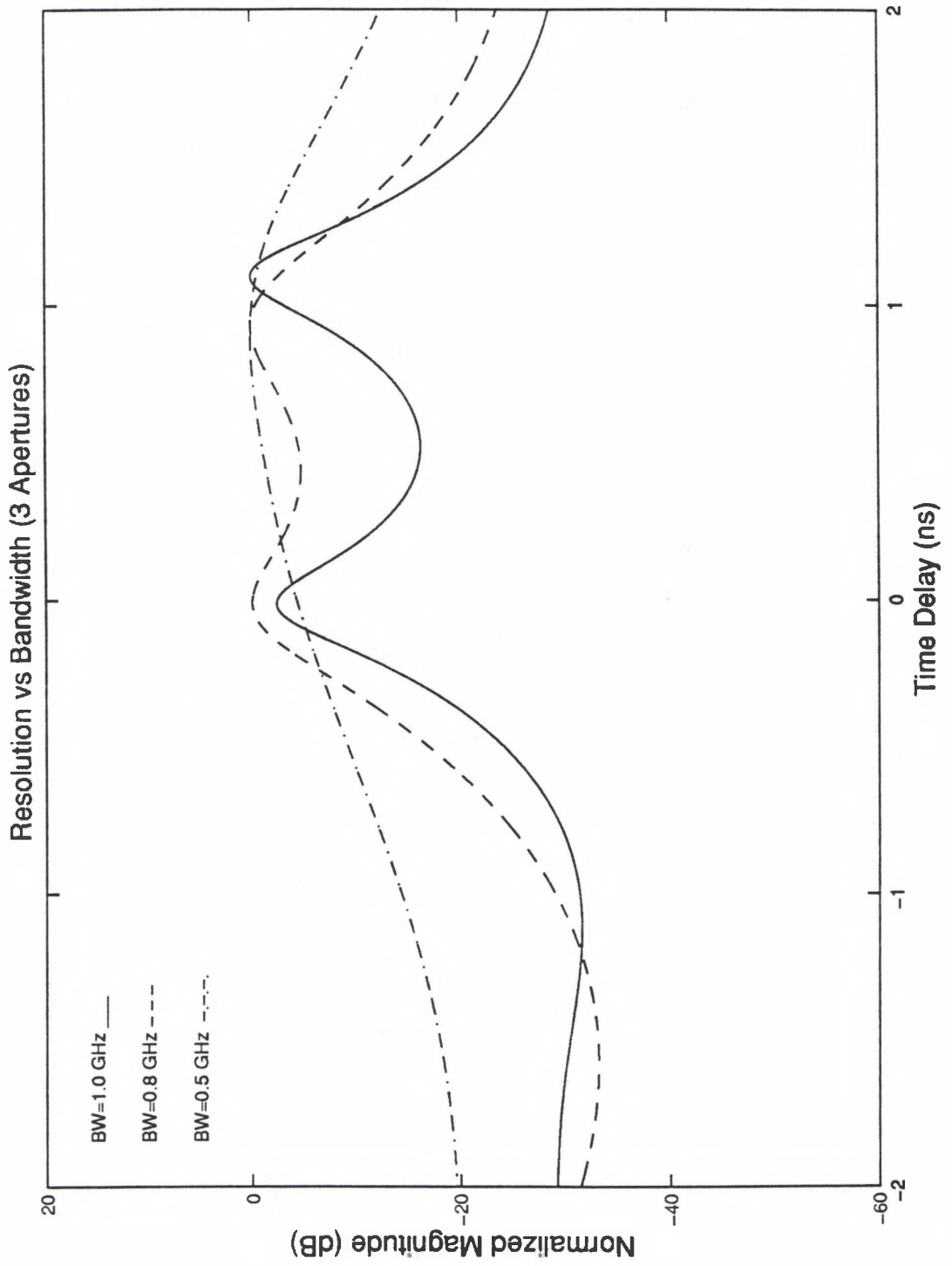


Figure 14. MUSIC Spectra Using 3 Apertures

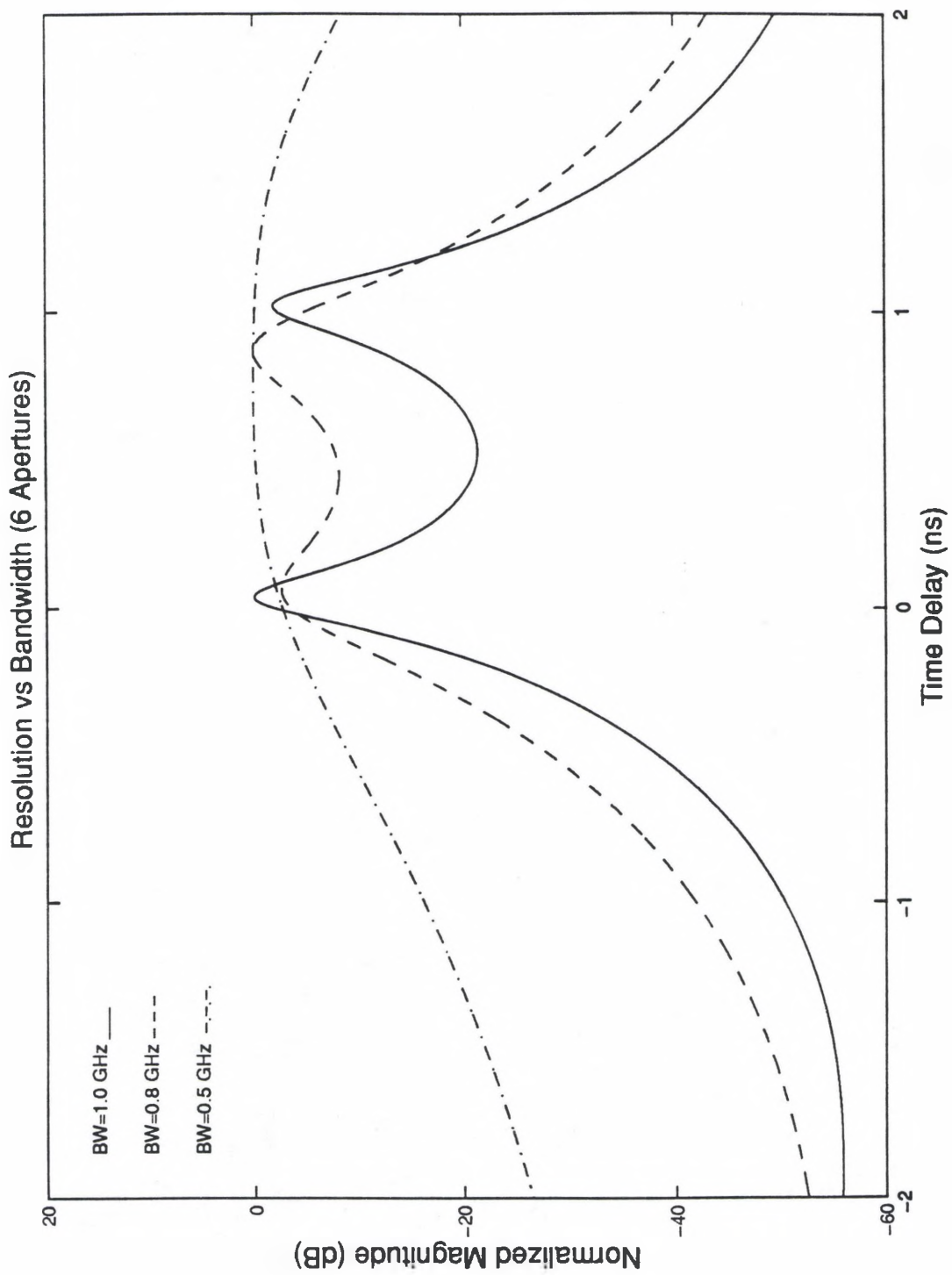


Figure 15. MUSIC Spectra Using 6 Apertures

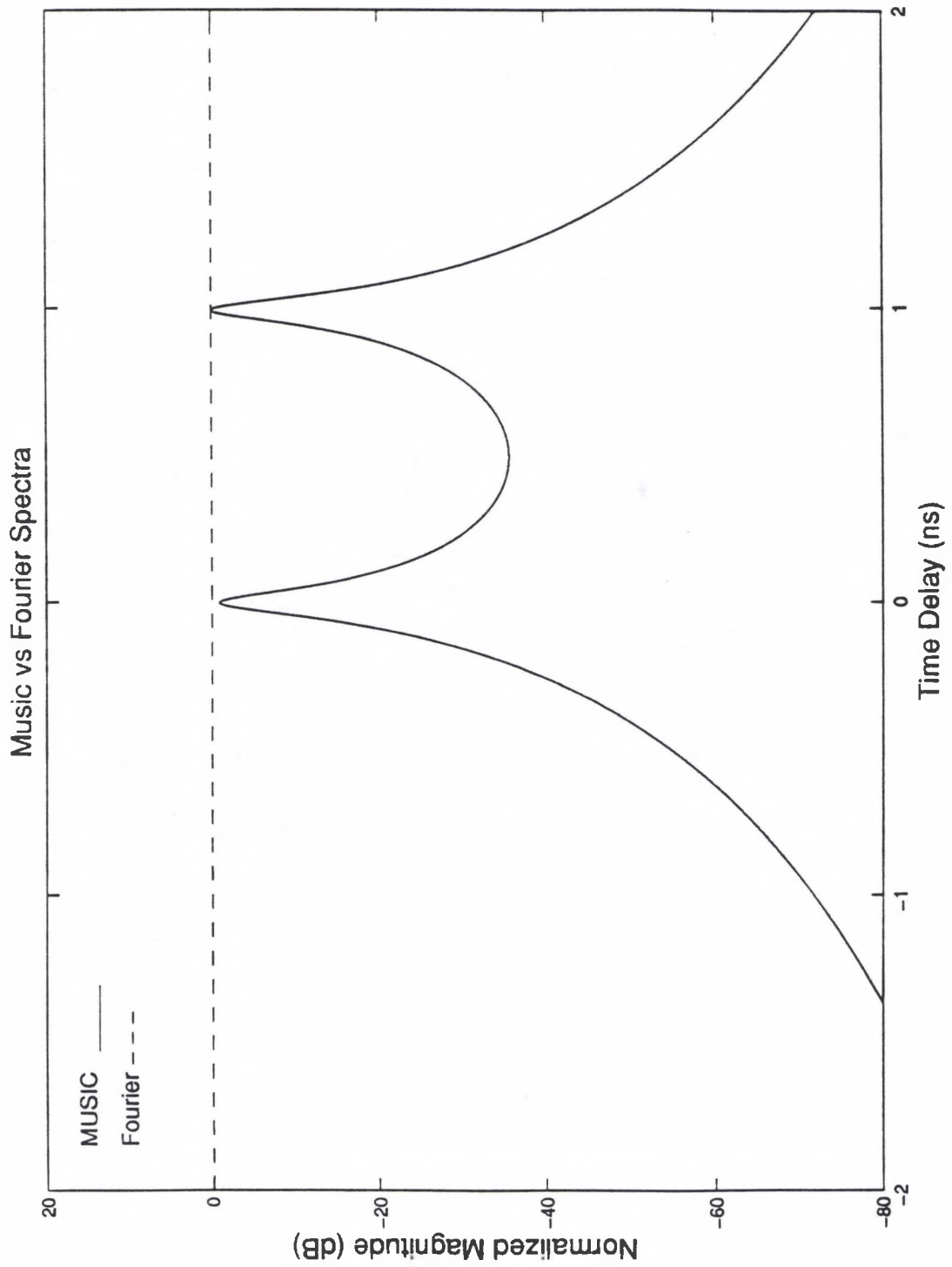


Figure 16. MUSIC and Fourier Spectra with .03 GHz Bandwidth and 2 Apertures

3.1.1.2 Accuracy

Parameters affecting accuracy will now be studied. Unlike the previous examples, the size of the correlation matrix is free to change according to the frequency increment and number of apertures used.

Figure 17 - Figure 20 plot MUSIC spectra depicting incremental changes in time delay estimation as a function of the number of apertures and correlation matrix size. Each case is based on two equal point sources at time delays of 0 and 1 ns respectively, and, a frequency band of 10-11 GHz with 20 dB SNR. The accuracy increases for each case until six apertures, where the scattering centers are accurately identified at 0 and 1 ns respectively. These figures show that accurate time delay estimation was achieved by six apertures. As such, the size of the correlation matrix has no effect on accuracy when the number of apertures is great enough to properly decorrelate the data for a sufficient bandwidth.

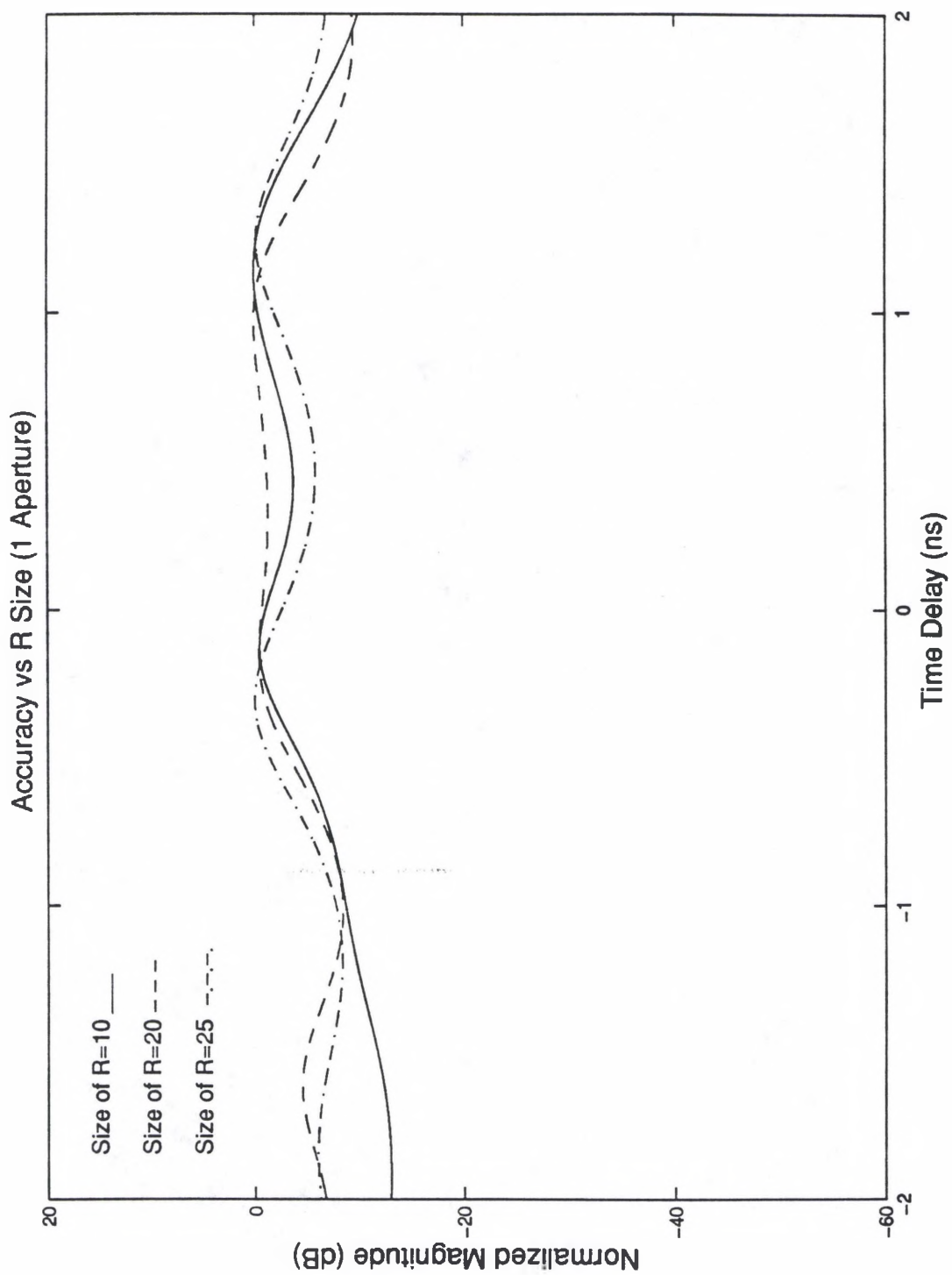


Figure 17. MUSIC Spectra Using 1 Aperture

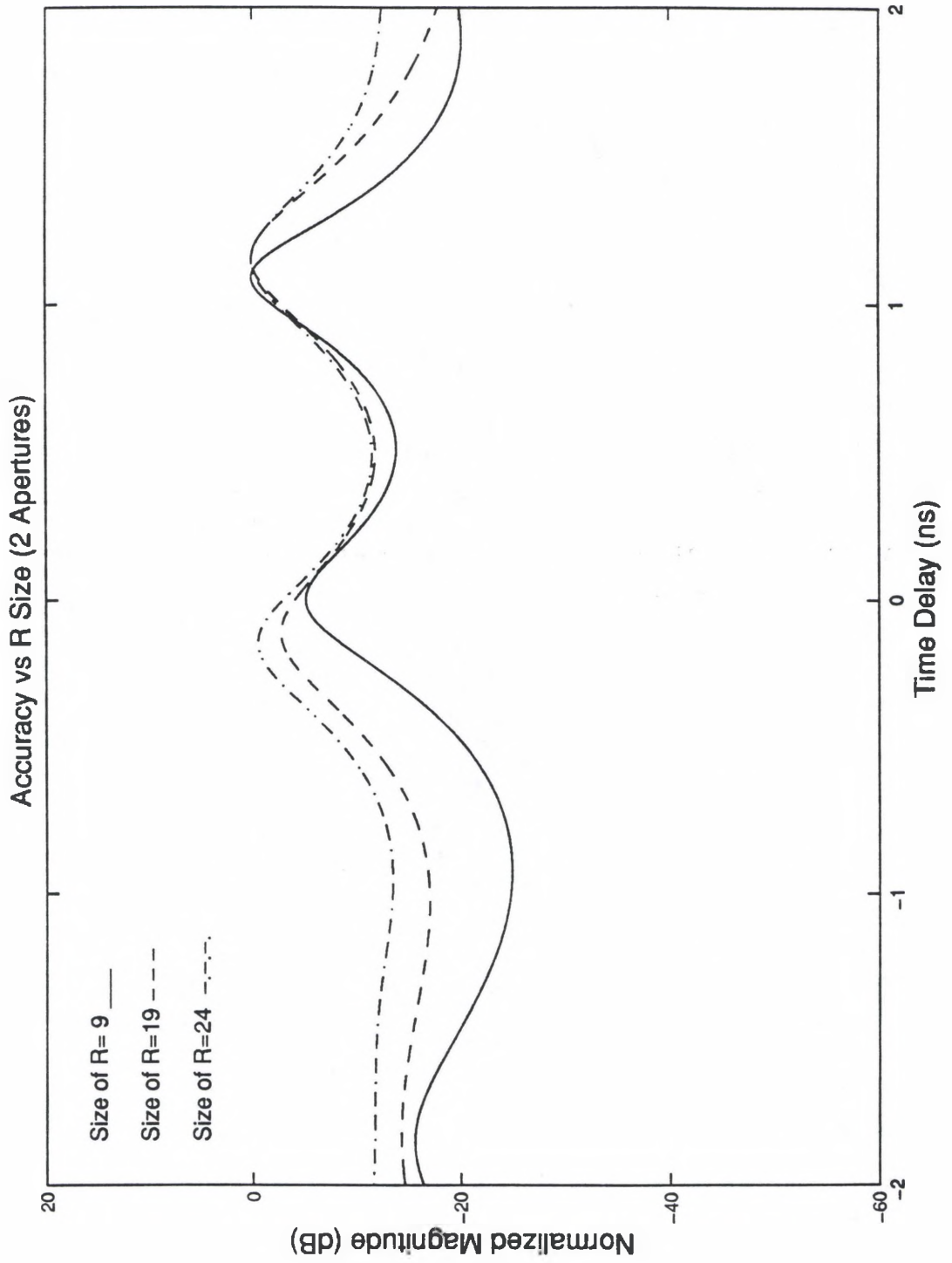


Figure 18. MUSIC Spectra Using 2 Apertures

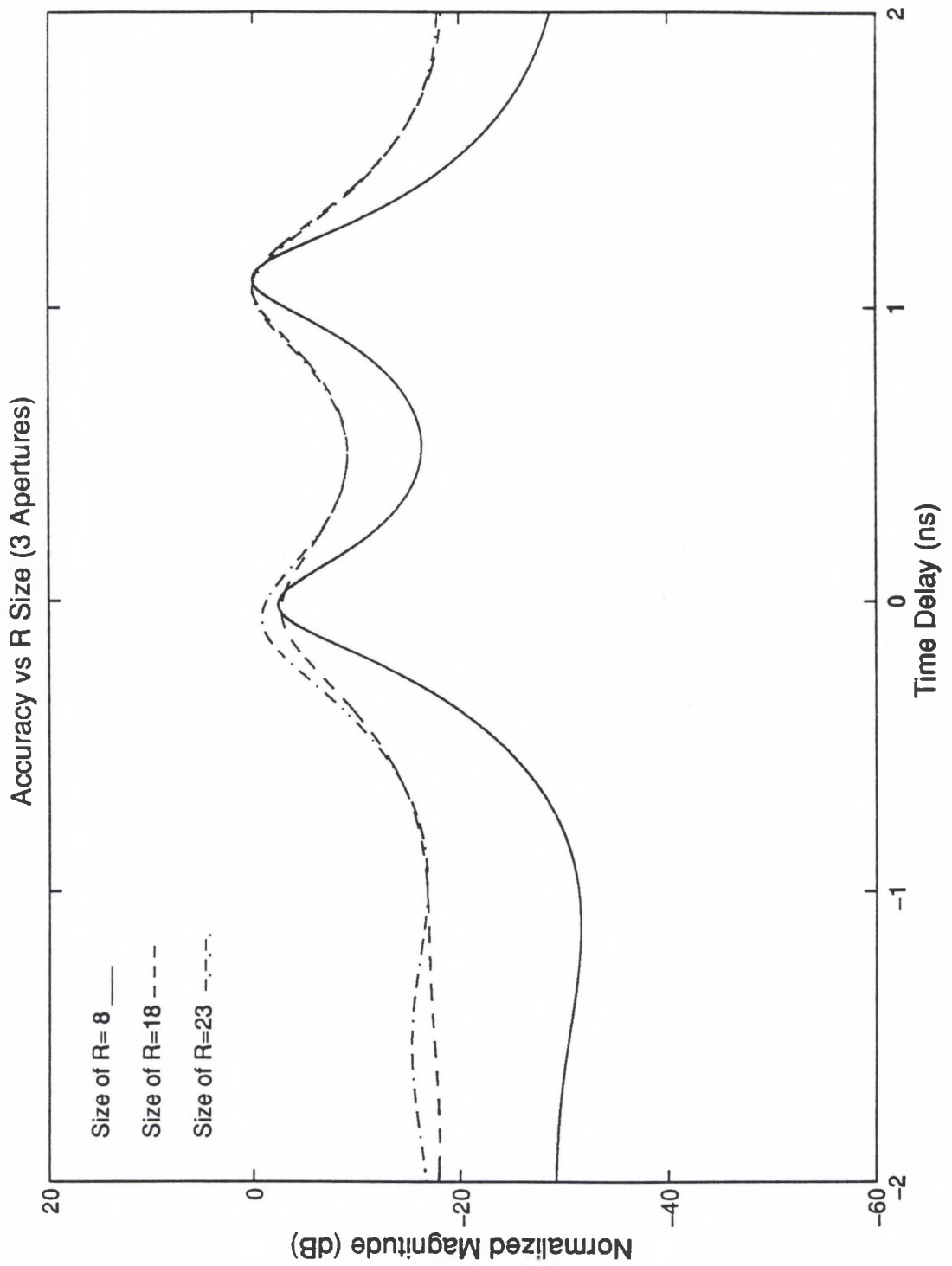


Figure 19. MUSIC Spectra Using 3 Apertures

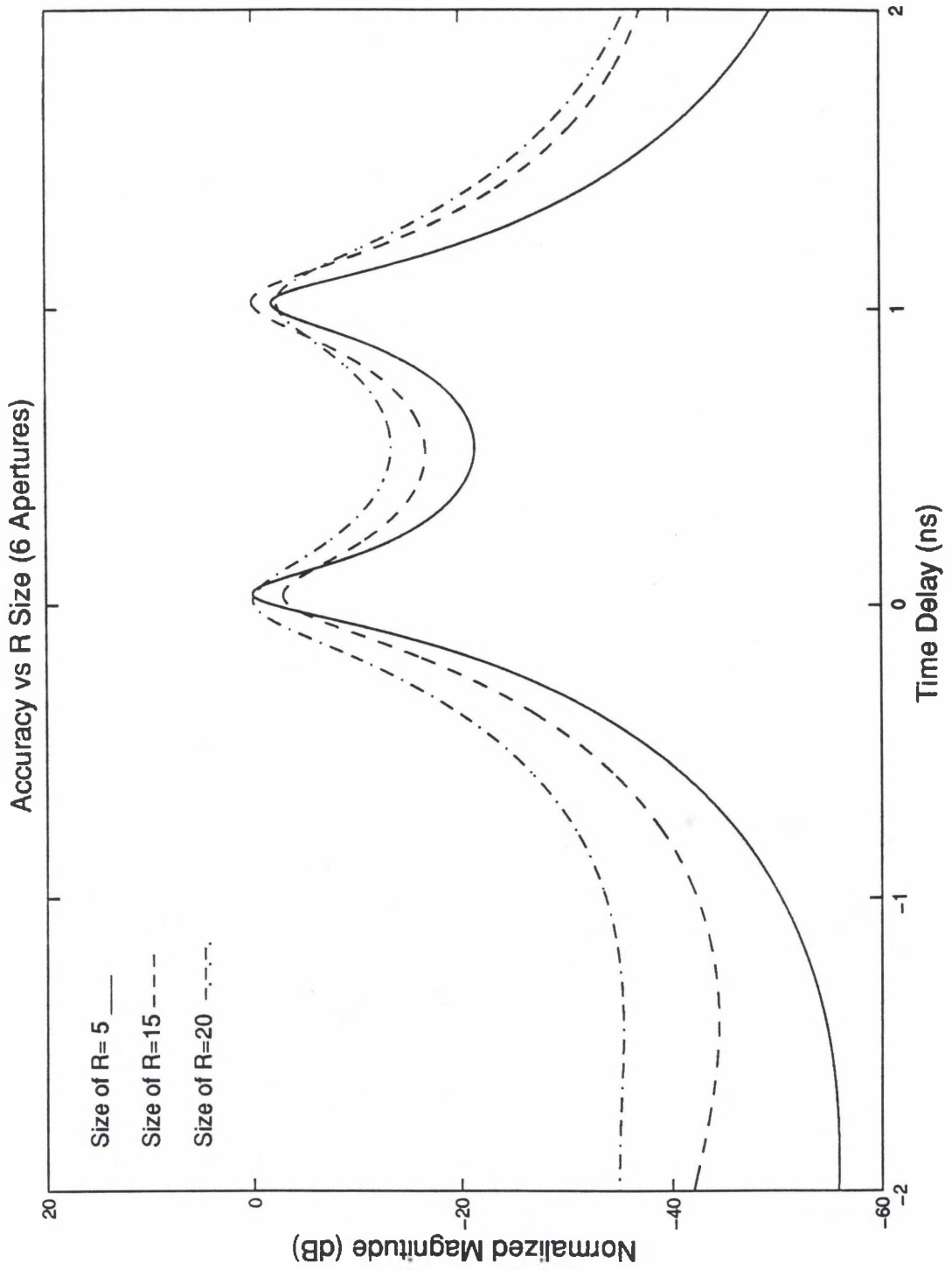


Figure 20. MUSIC Spectra Using 6 Apertures

3.2 Synthetic Data Analysis

The ability to decompose various types of scattering centers from synthetic signals will now be presented. Five different source compositions will be tested under a "just resolved" and "fully resolved" parameter set. The phrase "just resolved" is defined as a MUSIC spectrum computed from a minimum bandwidth which reveals distinct peaks that reflect the actual number of sources present. A "fully resolved" set is a MUSIC spectrum obtained from the maximum available or target specific bandwidth. All of the synthetic cases were performed using 16 apertures and a 20 dB SNR. Additional parameters specific to each set are shown in Table 1.

Table 1. Synthetic Data Parameters

Case Number	Number of Sources	Source Types 1 = Constant 2 = "Linear" 3 = Resonant	MUSIC Bandwidth/ Increment (GHz)	MUSIC Bandwidth/ Increment (GHz)	Regression Polynomial Order / Bandwidth (GHz)
			"Just Resolved"	"Fully Resolved"	
1	2	1-1	10.3-10.7/.02	12.0-18.0/.2	0/1
2	3	1-1-1	10.0-11.5/.05	12.0-18.0/.2	0/1
3	2	2-2	9.7-10.3/.02	12.0-18.0/.2	1/4*
4	3	2-3-2	9.5-10.5/.04	7.0-13.0/.2	0/1
5	3	3-3-3	4.0-12.0/.4	2.0-17.5/.5	0/1

* For the "just resolved" case, a regression polynomial order / bandwidth of 0/1 was used.

The results for each synthetic case are presented in five plots. The first plot shows the exact frequency response of the individual scattering centers. The second plot is an overlay of the MUSIC spectrum and the Fourier spectrum showing the estimated location of the centers using a "just resolved" bandwidth. The third plot is the estimated frequency response for each center also using a "just resolved" bandwidth. The fourth and fifth plots are the same as the second and third, respectively, except using a "fully resolved" bandwidth.

3.2.1 Synthetic Case 1

This case is designed to be a simple scenario as Figure 21 clearly shows. Since both scattering centers have the same amplitude, this plot appears to show only one line, although there are two. The error in estimated frequency response for the "just resolved" case (Figure 23)

is so pronounced. The primary source of error is the miscalculation in the scattering center locations (Figure 22). The exact versus estimated locations are as follows:

Table 2. Location of Scattering Centers for Synthetic Case 1

	Exact Time Delay (ns)	"Just Resolved" Time Delay (ns)	"Fully Resolved" Time Delay (ns)
Source 1	0	-.1153	0.002
Source 2	1	1.3548	1.0029

Both the MUSIC spectrum and estimated frequency responses for the "fully resolved" case show excellent agreement with the exact solution and are shown in Figure 24 and Figure 25.

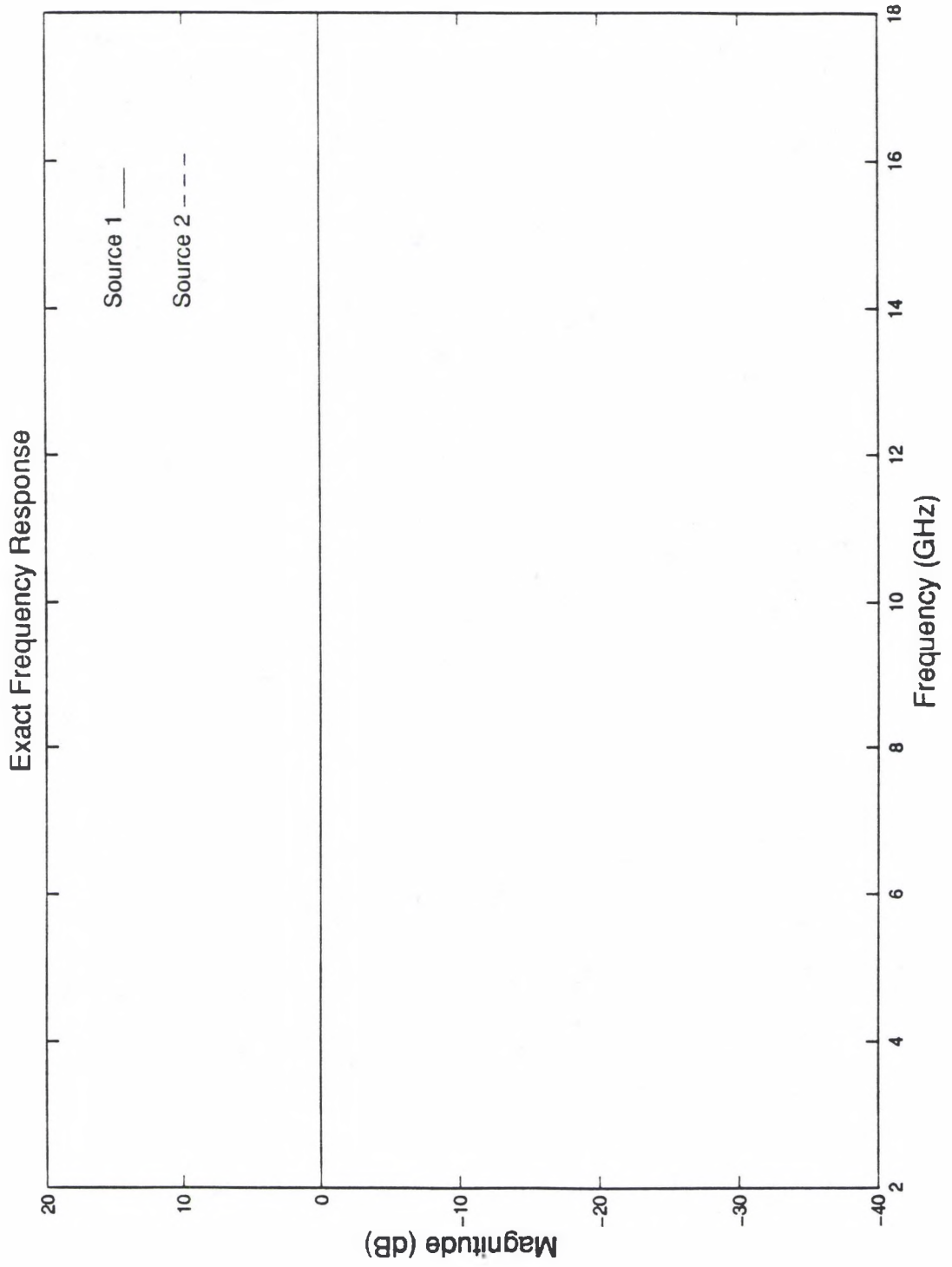


Figure 21. Exact Frequency Response for Synthetic Case 1

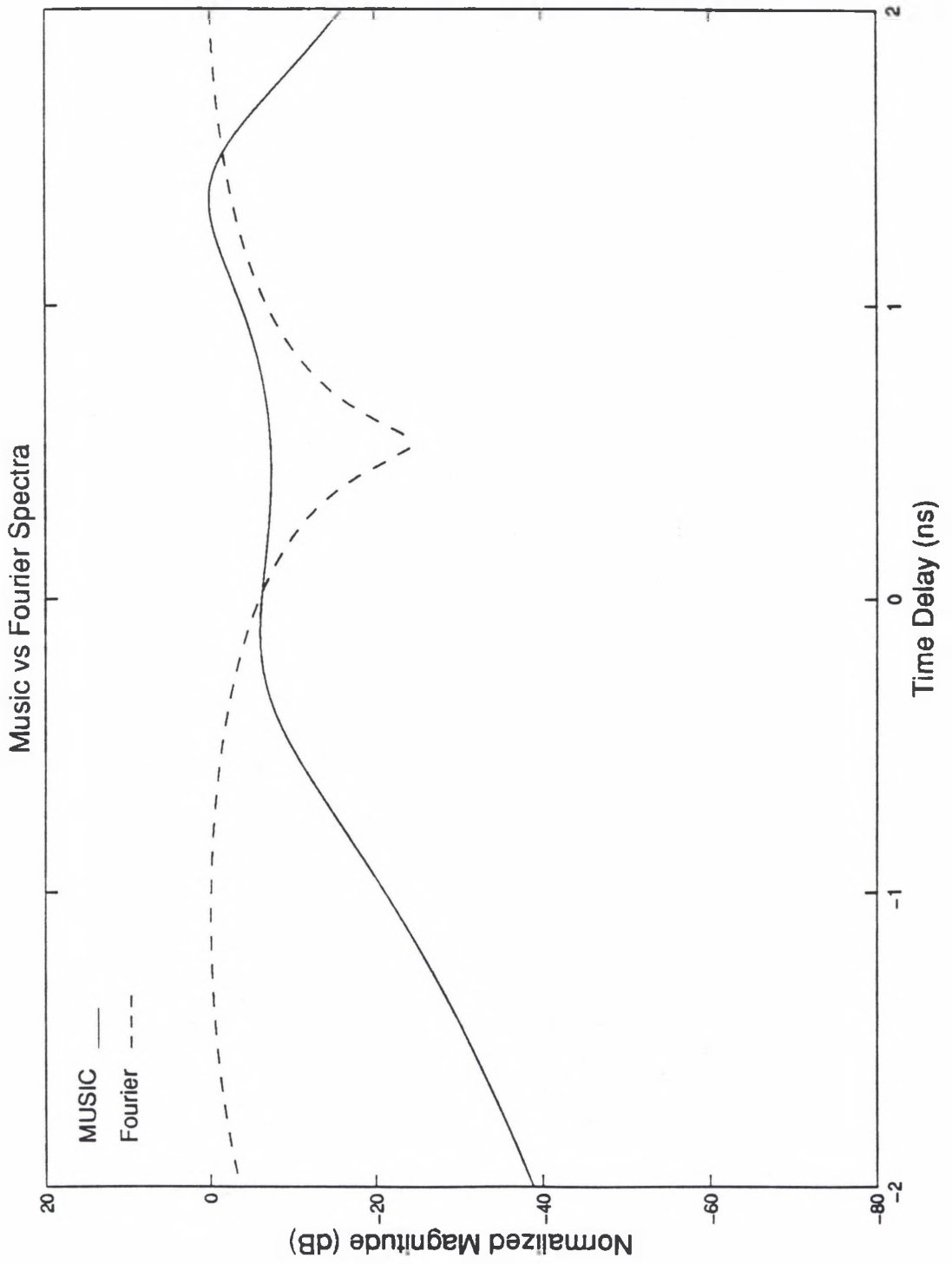


Figure 22. MUSIC Spectrum for Synthetic Case 1 ("Just Resolved")

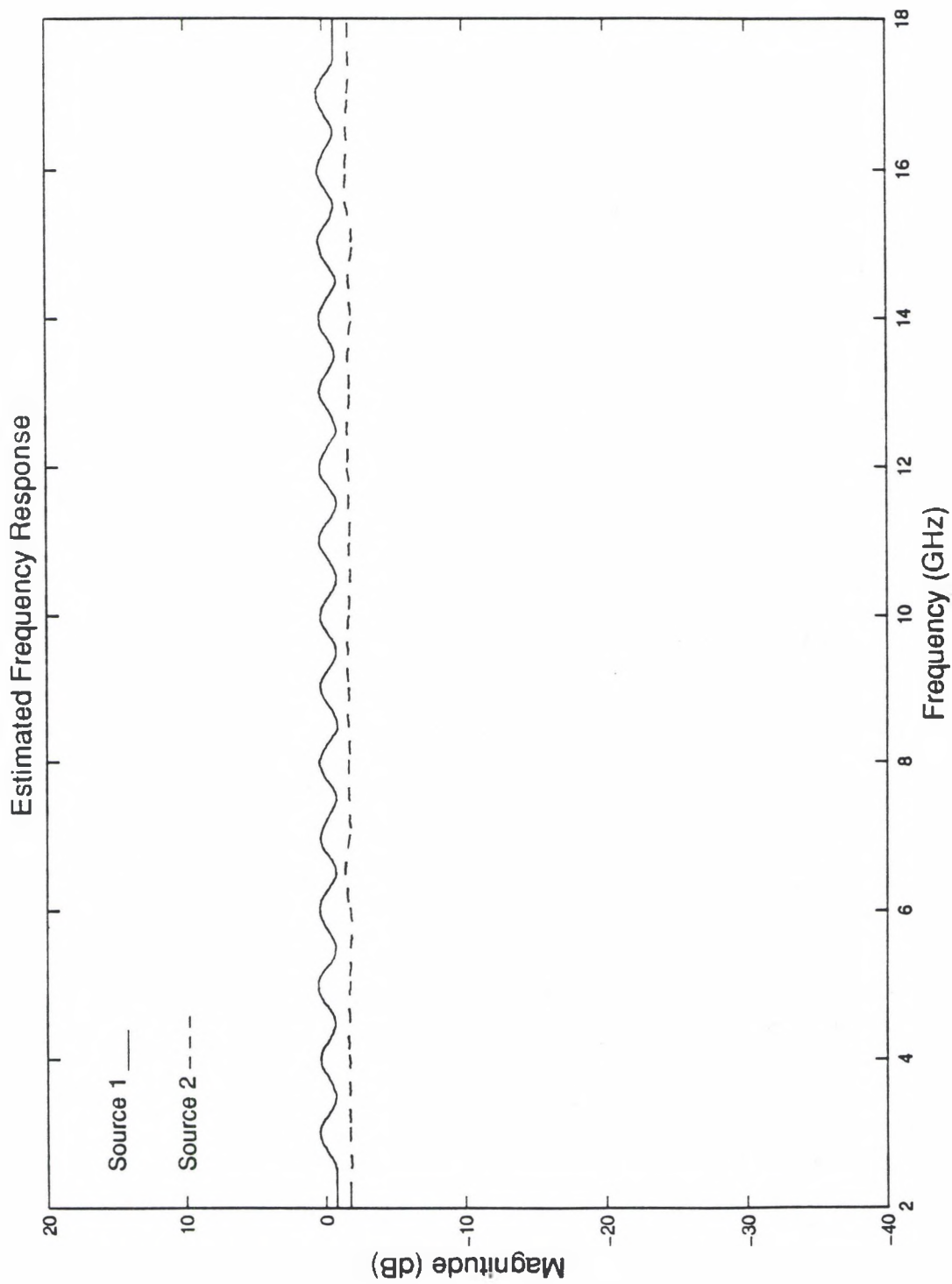


Figure 23. Estimated Frequency Response for Synthetic Case 1 ("Just Resolved")

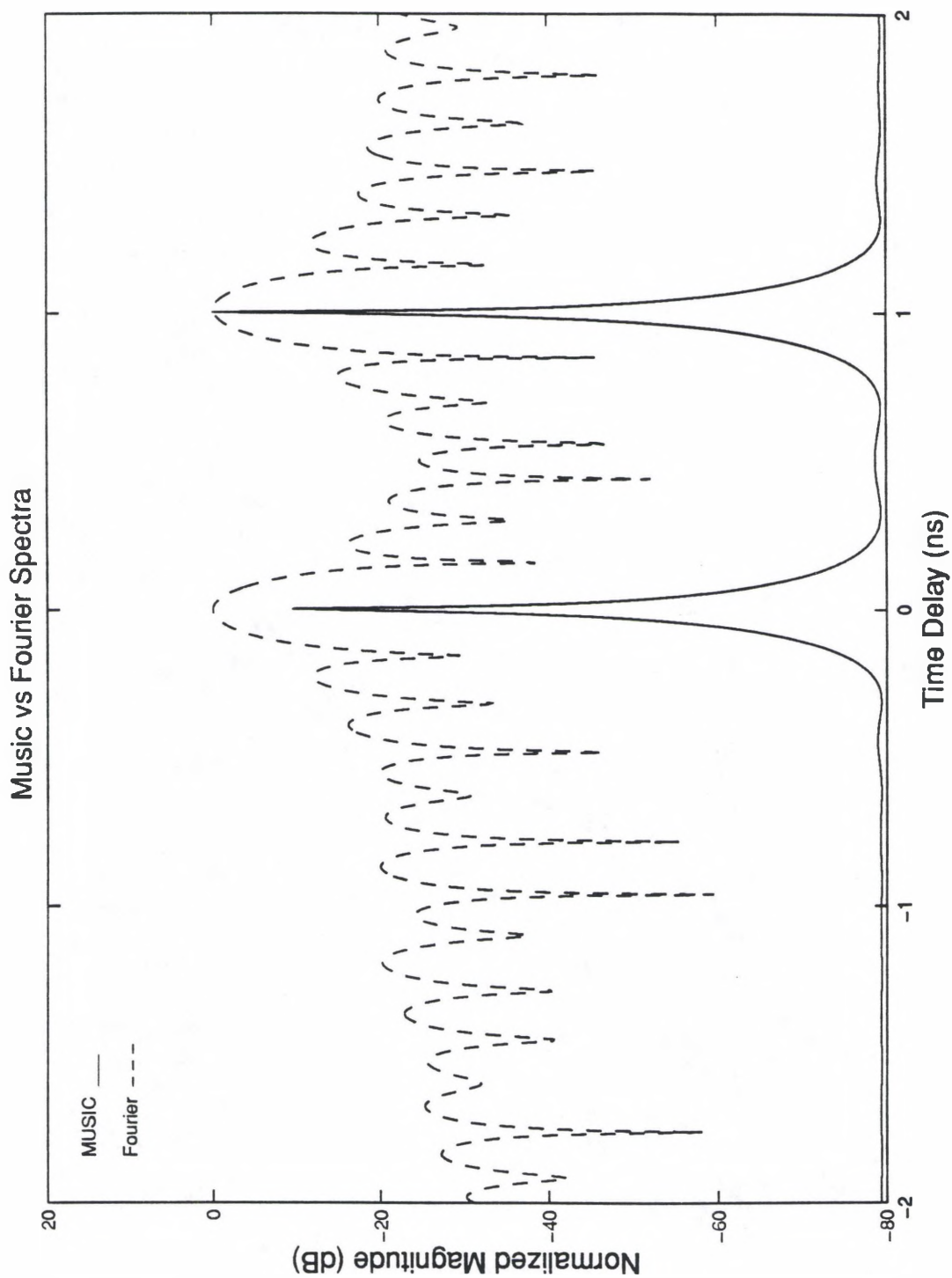


Figure 24. MUSIC and Fourier Spectra for Synthetic Case 1 ("Fully Resolved")

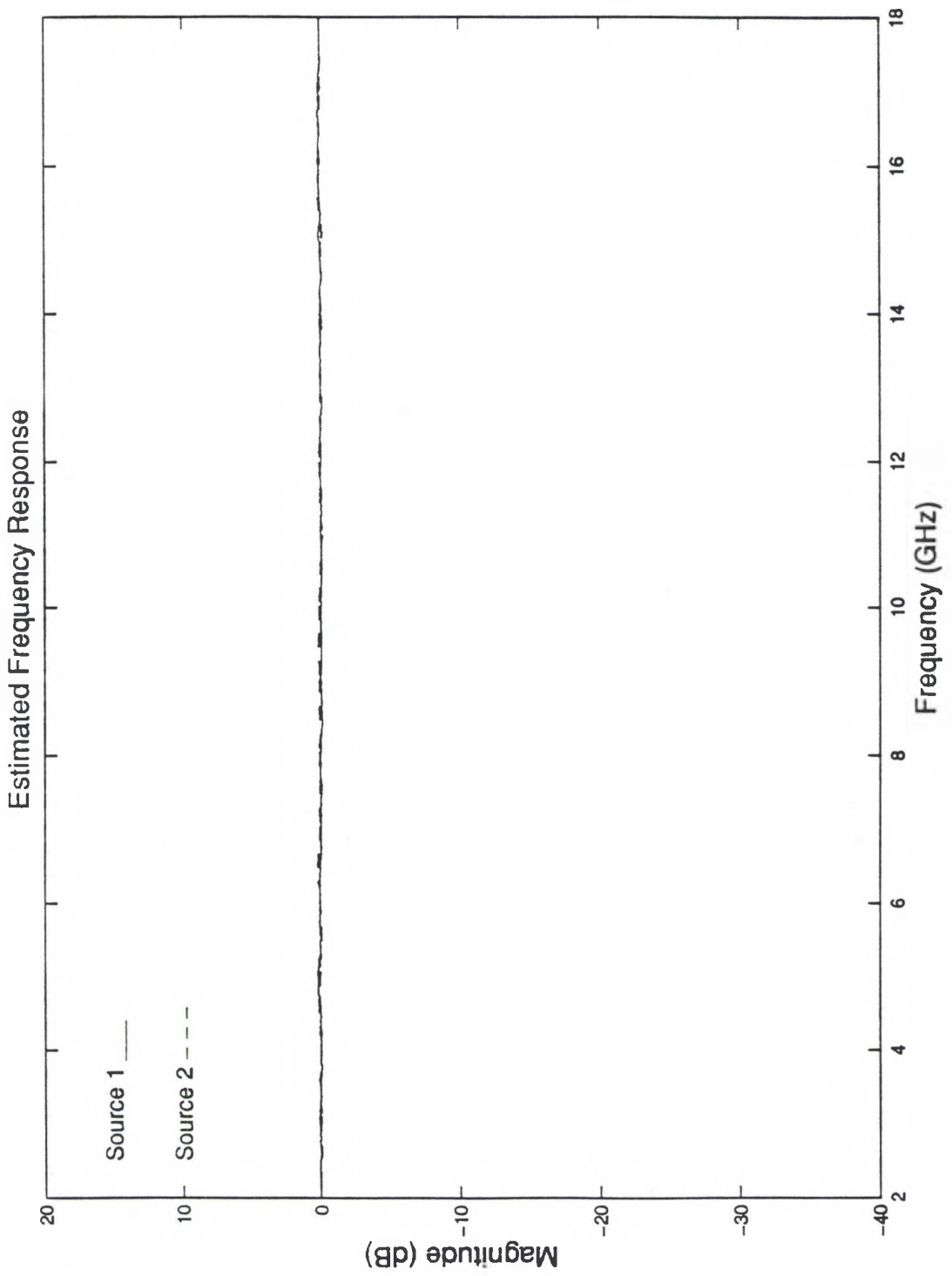


Figure 25. Estimated Frequency Response for Synthetic Case 1 ("Fully Resolved")

3.2.2 Synthetic Case 2

This case is primarily designed to test the method in a simple extended dynamic range situation as shown in Figure 26. In particular, the -20 dB Source is at the level of the noise (0 dB SNR) and is still resolvable in both MUSIC spectrum (Figure 27 and Figure 29) and estimated frequency response of scattering centers (Figure 28 and Figure 30). Both the "just" and "fully resolved" cases perform quite well in this scenario, which is due to an accurate estimation of the scattering center locations as shown below.

Table 3. Location of Scattering Centers for Synthetic Case 2

	Exact Time Delay (ns)	"Just Resolved" Time Delay (ns)	"Fully Resolved" Time Delay (ns)
Source 1	-1	-.9873	-.9951
Source 2	0	-.0059	0.002
Source 3	1	-1.0342	1.0068

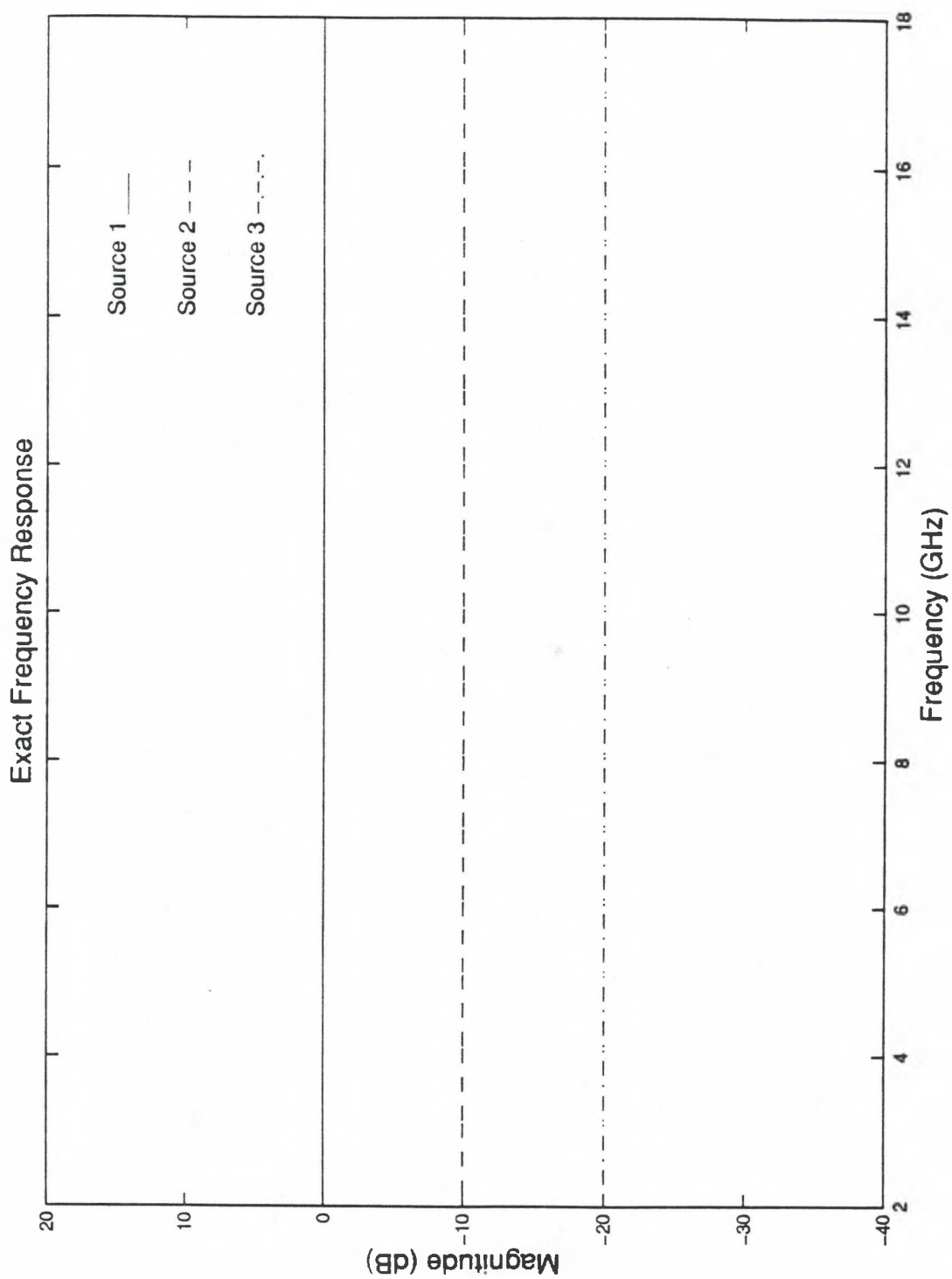


Figure 26. Exact Frequency Response for Synthetic Case 2

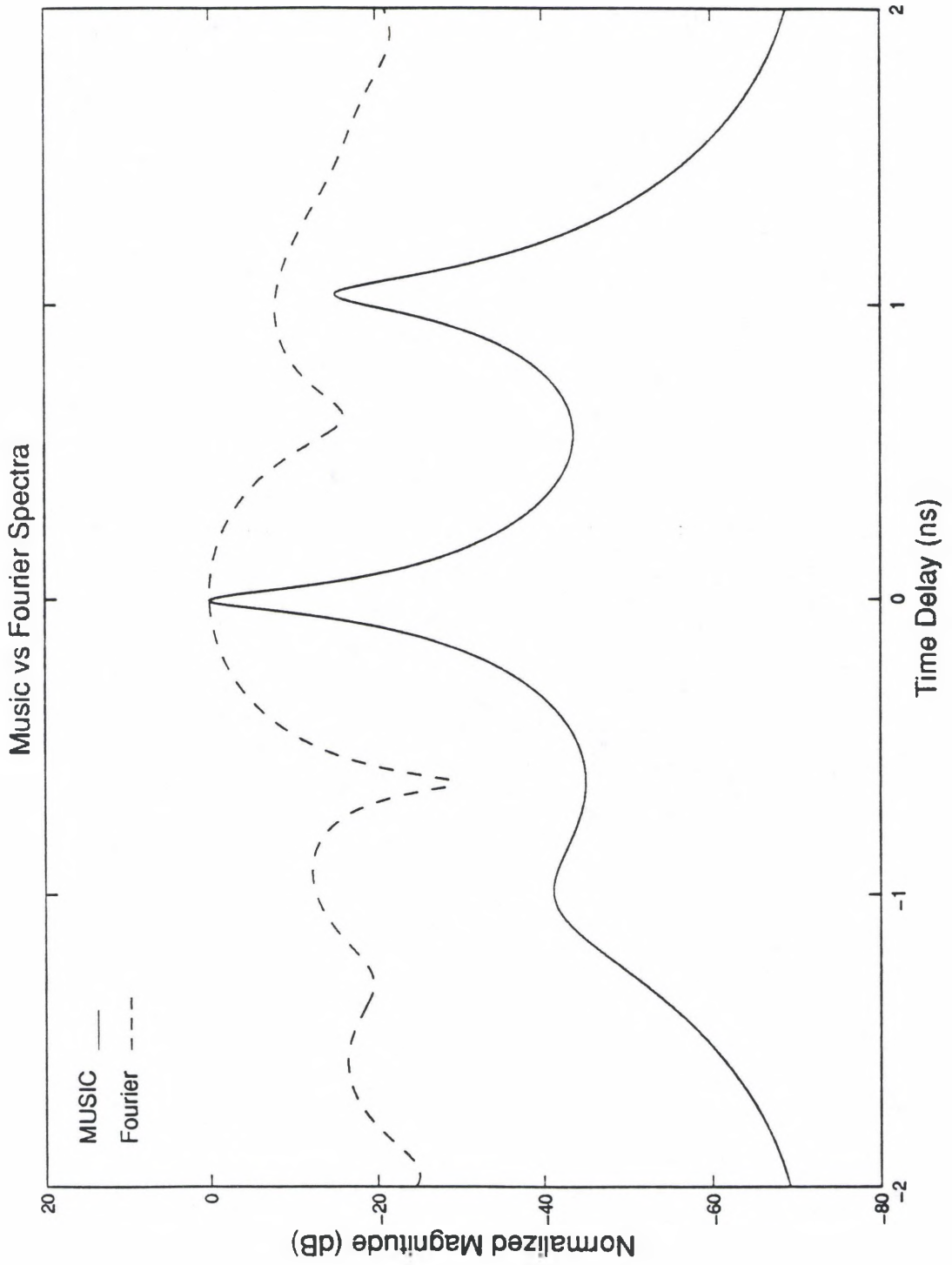


Figure 27 MUSIC and Fourier Spectra for Synthetic Case 2 ("Just Resolved")

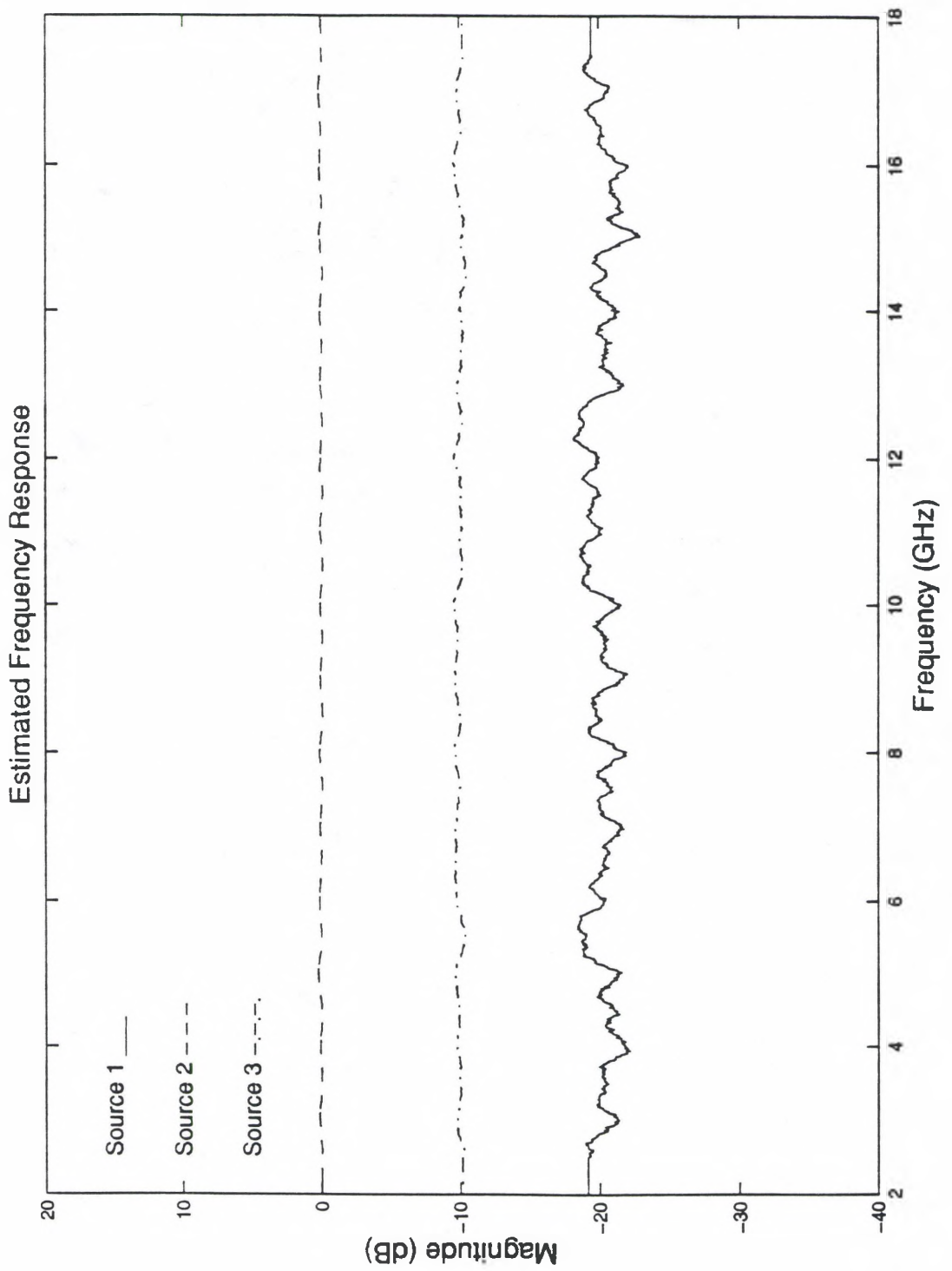


Figure 28. Estimated Frequency Response for Synthetic Case 2 ("Just Resolved")

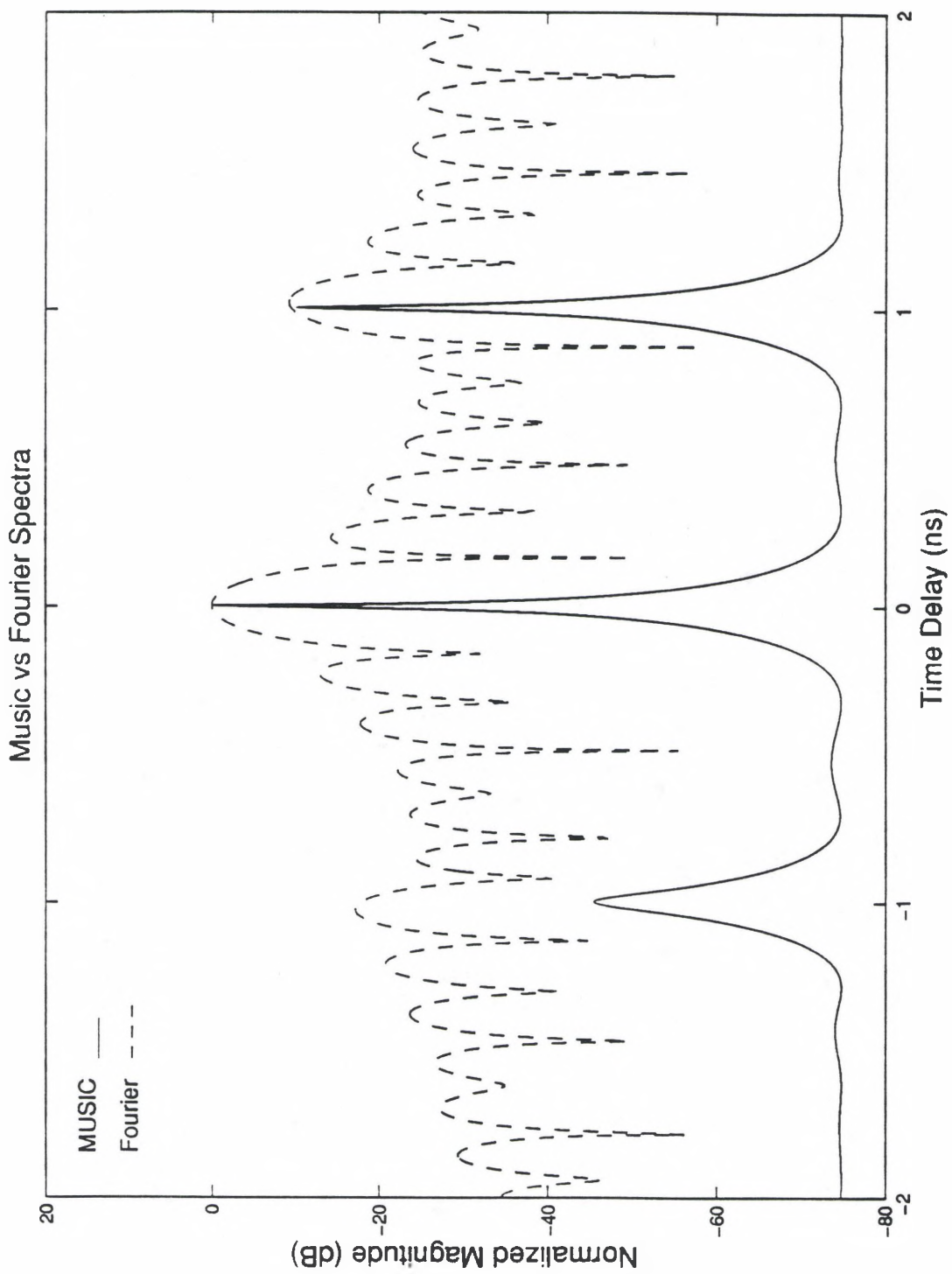


Figure 29 MUSIC and Fourier Spectra for Synthetic Case 2 ("Fully Resolved")

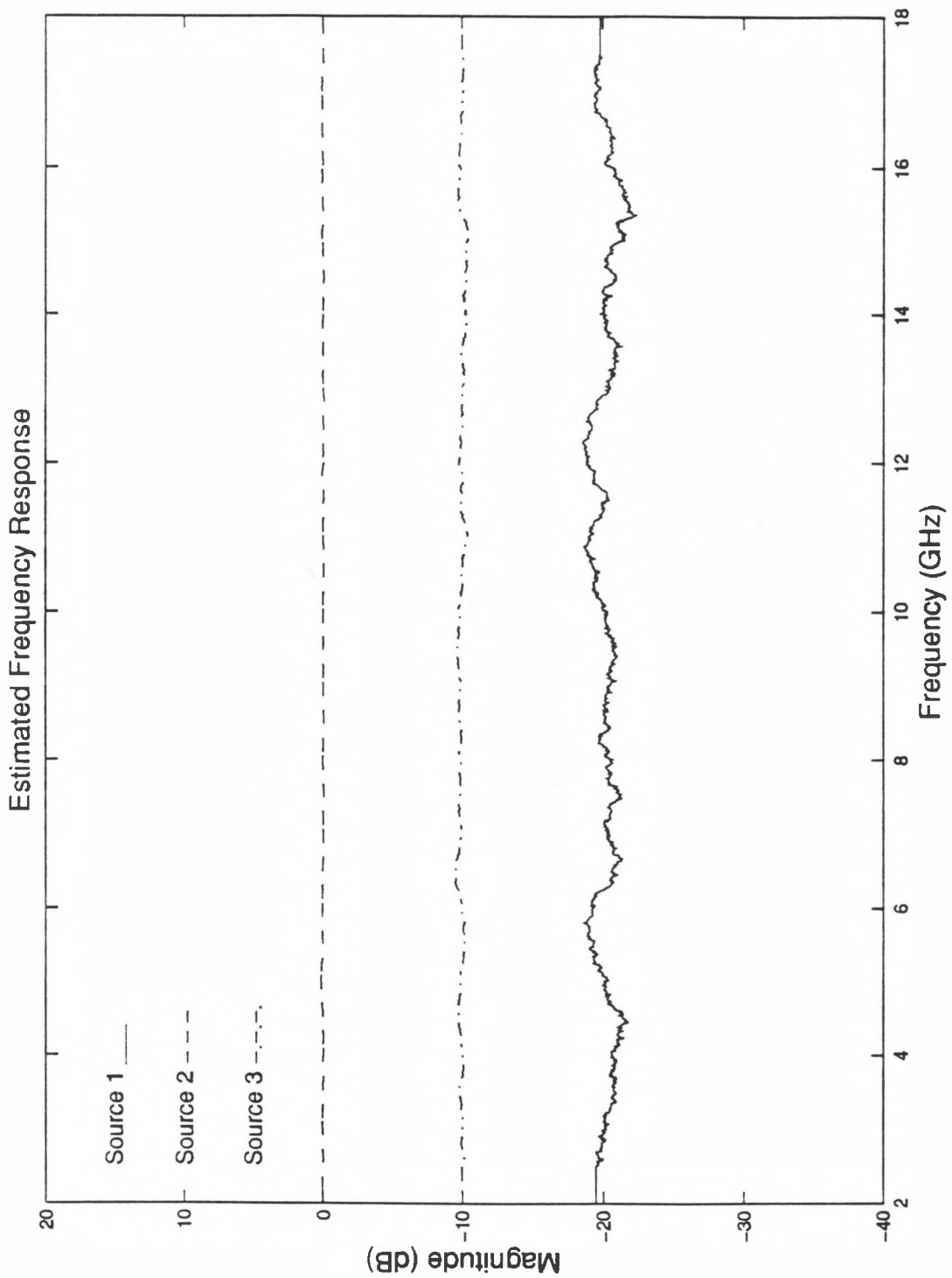


Figure 30 Estimated Frequency Response for Synthetic Case 2 ("Fully Resolved")

3.2.3 Synthetic Case 3

This scenario shows how the SNR can affect a non-constant source as it approaches the noise level. As the exact frequency response shows in Figure 31, each source's frequency response begins at one end of the band at a maximum of 0 dB and extends down to -10 dB at the opposite end of the band. Both the "just" and "fully resolved" cases correctly identify the sources as "linear", but the "just resolved" frequency responses (Figure 33) are incorrect in slope and magnitude at 2 GHz. The estimated frequency response is better for the "fully resolved" case. The time delays for both cases (Figure 32 and Figure 34) are shown in the following table.

Table 4. Location of Scattering Centers for Synthetic Case 3

	Exact Time Delay (ns)	"Just Resolved" Time Delay (ns)	"Fully Resolved" Time Delay (ns)
Source 1	0	-0.0137	0.002
Source 2	1	0.08426	1.0029

The method performs best when it accurately identifies the locations of the scattering centers as shown in Figure 35, in which the slopes and magnitudes of the frequency responses are accurately estimated.

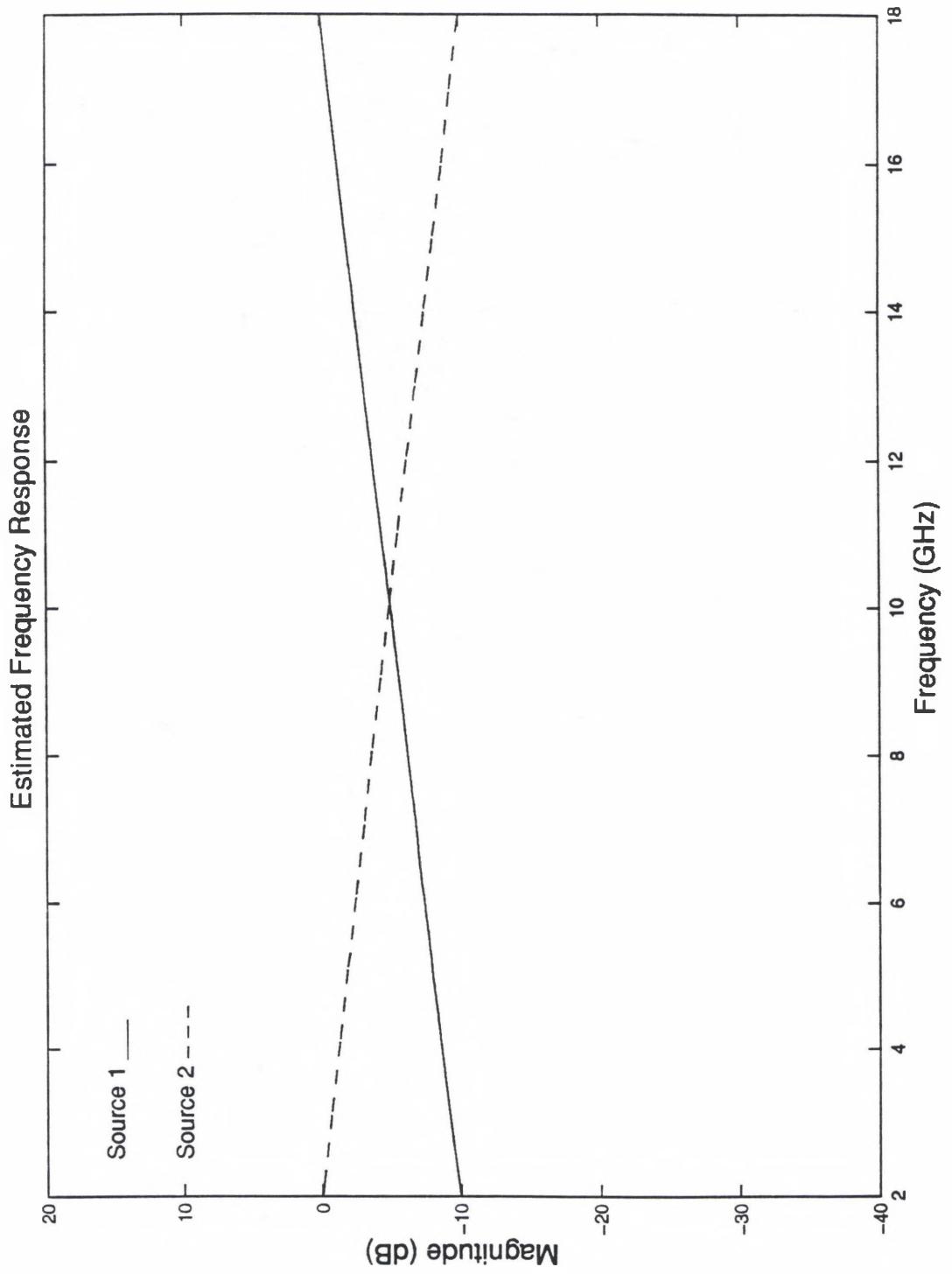


Figure 31. Exact Frequency Response for Synthetic Case 3

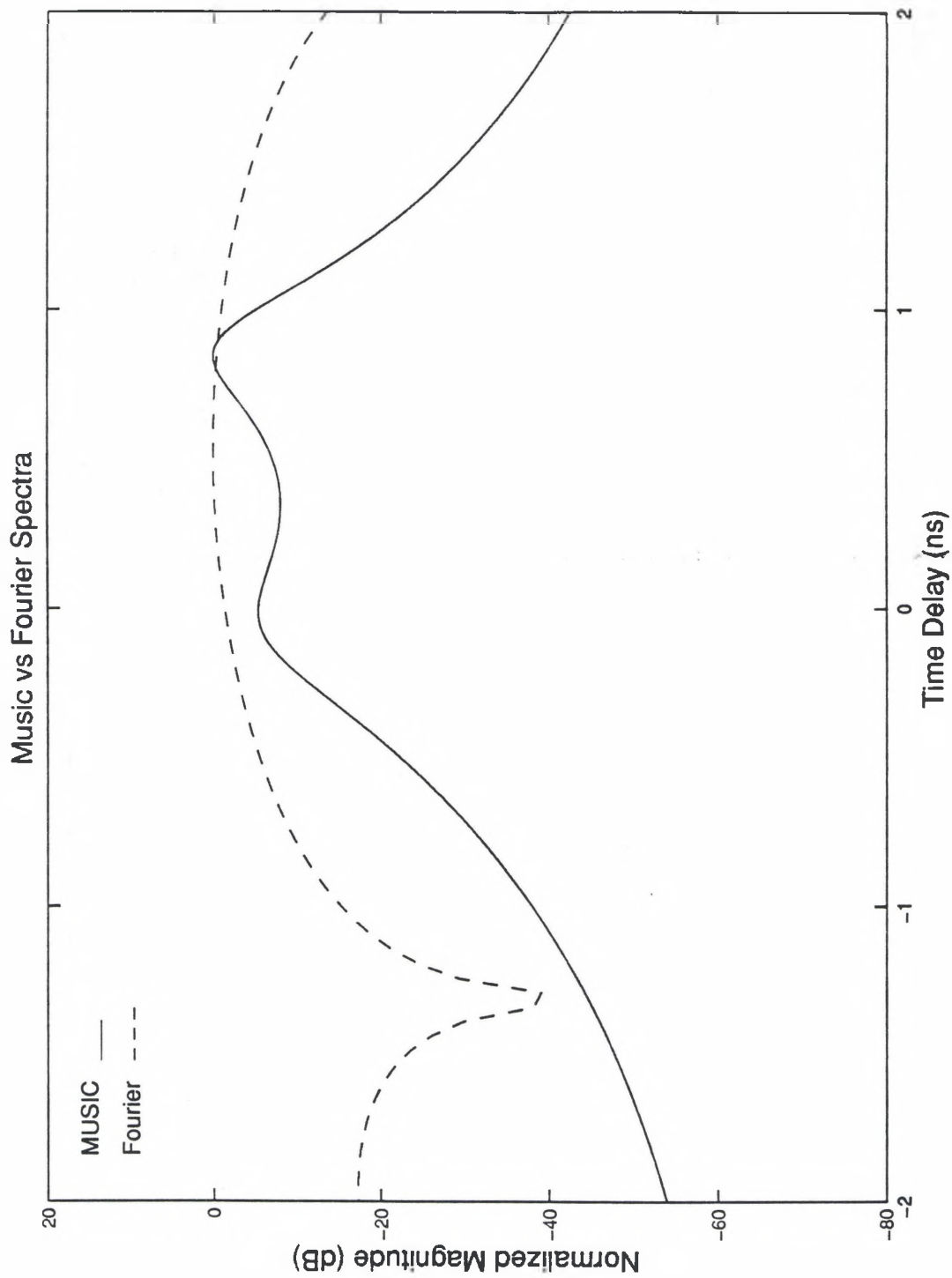


Figure 32. MUSIC and Fourier Spectra for Synthetic Case 3 ("Just Resolved")

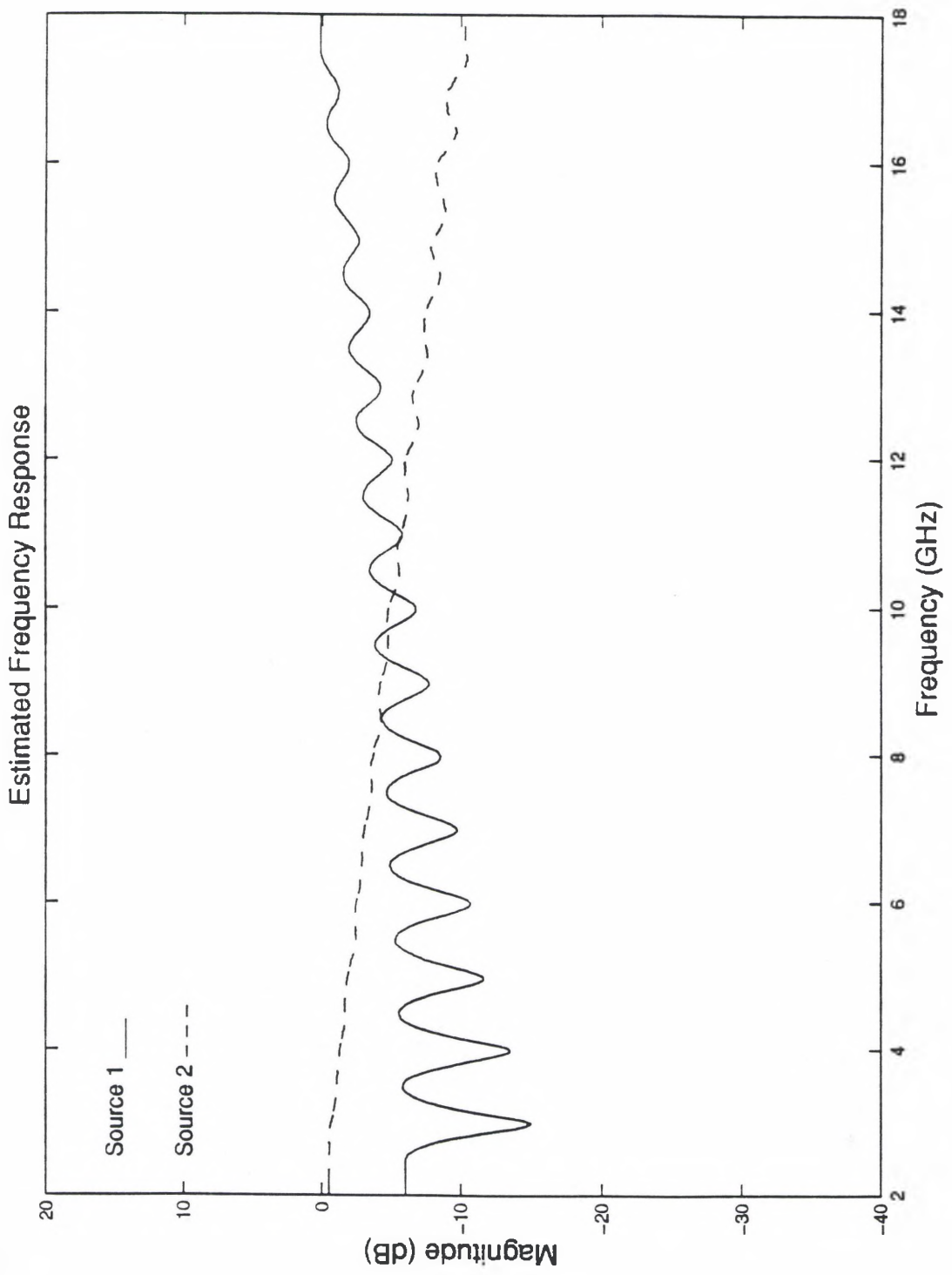


Figure 33 Estimated Frequency Response for Synthetic Case 3 ("Just Resolved")

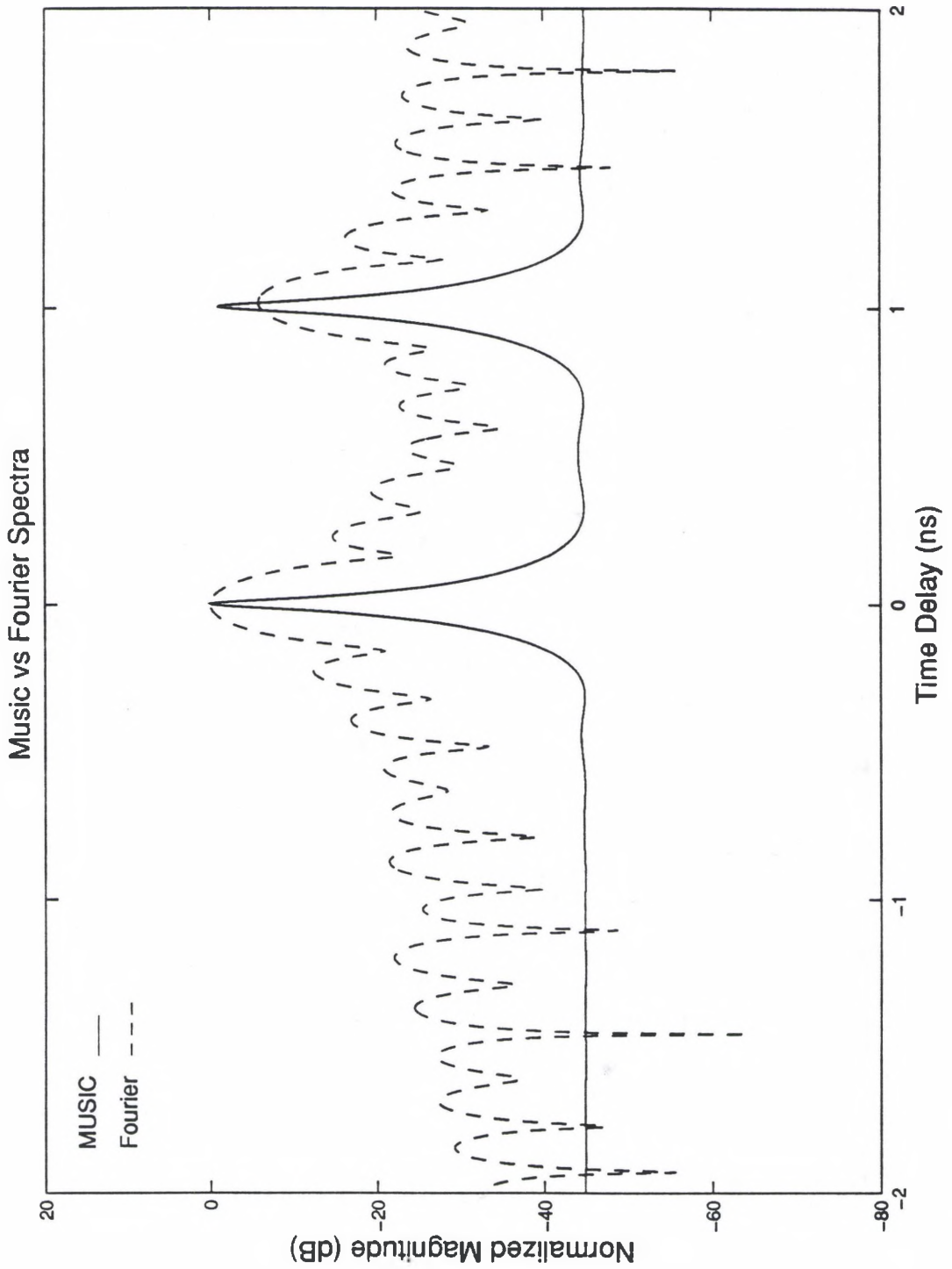


Figure 34. MUSIC and Fourier Spectra for Synthetic Case 3 ("Fully Resolved")

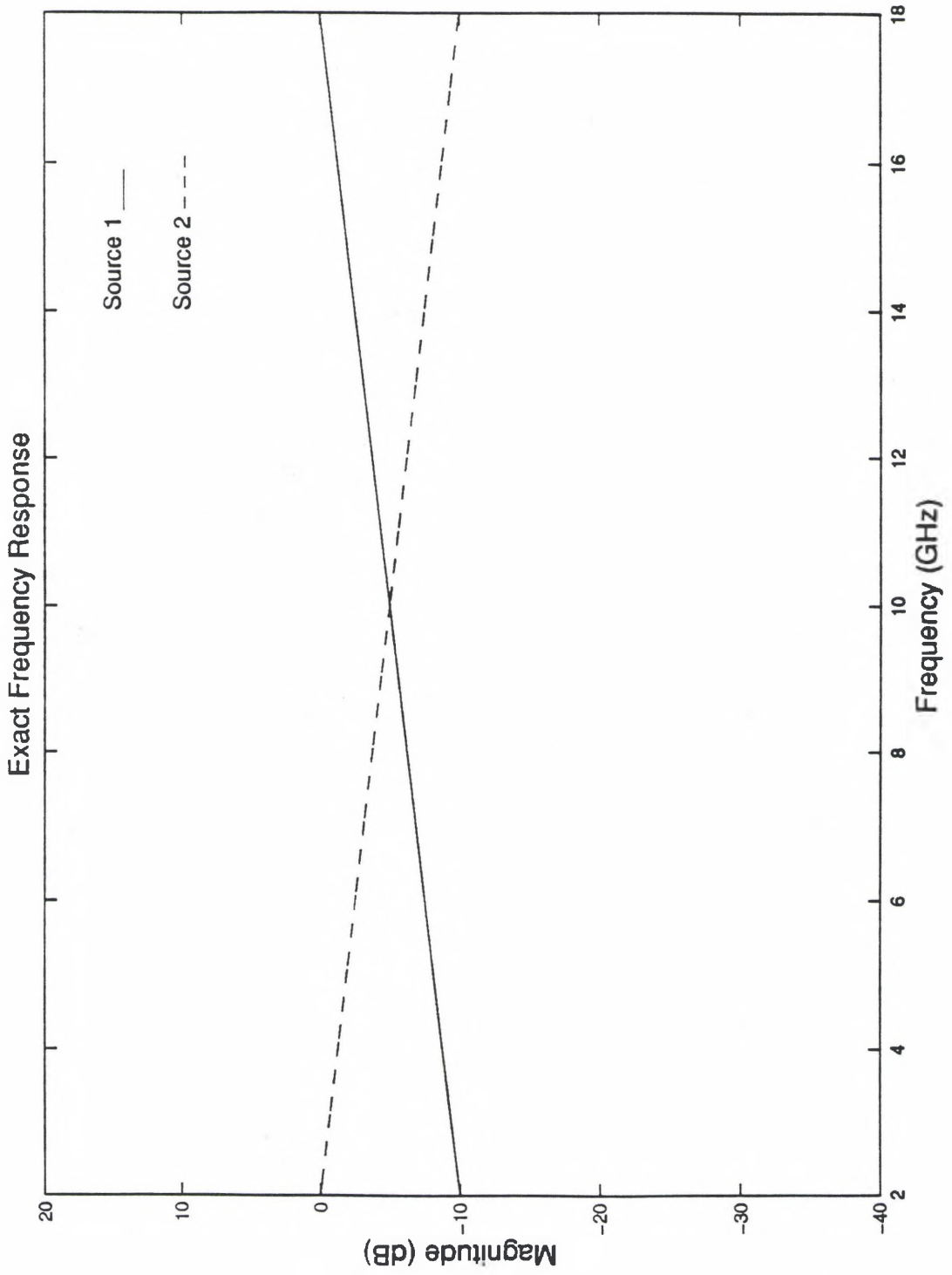


Figure 35. Estimated Frequency Response for Synthetic Case 3 ("Fully Resolved")

3.2.4 Synthetic Case 4

This case is designed to test the method in three areas. First, can the three sources be identified in the MUSIC spectrum? Second, can the method estimate the character of the frequency responses for each of the sources? Third, can the method estimate the lower amplitude regions of each of the sources as they approach, and eventually are overcome by noise?

Figure 36 shows the exact frequency response for each of the three scattering centers. The first and third sources are "linear". The third corresponds to a resonance with a center frequency of 10 GHz.

The MUSIC spectrum for the "just resolved", as its name reflects, barely resolved the first "linear" source. However, it did adequately estimate the location of each of the three source locations as shown in Figure 37.

Table 5. Location of Scattering Centers for Synthetic Case 4

	Exact Time Delay (ns)	"Just Resolved" Time Delay (ns)	"Fully Resolved" Time Delay (ns)
"Linear" 1	-1	-0.827	-0.9951
Resonance	0	0.1075	0.002
"Linear" 2	1	0.827	.9951

Figure 38 shows the frequency response of each of the scattering sources based on the locations obtained from the "just resolved" case. For each source, the method adequately estimated the character. However, the magnitudes for each are degraded as the levels approach the noise. Most interesting is that even though it was able to reconstruct the resonance it improperly estimated the center frequency. This is due to the error in location of the scattering center. The "fully resolved" MUSIC spectrum (Figure 39) correctly located the three sources and, as a result,

correctly identified the resonant frequency at 10 GHz as shown in Figure 40. This figure also demonstrates its ability to estimate the "linear" and resonant frequency responses quite well.

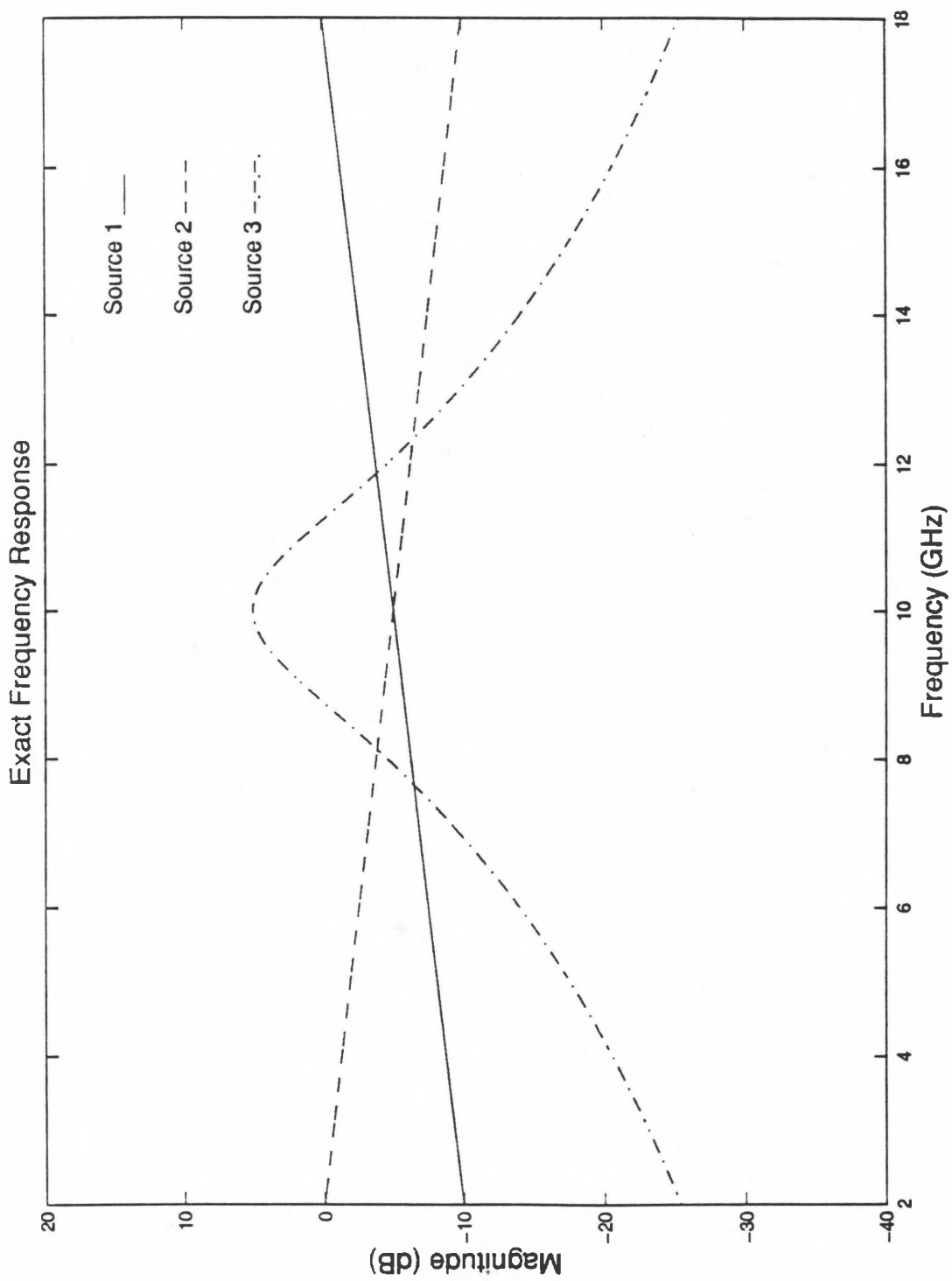


Figure 36. Exact Frequency Response for Synthetic Case 4

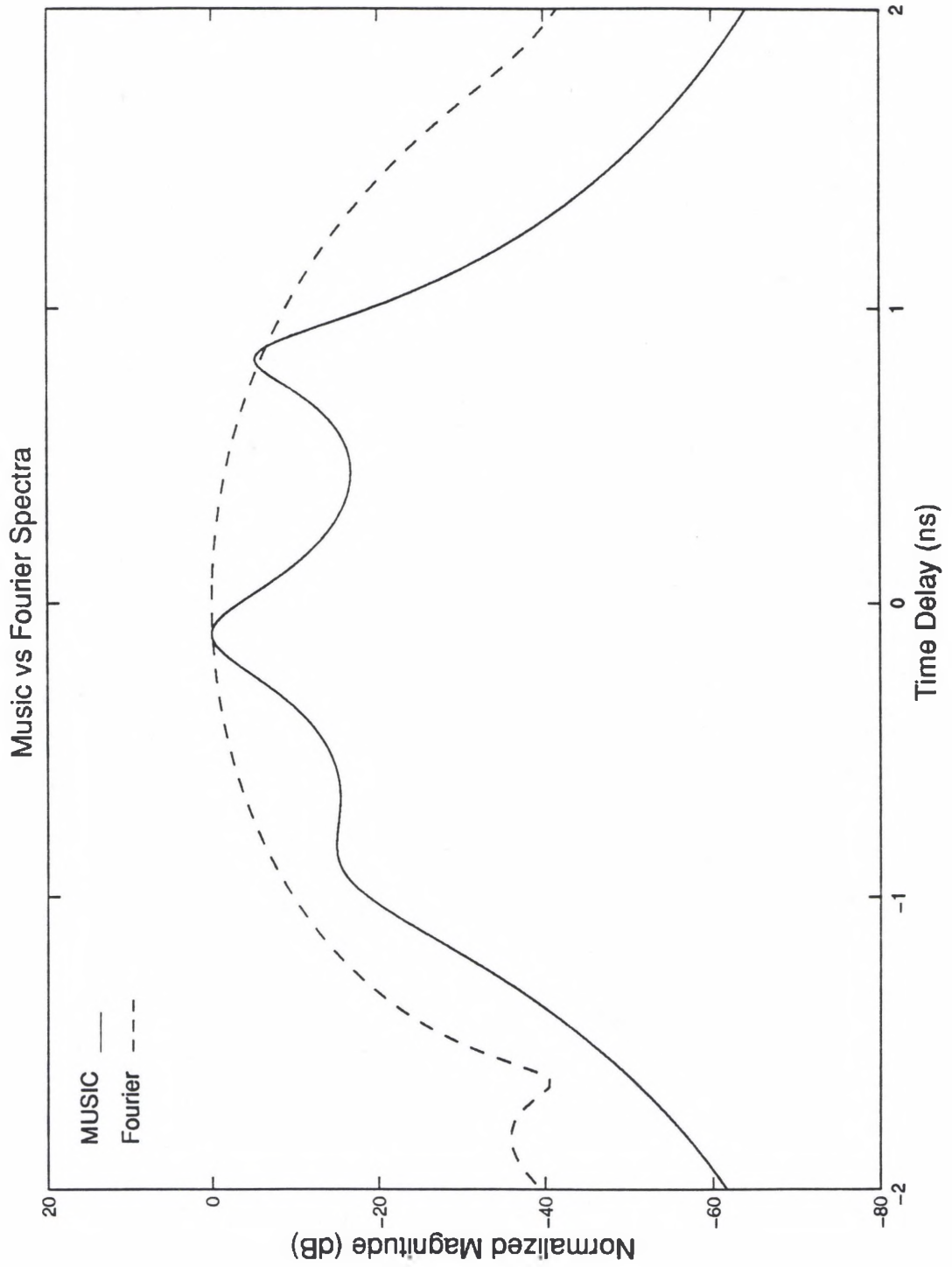


Figure 37. MUSIC and Fourier Spectra for Synthetic Case 4 ("Just Resolved")

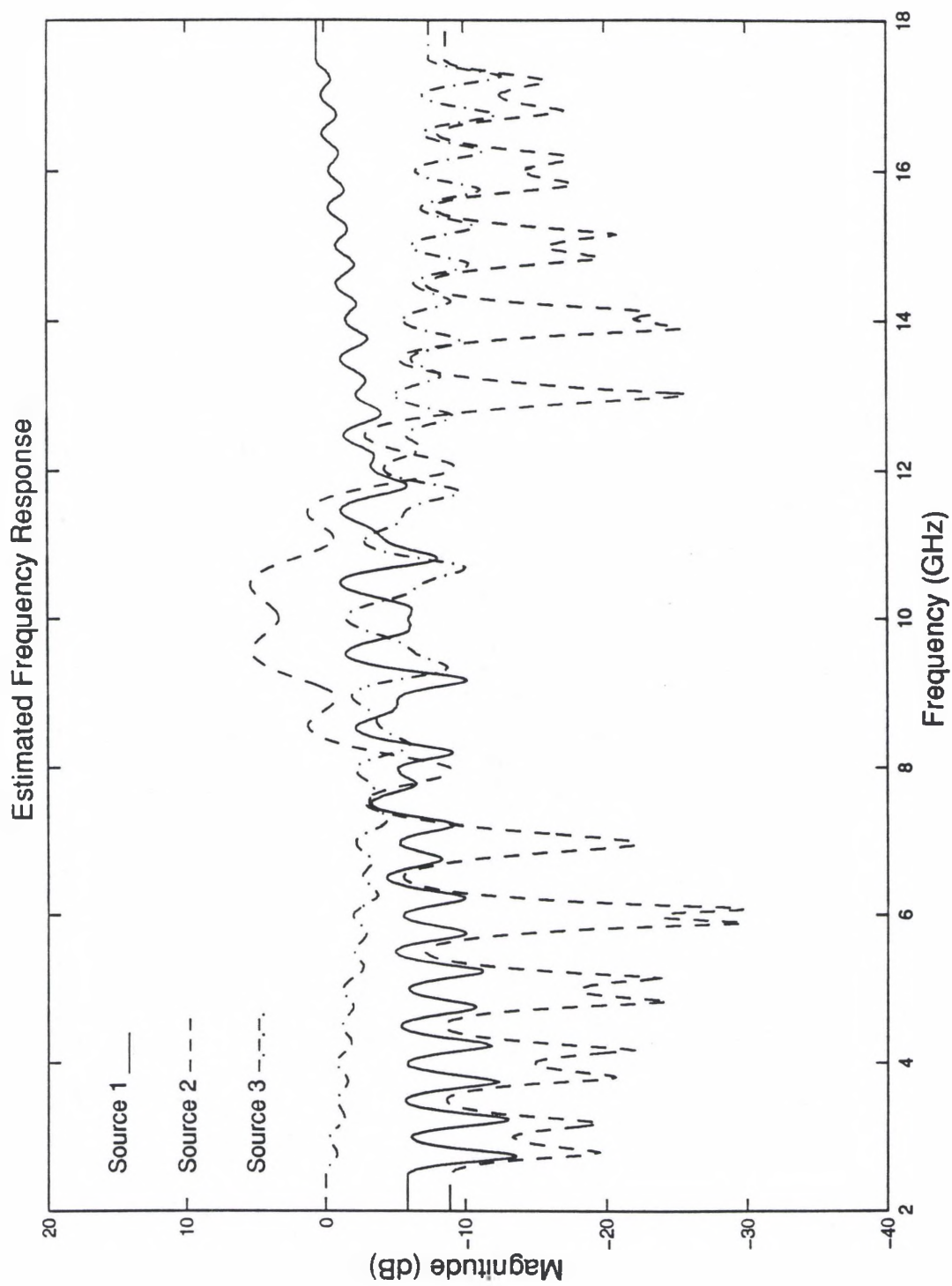


Figure 38. Estimated Frequency Response for Synthetic Case 4 ("Just Resolved")

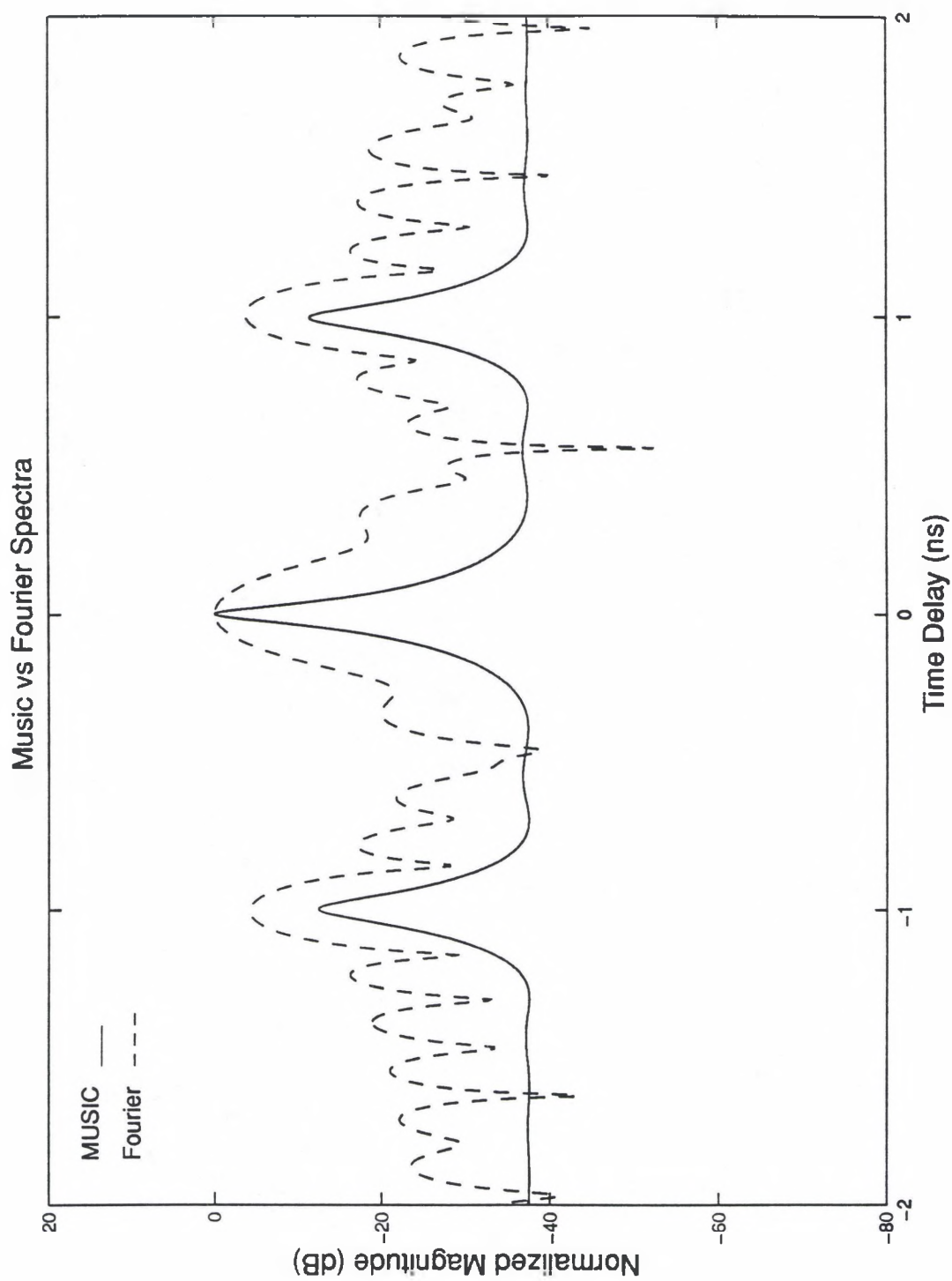


Figure 39. MUSIC and Fourier Spectra for Synthetic Case 4 ("Fully Resolved")

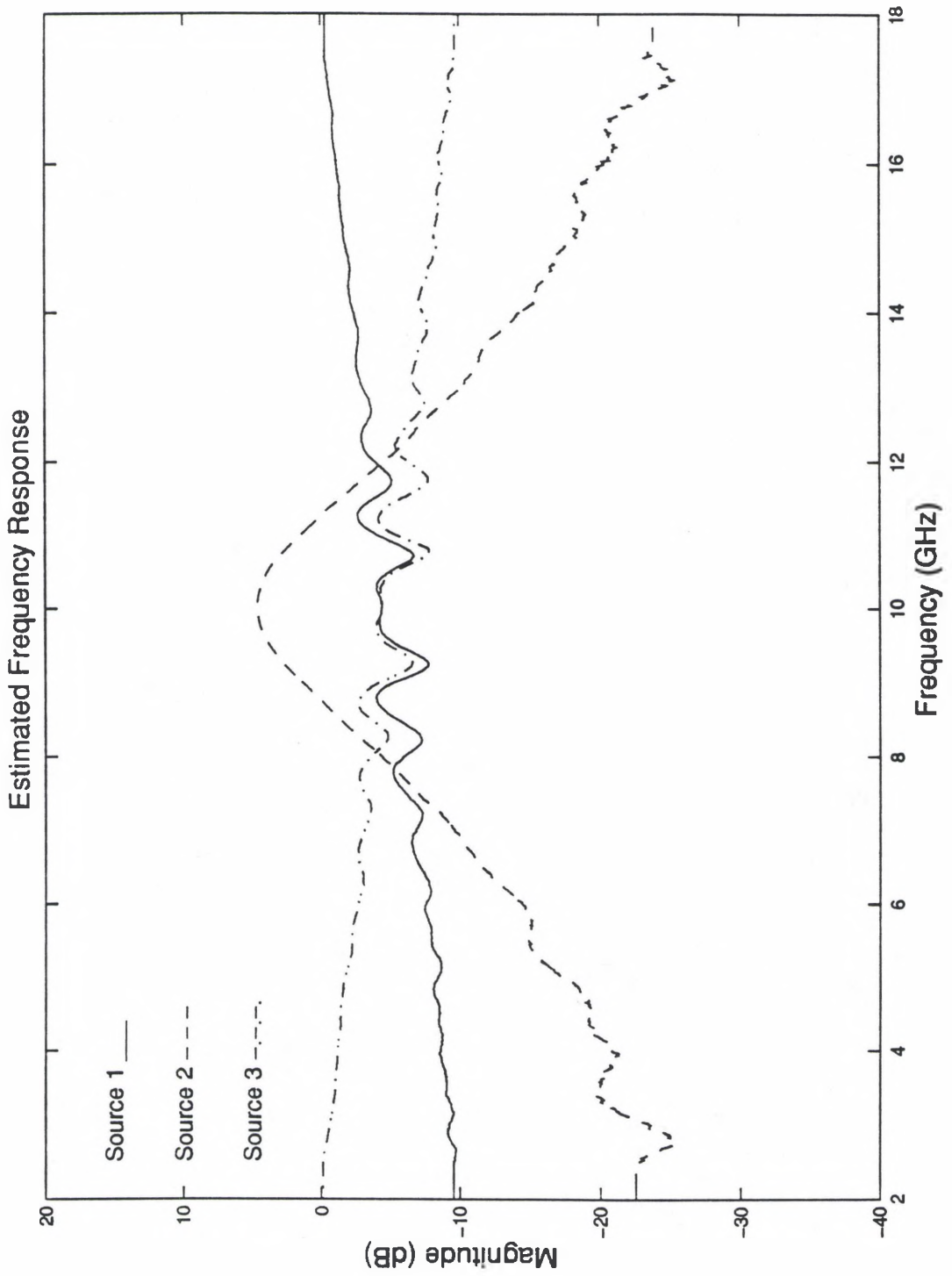


Figure 40. Estimated Frequency Response for Synthetic Case 4 ("Fully Resolved")

3.2.5 Synthetic Case 5

This scenario is designed to test the method under different resonances at multiple magnitudes. Figure 42 shows three resonant sources located at 5, 10 and 15 GHz with magnitudes of 15, 5 and 0 dB respectively. The "just resolved" case is shown to have a bandwidth of 8 GHz. This appears, at first glance, to be a significant bandwidth for a "just resolved" condition. However, at less than this, the MUSIC spectrum could not adequately resolve the sources. This is due to the large separation between resonant peaks. Even under this 8 GHz bandwidth, the MUSIC spectrum significantly erred in locating the 15 GHz resonance as seen in Figure 43. The corresponding estimated frequency response for each of the resonances is shown in Figure 44. As this figure clearly demonstrates, such a location error significantly degraded the method's ability to reconstruct the individual frequency responses. The figure also shows all three resonant magnitudes as less than the exact and the resonant frequencies are mis-identified. However, for the "fully resolved" case, the MUSIC spectrum (Figure 44) and frequency response of the sources (Figure 45) performed quite well. In each of these figures both the magnitudes and center frequencies are properly estimated. The locations for each of the resonances are shown in Table 6.

Table 6. Location of Scattering Centers for Synthetic Case 5

	Exact Time Delay (ns)	"Just Resolved" Time Delay (ns)	"Fully Resolved" Time Delay (ns)
Resonance 1 - 5 GHz	-1	-0.9912	-.9912
Resonance 2 - 10 GHz	0	0.0059	-0.0176
Resonance 3 - 15 GHz	1	1.5112	1.0068

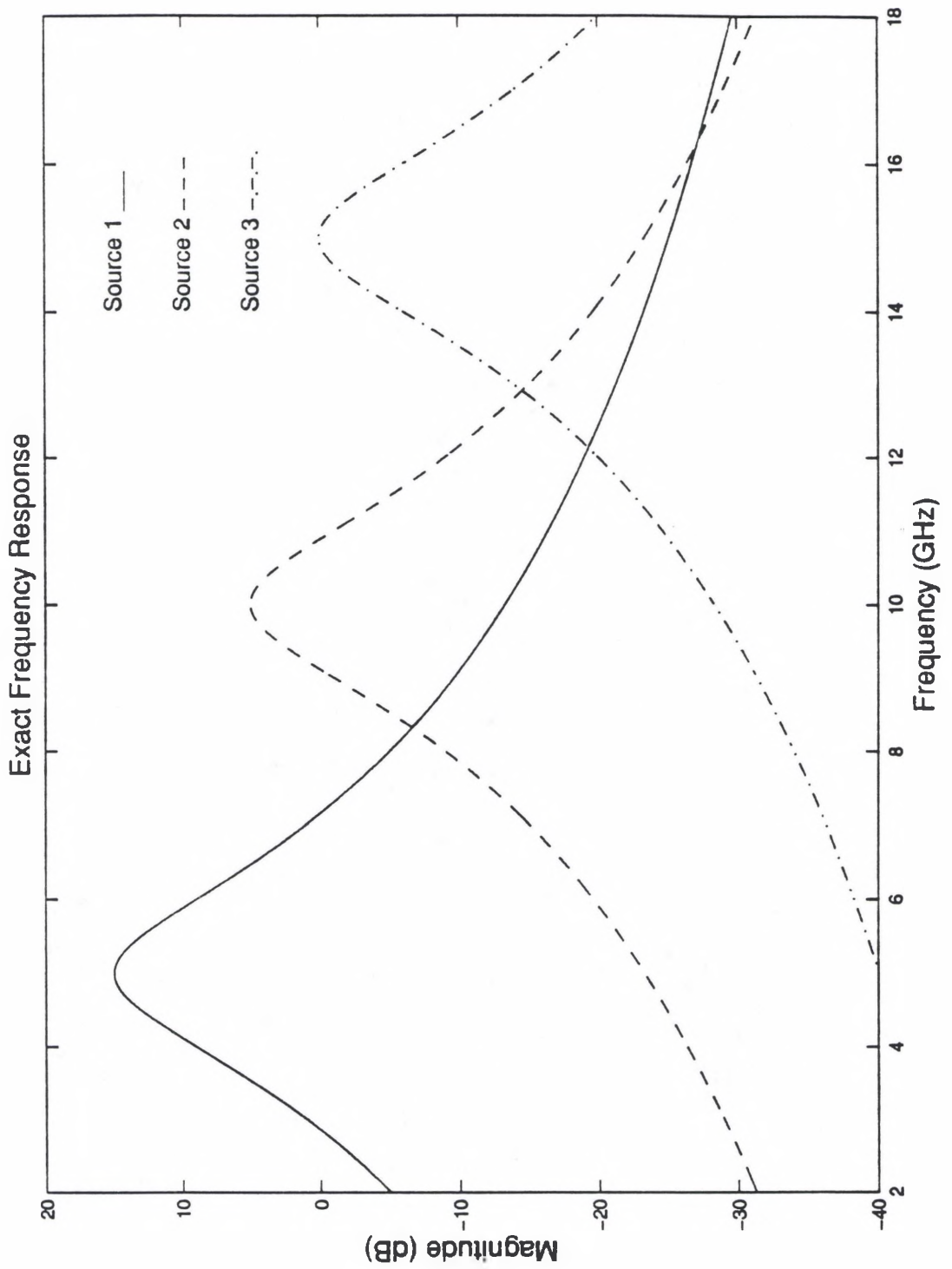


Figure 41. Exact Frequency Response for Synthetic Case 5

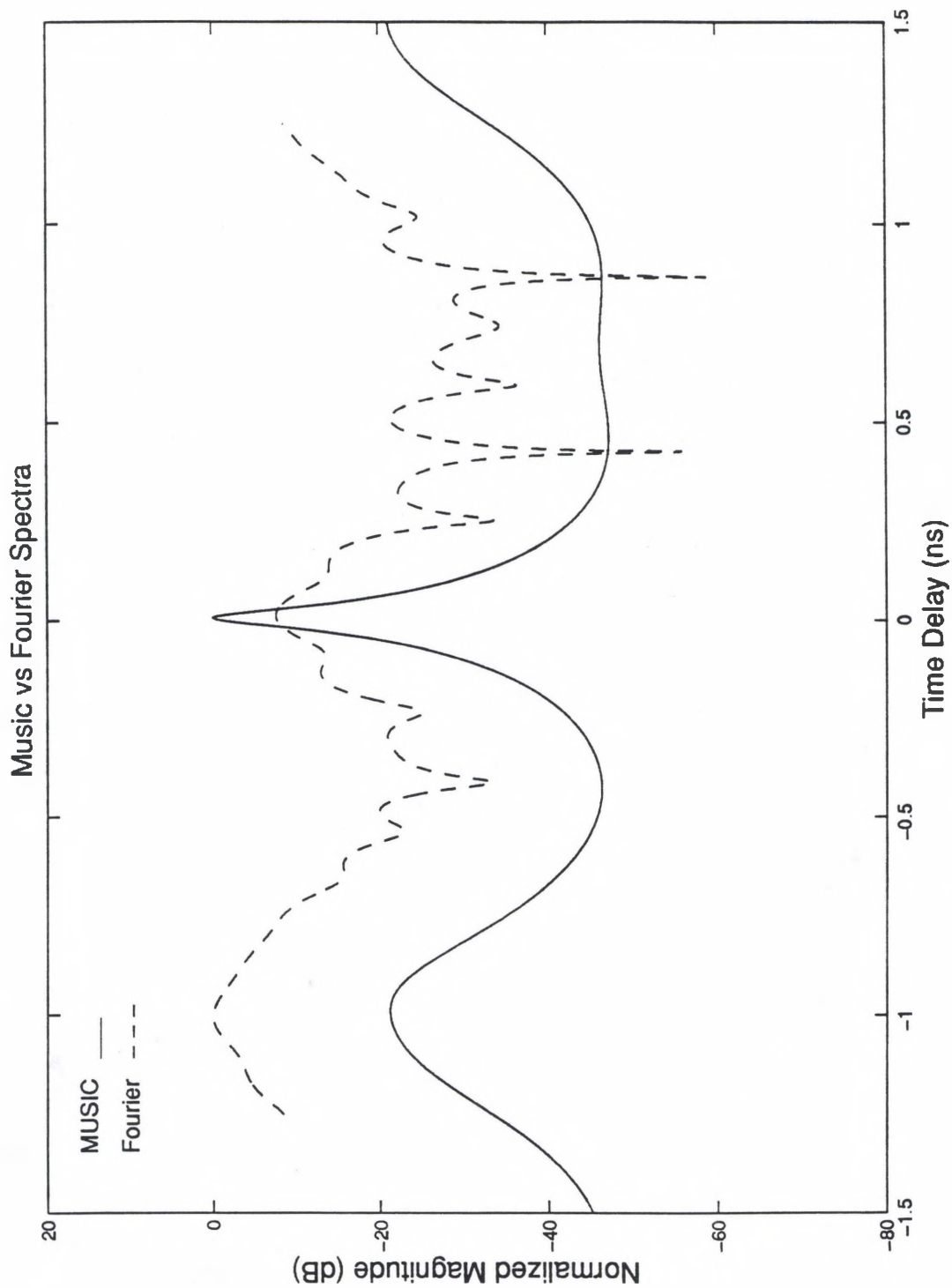


Figure 42. MUSIC and Fourier Spectra for Synthetic Case 5 ("Just Resolved")

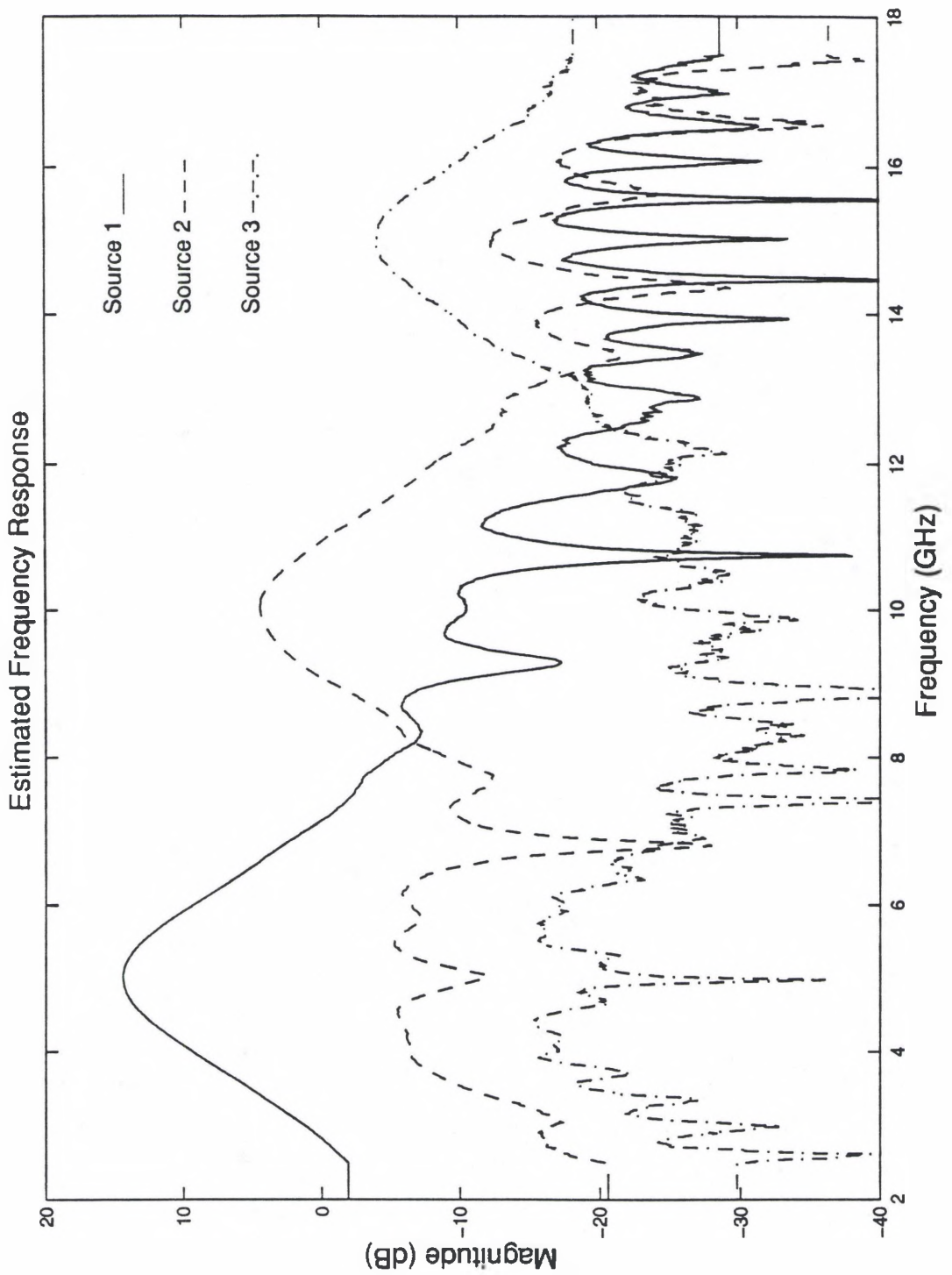


Figure 43. Estimated Frequency Response for Synthetic Case 5 ("Just Resolved")

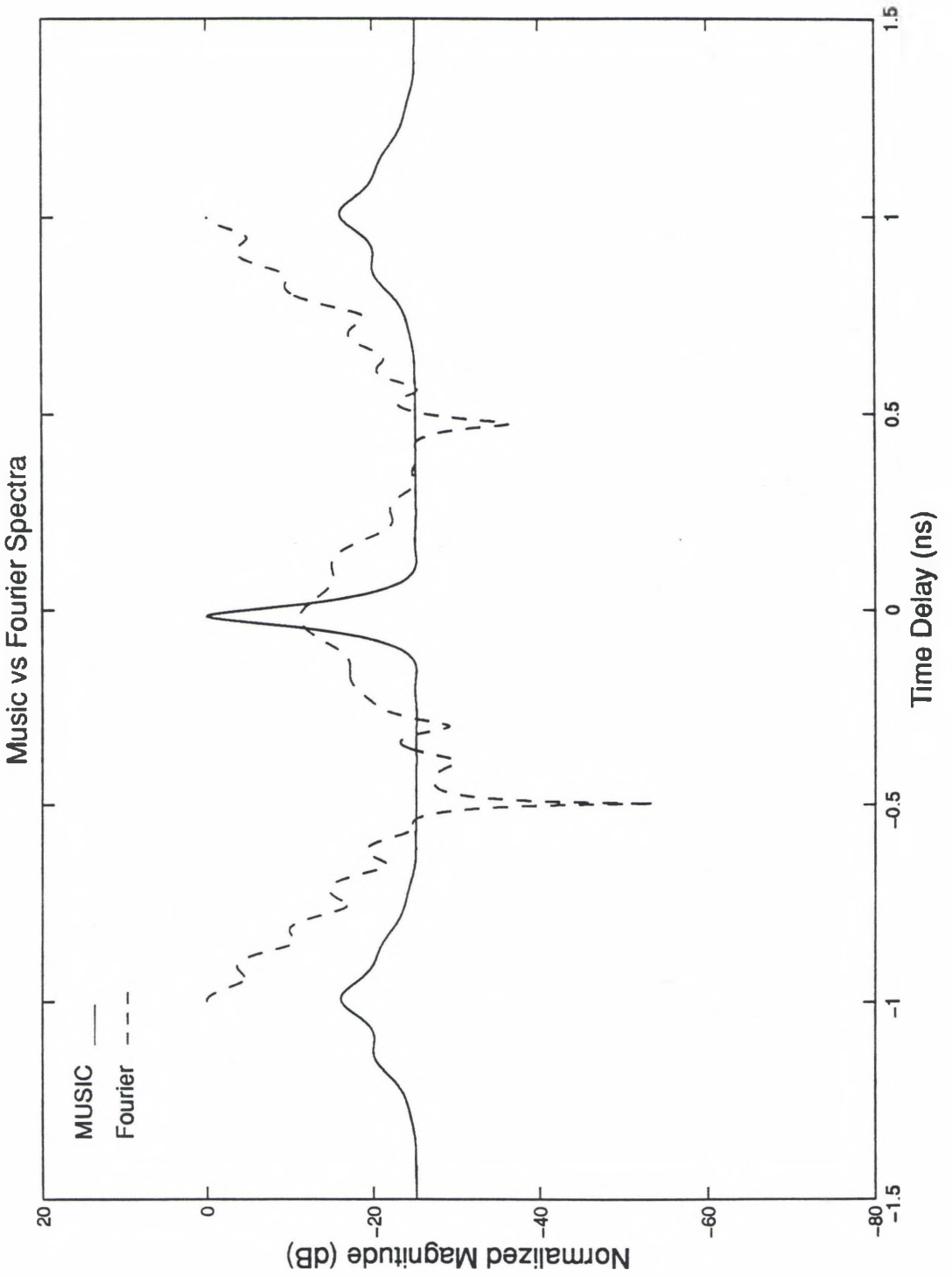


Figure 44. MUSIC and Fourier Spectra for Synthetic Case 5 ("Fully Resolved")

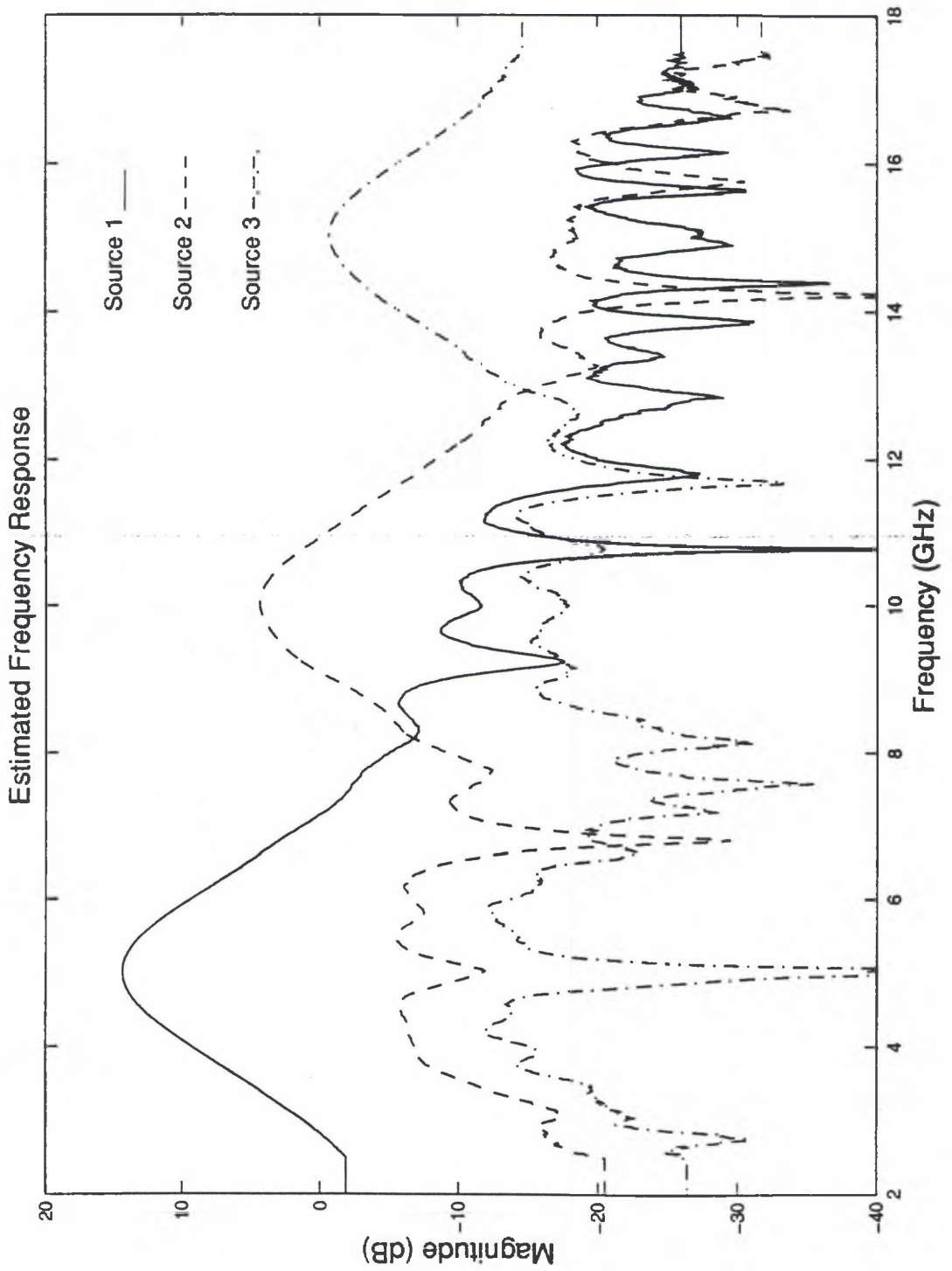


Figure 45. Estimated Frequency Response for Synthetic Case 5 ("Fully Resolved")

3.3 Measured Data

This section will present results from five measured data sets. The section begins with a brief description of the measurement test range used and is followed by a discussion of the targets selected with their estimated MUSIC spectra and frequency responses of the individual scattering centers.

The measured data was collected on the Advanced RCS Measurement Range (ARMR) at Wright-Patterson Air Force Base. The ARMR is a dual-reflector/dual chamber Gregorian compact range¹⁶ (Figure 46- side view). The ARMR offers a planar wavefront produced by a linear, time-invariant (LTI) radar system. Figure 47 shows a histogram of the typical receiver noise found in a 2-18 GHz sampling of the ARMR radar receiver.

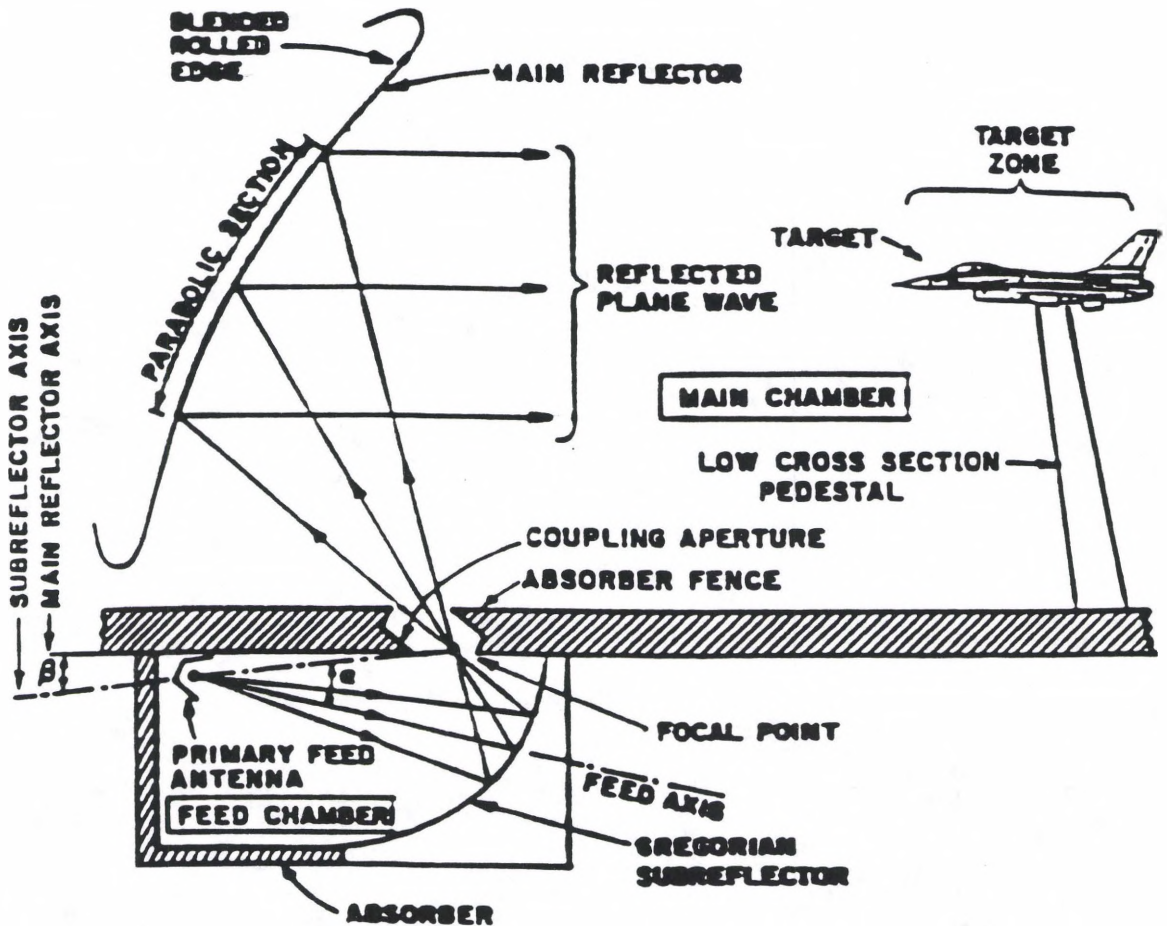


Figure 46. Side View of RCS Measurement Range at Wright-Patterson AFB

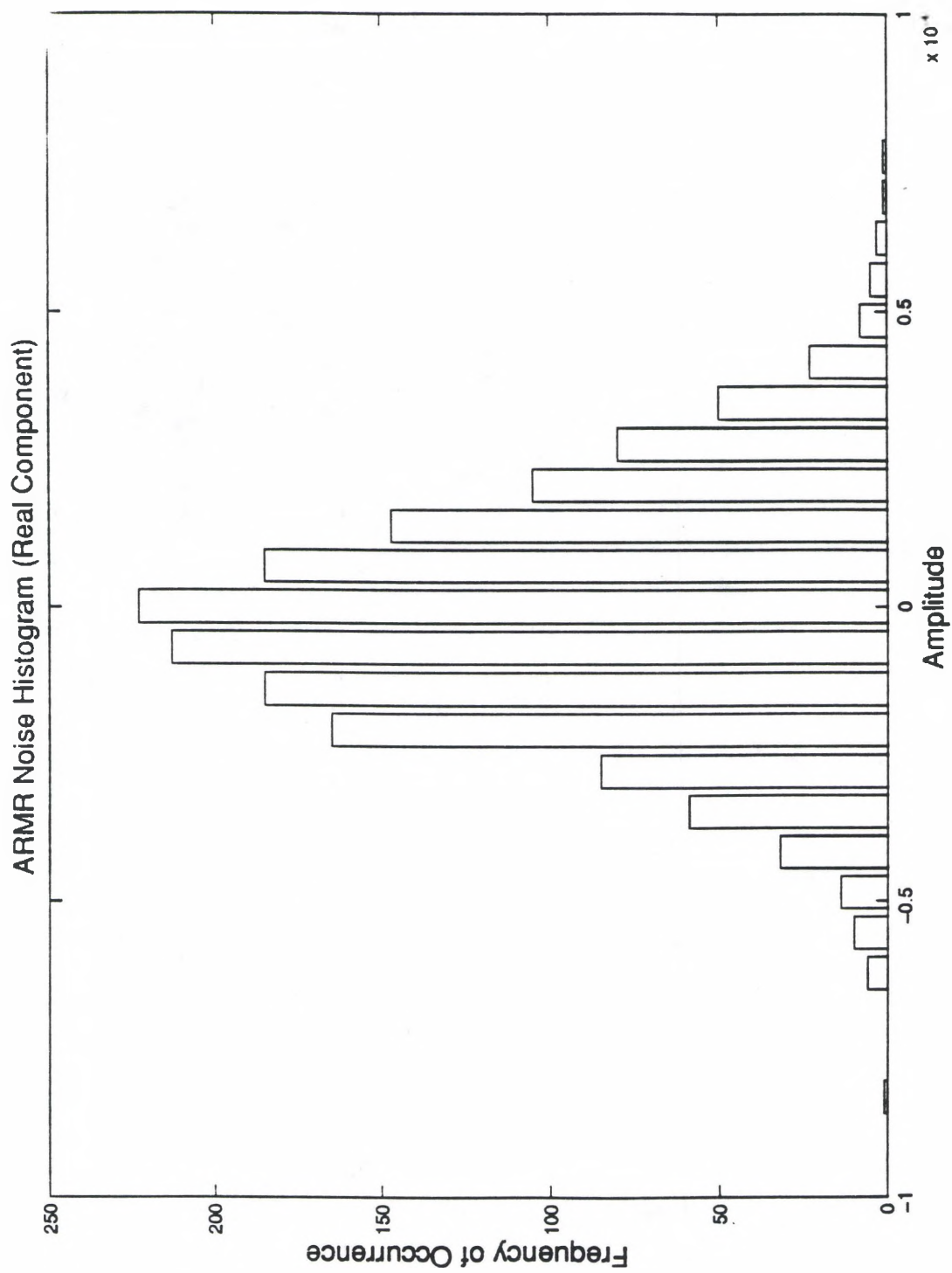


Figure 47. ARMR Radar Noise Histogram

The measured data is designed to challenge the method under various situations. However, unlike their synthetic counterparts, the measured data will be studied under fully-resolved conditions only. These parameters are listed in Table 7.

Table 7. Measured Data Parameters

Case Number	Description	Source Types	MUSIC Bandwidth/ Increment (GHz) "Fully Resolved"	Regression Polynomial Order/ Bandwidth (GHz)
1	8 inch sphere	Specular with creeping wave	2.0-11.3/.3	1/4
2	9.6 inch ogive	Forward scattering & low SNR	2.0-11.3/.3	1/4
3	.7 inch wire	Resonance	2.0-17.5/.5	0/1
4	foam block with embedded wooden rod	Dielectric with strong inhomogeneity	12.0-18.0/.2	0/1
5	foam block minus wooden rod	Dielectric with weak inhomogeneity	15.0-18.0/.1	0/1

3.3.1 Measured Case 1

The sphere is a canonical target which offers both specular and creeping wave returns which are well understood. It is customary to measure the sphere atop a short Styrofoam column. This measurement geometry is shown in Figure 48. According to the Mie series solution¹⁷ for an 8 inch sphere, there should be a specular return from the front of the sphere and a creeping wave return at

$$t_{\text{creep}} = \frac{r(\pi + 2)_{\text{inches}}}{11.802_{\text{inches}/\text{ns}}} \quad (35)$$

time delay behind the specular response. Where r is the radius of the sphere (in inches). The sphere under study, however, is showing three sources in the MUSIC spectrum (Figure 49). The

first response, the specular return from the sphere, is located at -0.6471 ns. The next source, located at -0.4399 ns, is a result of mounting the sphere too close to a flat absorbing cap atop the support structure and is an error term. This response is a multi-path error source caused as the plane wave scatters from the sphere, down to the cap, back to the sphere and ultimately returns to the receiver. Finally, the third response, located at 1.32 ns is from the creeping wave. Figure 50 shows the frequency response of each of the responses. Figure 51 shows the estimated MUSIC spectrum obtained from measured data overlaid with the MUSIC spectrum obtained from the Mie series data. This figure shows good agreement for both the specular and creeping wave returns. The time delay offset between the two spectra is due to the measured sphere not being located at the phase center of its reference target. This offset is arbitrary and of no consequence to the data accuracy as long as the shift is in the same amount and direction at both source locations. Figure 52 shows the estimated frequency responses of the specular and creeping wave responses obtained from the measured data overlaid with those of the Mie series data. The measured specular return shows excellent agreement across the entire band. However, the creeping wave begins to degrade after 11 GHz. This is due to increases in the chamber background level and errors in the estimation of the frequency response due to the third error term. Figure 53 shows the total sphere frequency response from 2 - 18 GHz based on three different sets of data. First, the frequency response from the Mie series is plotted directly as a reference. Second, the sphere frequency response from the Mie series after optimal extraction is shown to reveal any errors introduced by the process. The third curve is the output of the optimal extraction using the measured data - corrected for the error term. As the figure clearly shows, there is excellent agreement between measured and exact solutions, until the creeping wave becomes poorly estimated due to range clutter.

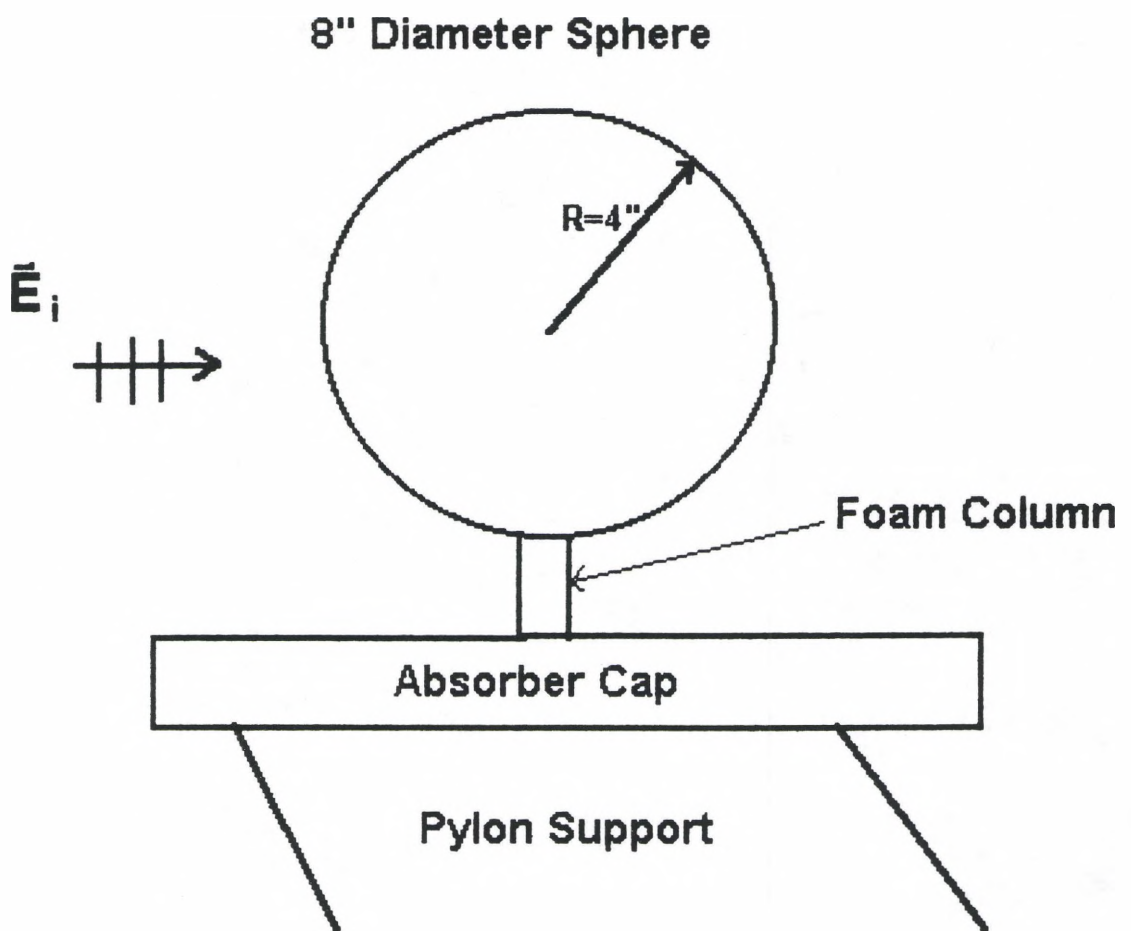


Figure 48. Measured Case 1 Geometry

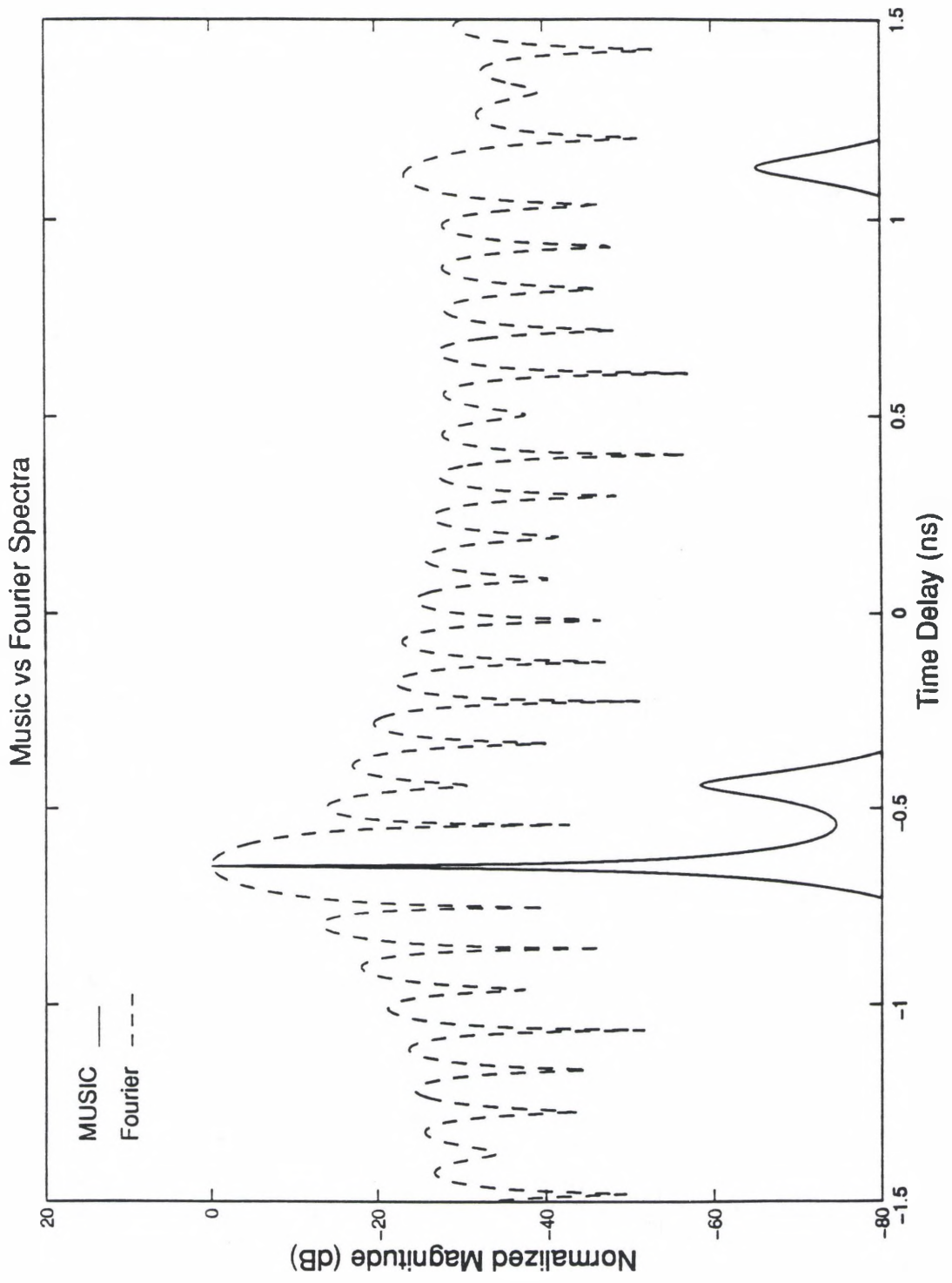


Figure 49. MUSIC and Fourier Spectra for Measured Case 1

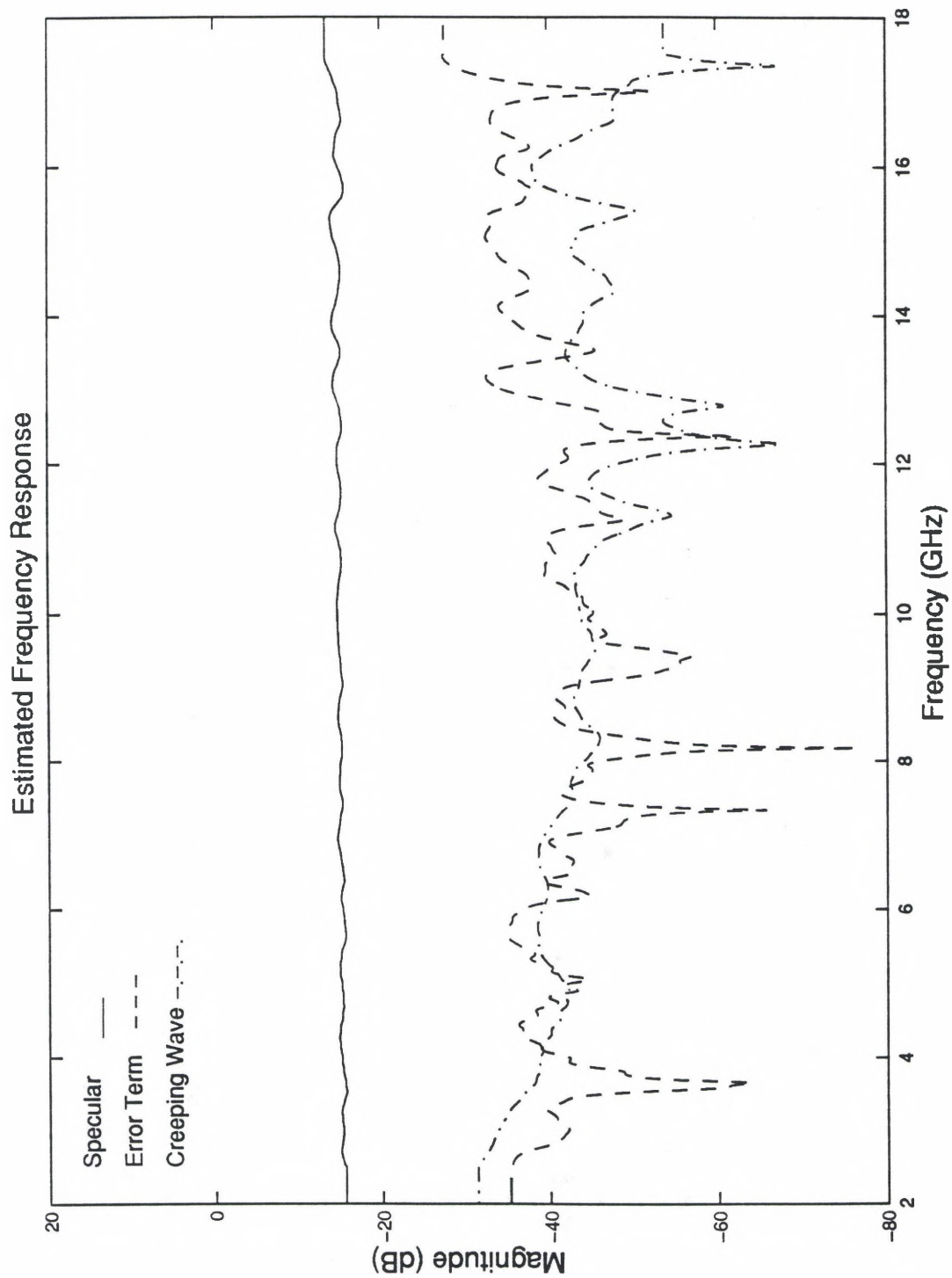


Figure 50. Estimated Frequency Response for Measured Case 1

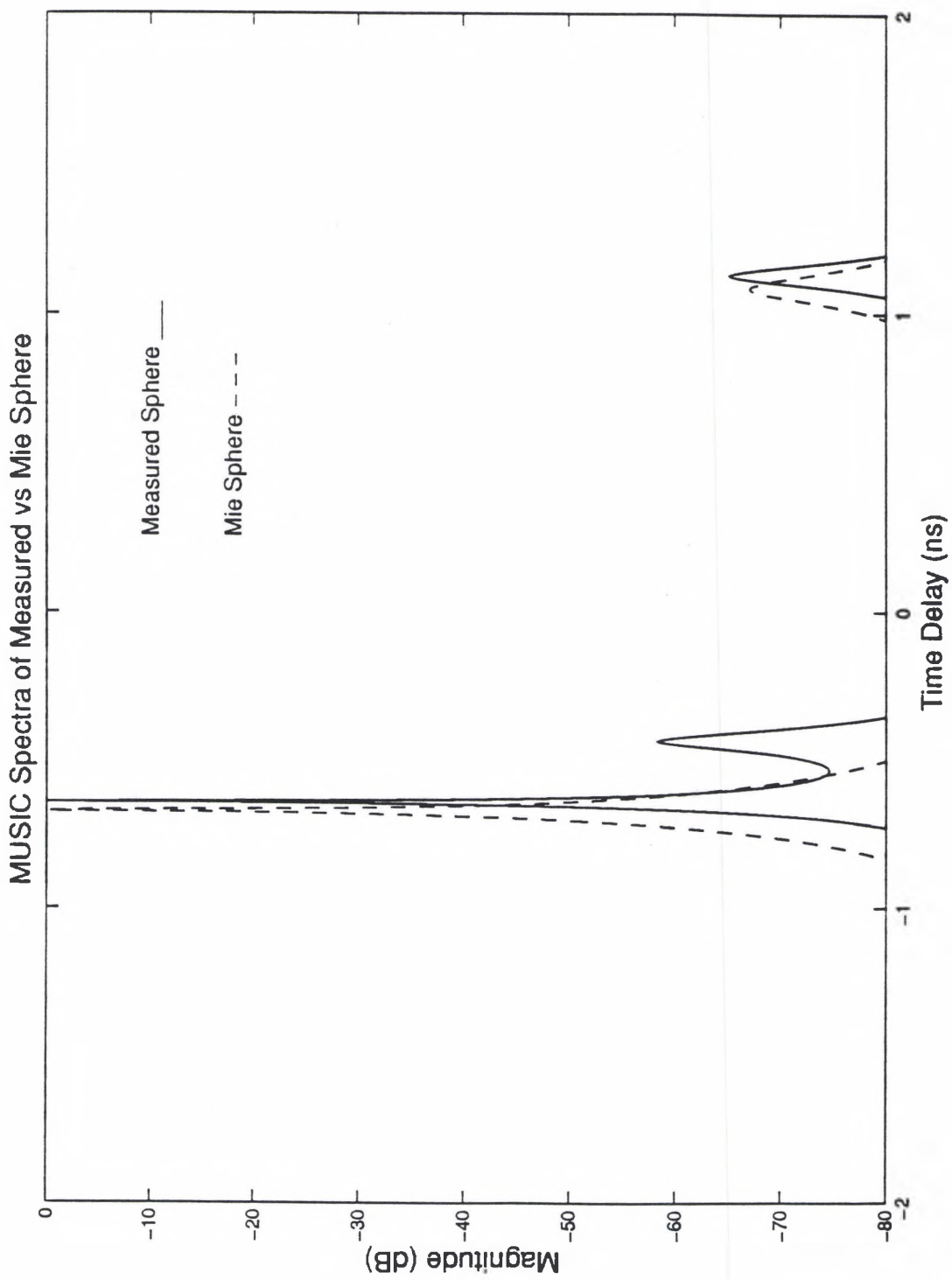


Figure 51. MUSIC Spectra for Measured Case 1

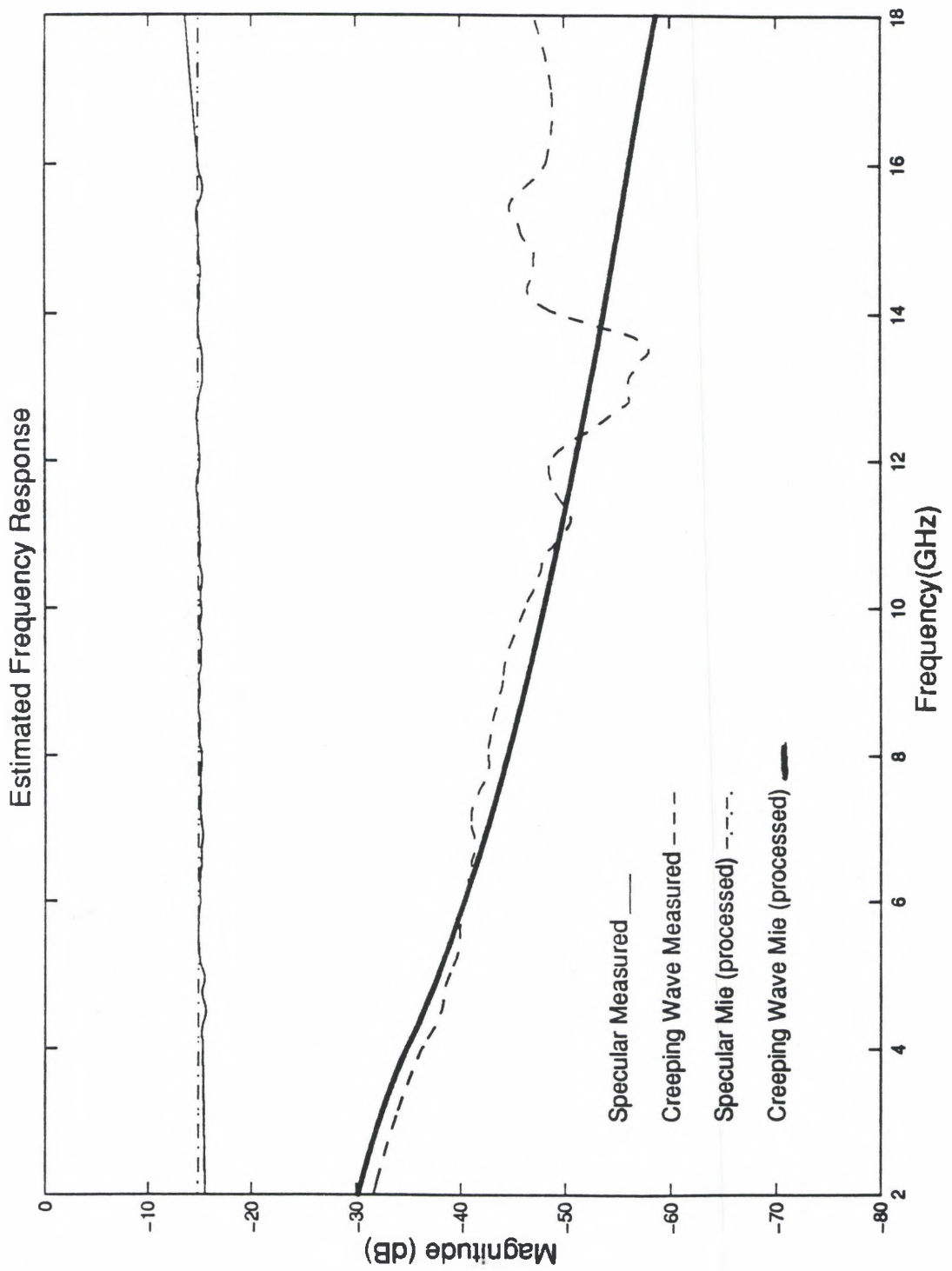


Figure 52 Estimated Frequency Response for Measured Case 1

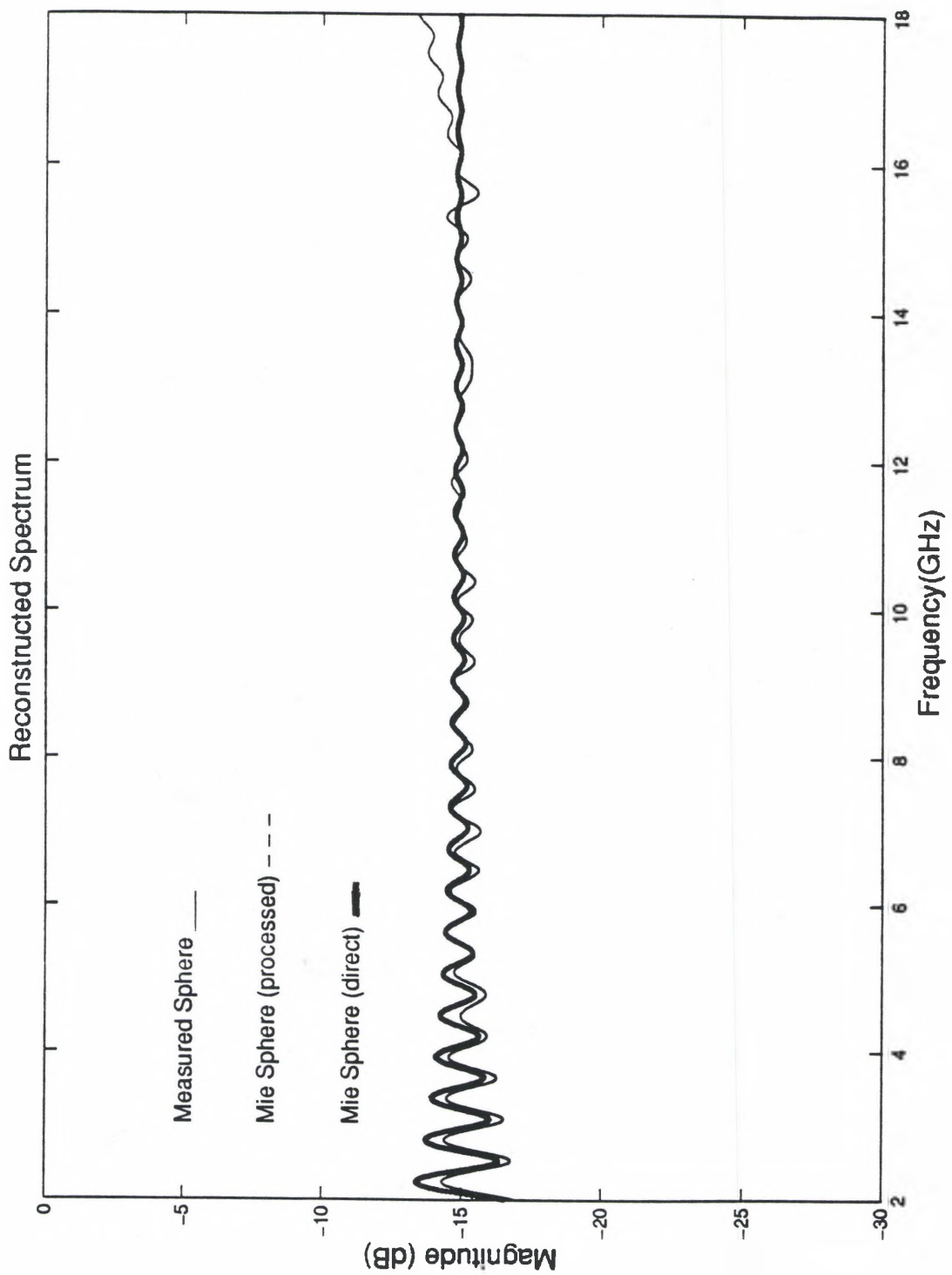


Figure 53 Reconstructed Frequency Response for Measured Case 1

3.3.2 Measured Case 2

The 9.6 inch ogive is a canonical target yet is difficult to measure accurately. It has a low signature across the 2-18 GHz region (low SNR). In addition to scattering from the ogive, there is also scattering from the boundary of a mounting surface. The mounting of this target is shown in Figure 54. This problem is highlighted in the MUSIC spectrum of Figure 55 where the interior two sources in the MUSIC spectrum are the Styrofoam cup support. The first and last responses at -.8465 and .7879 ns respectively correspond to the front and rear tips of the ogive. By converting the times of the front and rear tip responses to inches, one finds excellent agreement between the physical length of the target (9.6 inches) and the location of the response. For example, converting the electrical length of the ogive in nanoseconds to inches yields the following

$$\text{length}_{\text{inches}} = \frac{(.8465 + .7879)\text{ns}}{2} (11.802 \text{ inches / ns}) = 9.64 \text{ inches.} \quad (36)$$

Figure 56 shows the estimated frequency responses of each of the sources found in the MUSIC spectrum. As the frequency approaches the end of the band, the chamber background noise dominates the estimation algorithm. Figure 57 shows the MUSIC spectrum obtained from measured data overlaid with the MUSIC spectrum obtained from scattered fields computed using the CICERO¹⁸, body-of-revolution code. As in the case of the sphere, there is excellent agreement between the calculated and measured data. The offset in time between the two sets of data is, again, due to calibration offsets in the measurement process and is inconsequential to the accuracy of the data. Figure 58 shows an overlay of the estimated frequency response from measured data and CICERO. Good agreement is found between measured and calculated until the chamber background becomes excessive. Figure 59, shows the total ogive frequency response from 2-18 GHz based on three different sets of data. First, the frequency response from CICERO is plotted directly as a reference. Second, the ogive frequency response from CICERO after optimal extraction is shown to reveal any errors introduced by the process. The third curve is the output of the optimal extraction using the measured data - corrected for the

error terms. As in the previous figure, there is good agreement between measured and calculated data until limited by the chamber background noise.

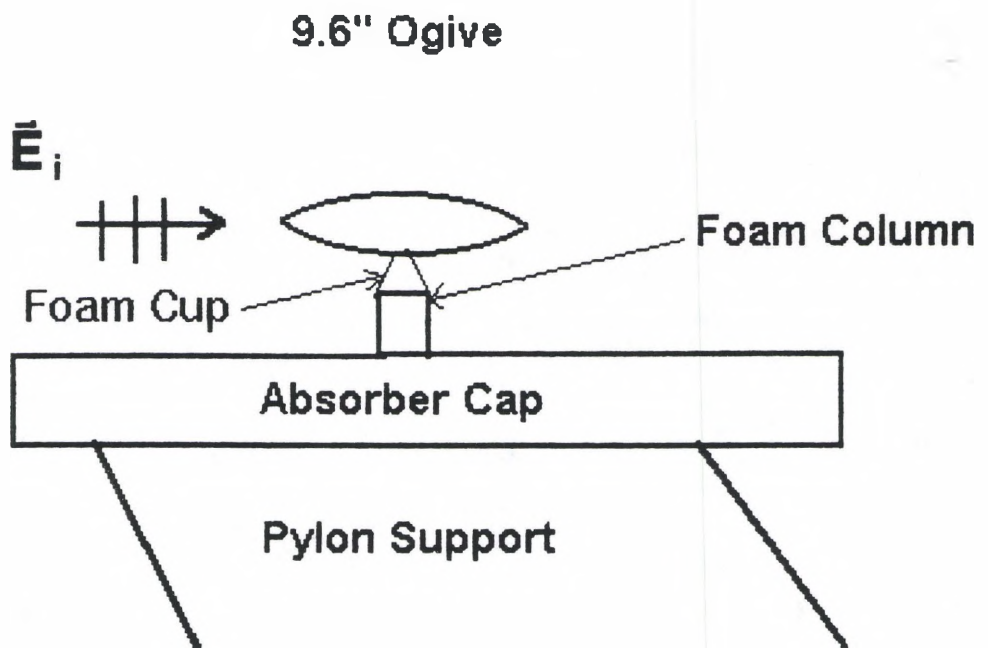


Figure 54. Measured Case 2 Geometry

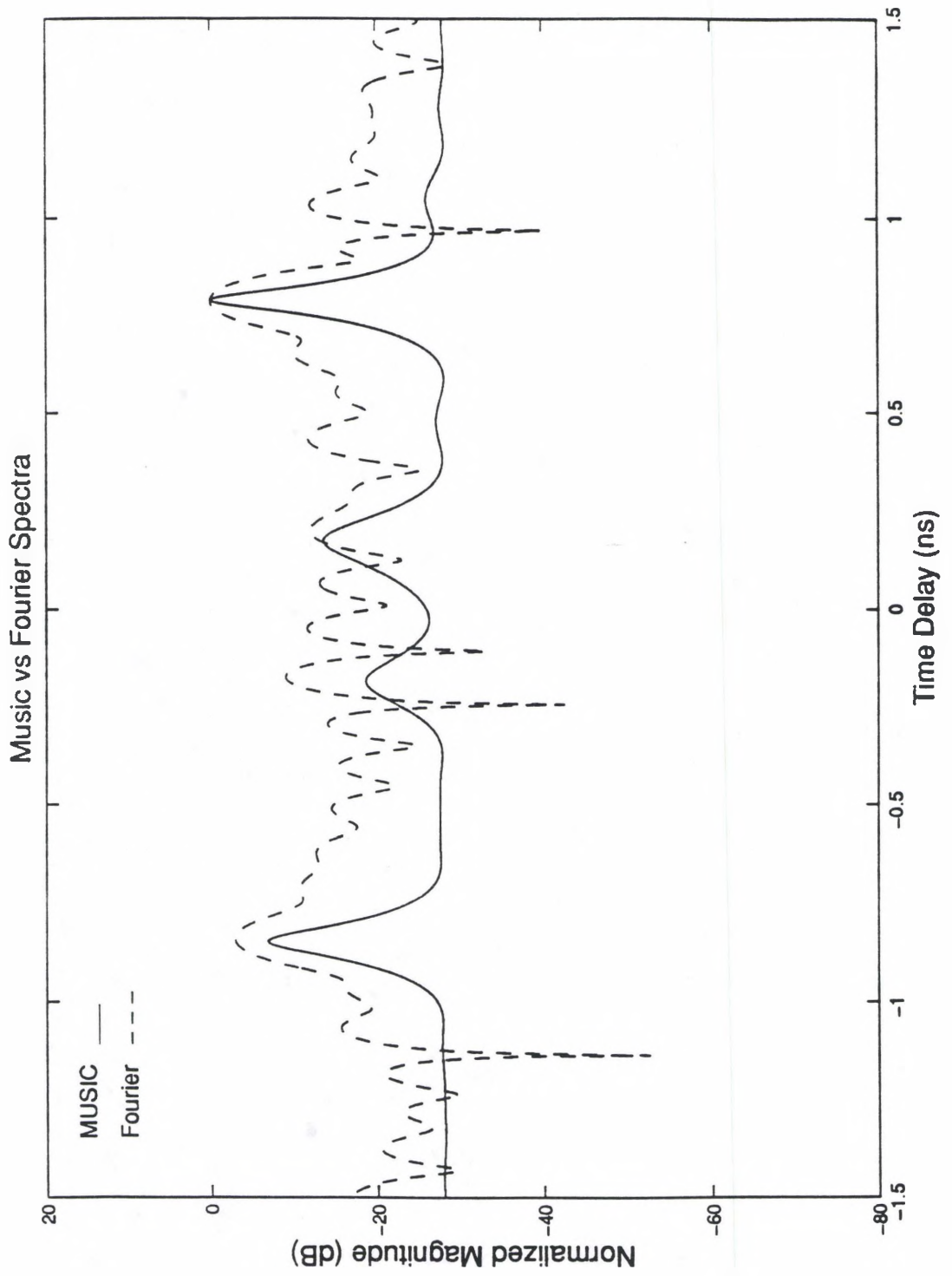


Figure 55. MUSIC and Fourier Spectra for Measured Case 2

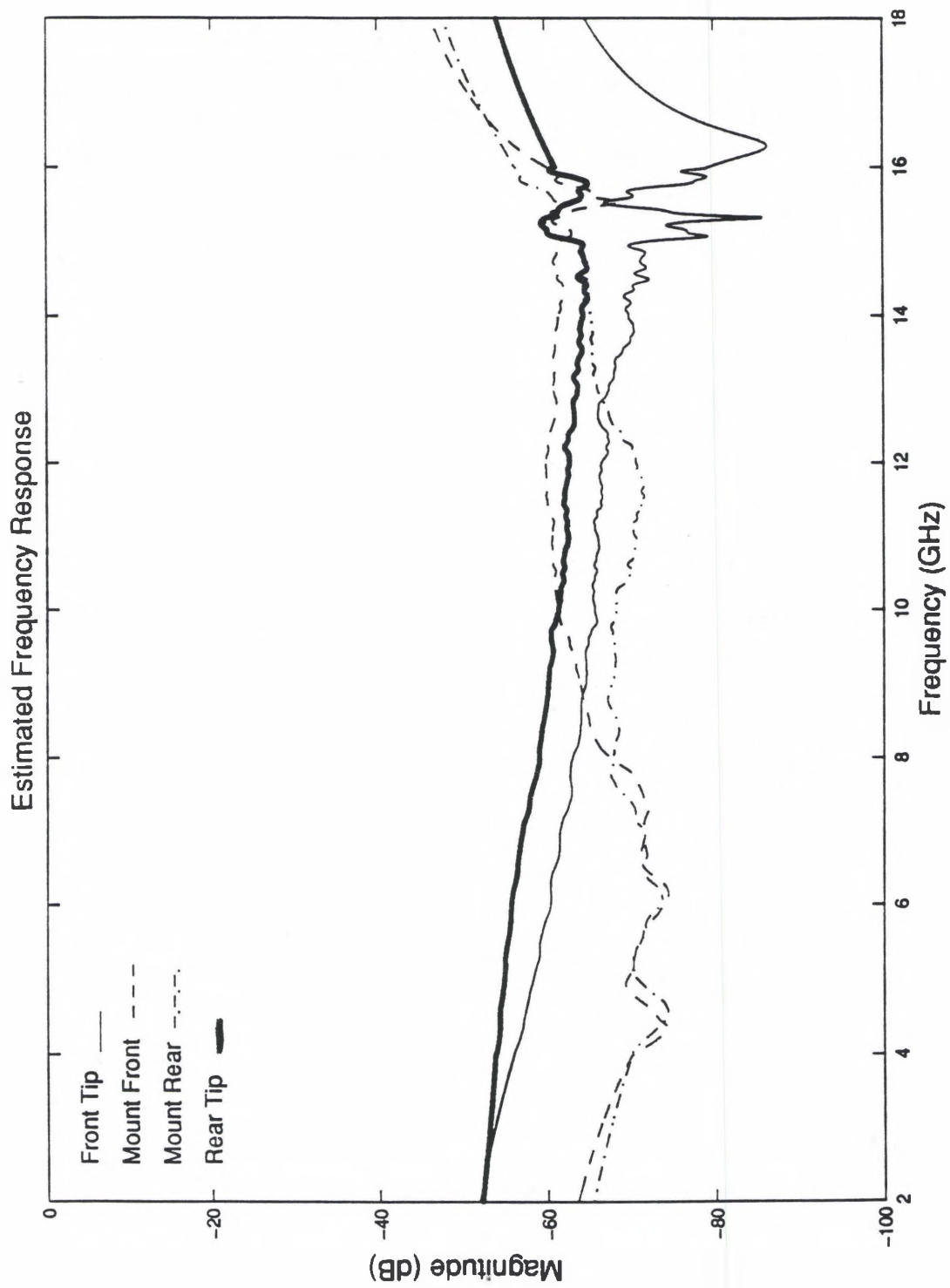


Figure 56. Estimated Frequency Response for Measured Case 2

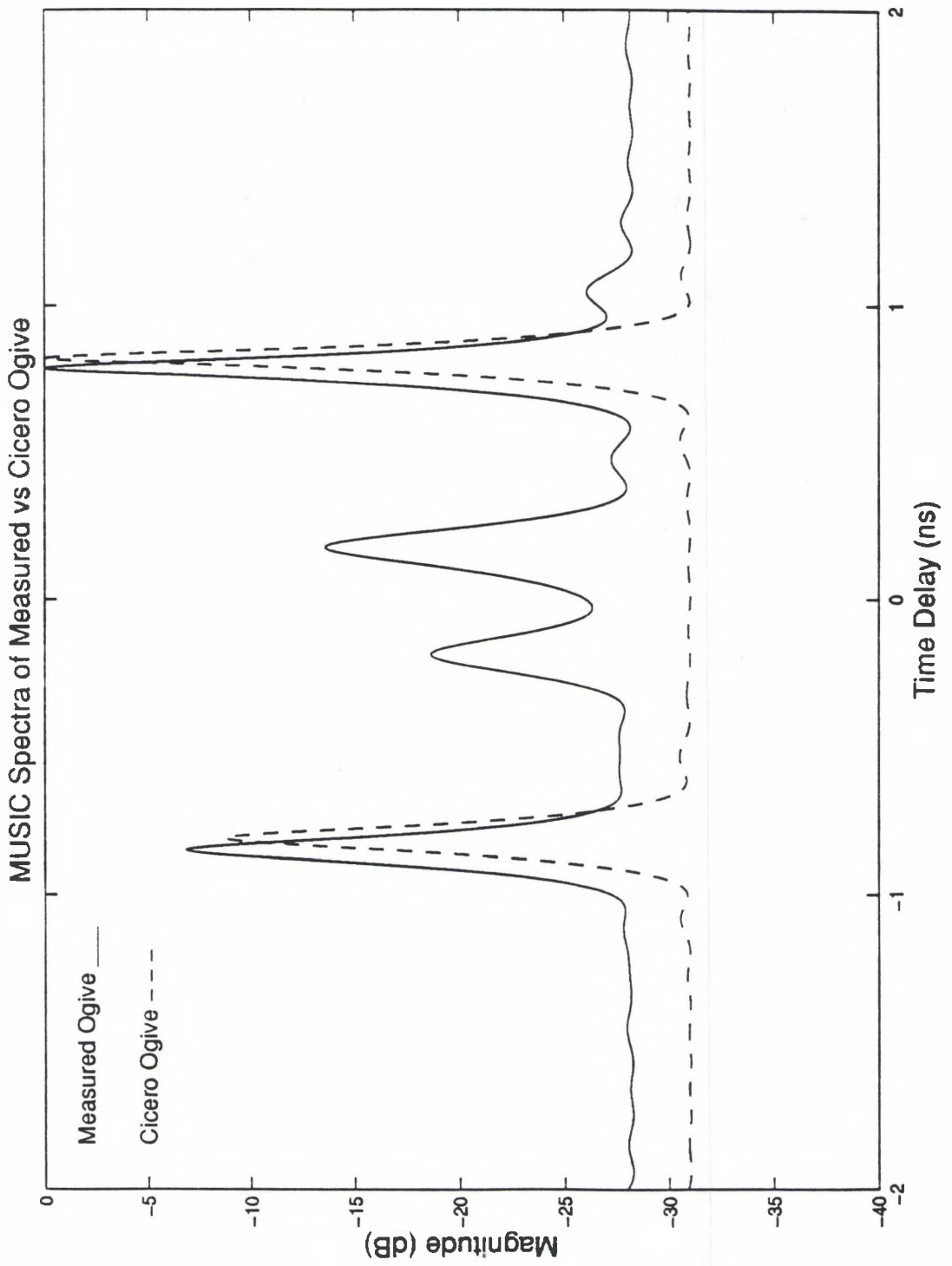


Figure 57. MUSIC Spectra for Measured Case 2

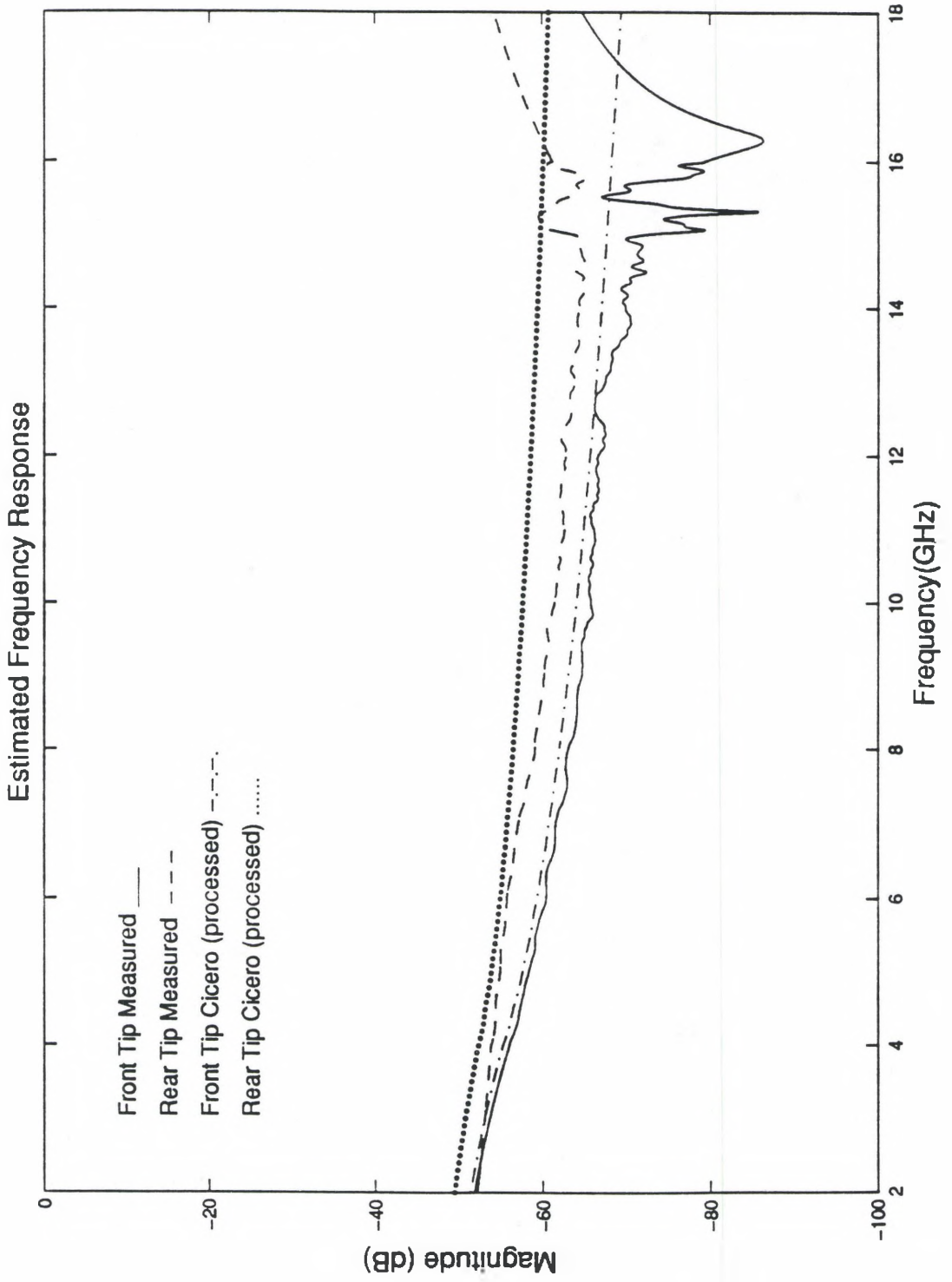


Figure 58. Estimated Frequency Response for Measured Case 2

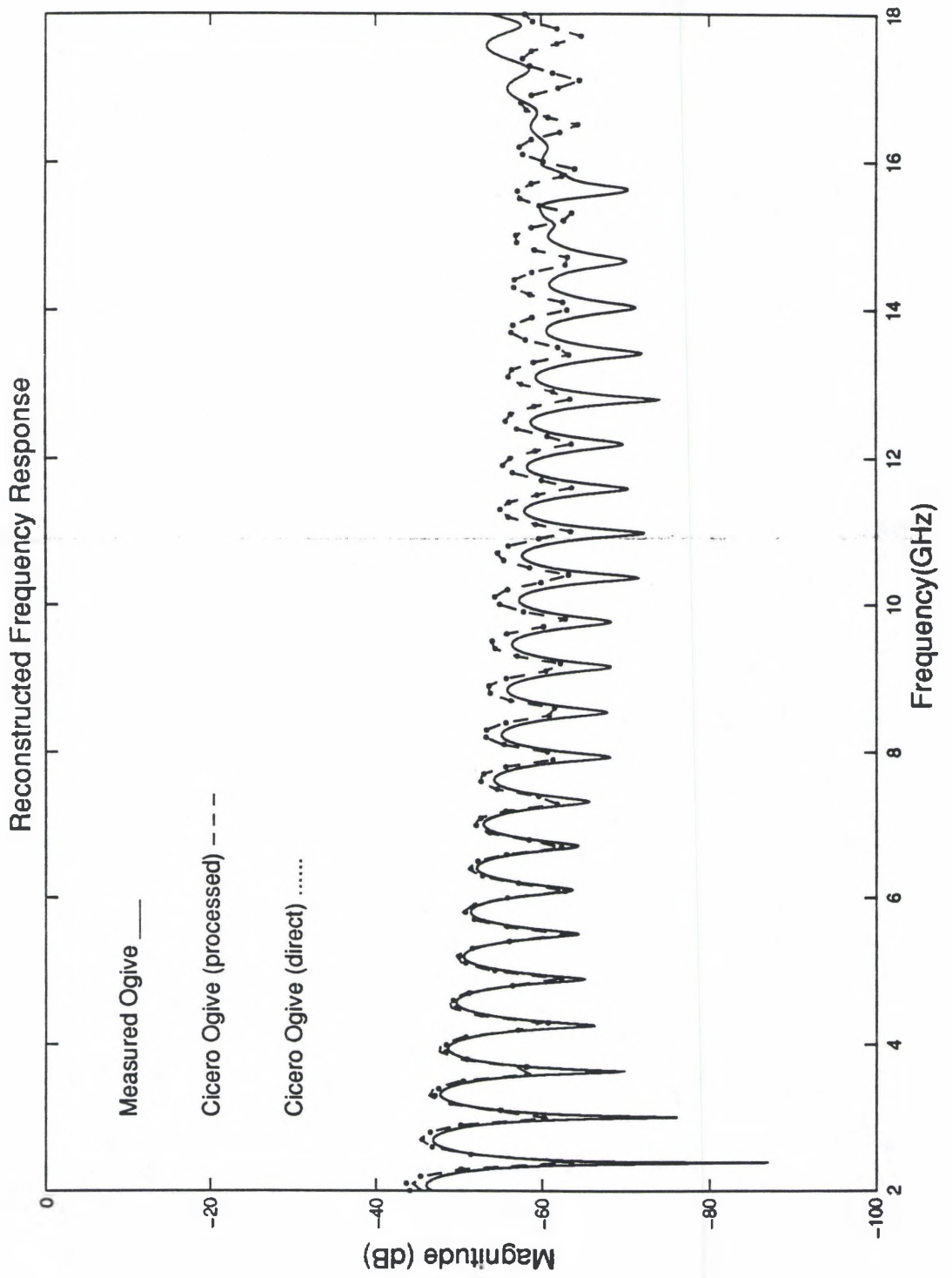


Figure 59. Reconstructed Frequency Response for Measured Case 2

3.3.3 Measured Case 3

The wire was selected as a canonical resonant source. The wire, approximately 0.7 inches in length, was mounted in foam as shown in Figure 60. Figure 61 shows the MUSIC and Fourier spectra overlaid. The spectrum shows four peaks in which the first peak is the specular scattering from the wire body. The additional three returns are the decaying amplitudes of the resonances in time. Since the resonant frequency should be approximately 8.5 GHz, the spacing of the time resonances should be $1/8.5$ GHz or 0.118 ns. The time separation between each of the peaks is .089, .11, and .102 ns respectively. Clearly, these time delays are within the accuracy of the MUSIC spectrum and the estimation of the resonant frequency. Figure 62 shows the frequency responses of each of the decaying time delaying centers.

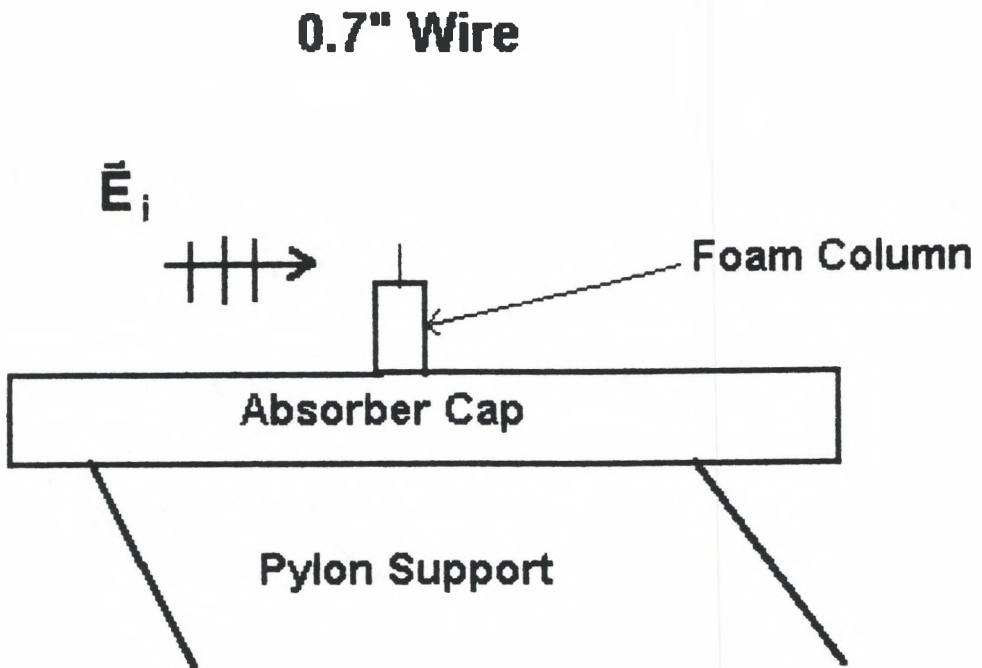


Figure 60. Measured Case 3 Geometry

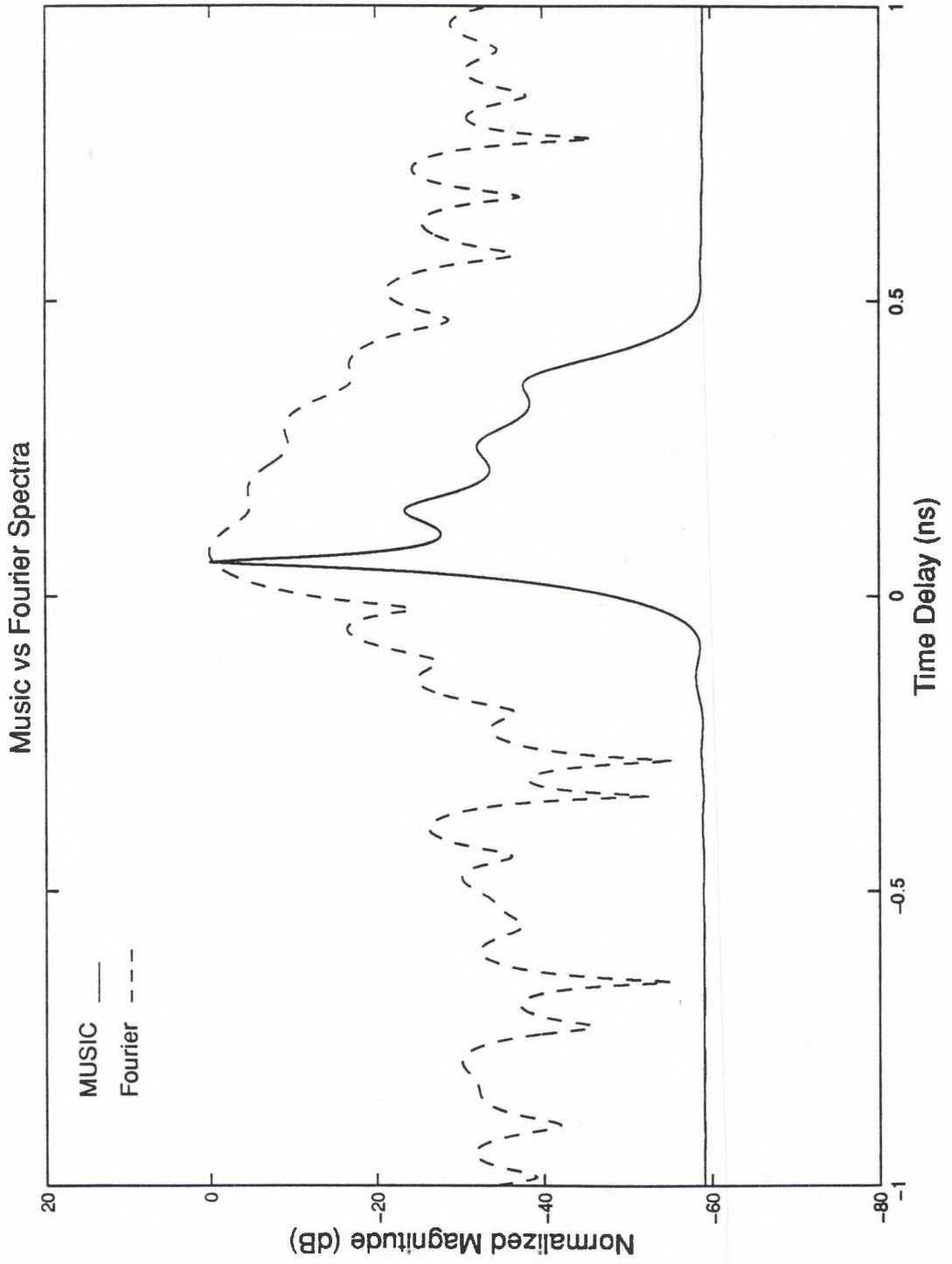


Figure 61. MUSIC and Fourier Spectra for Measured Case 3

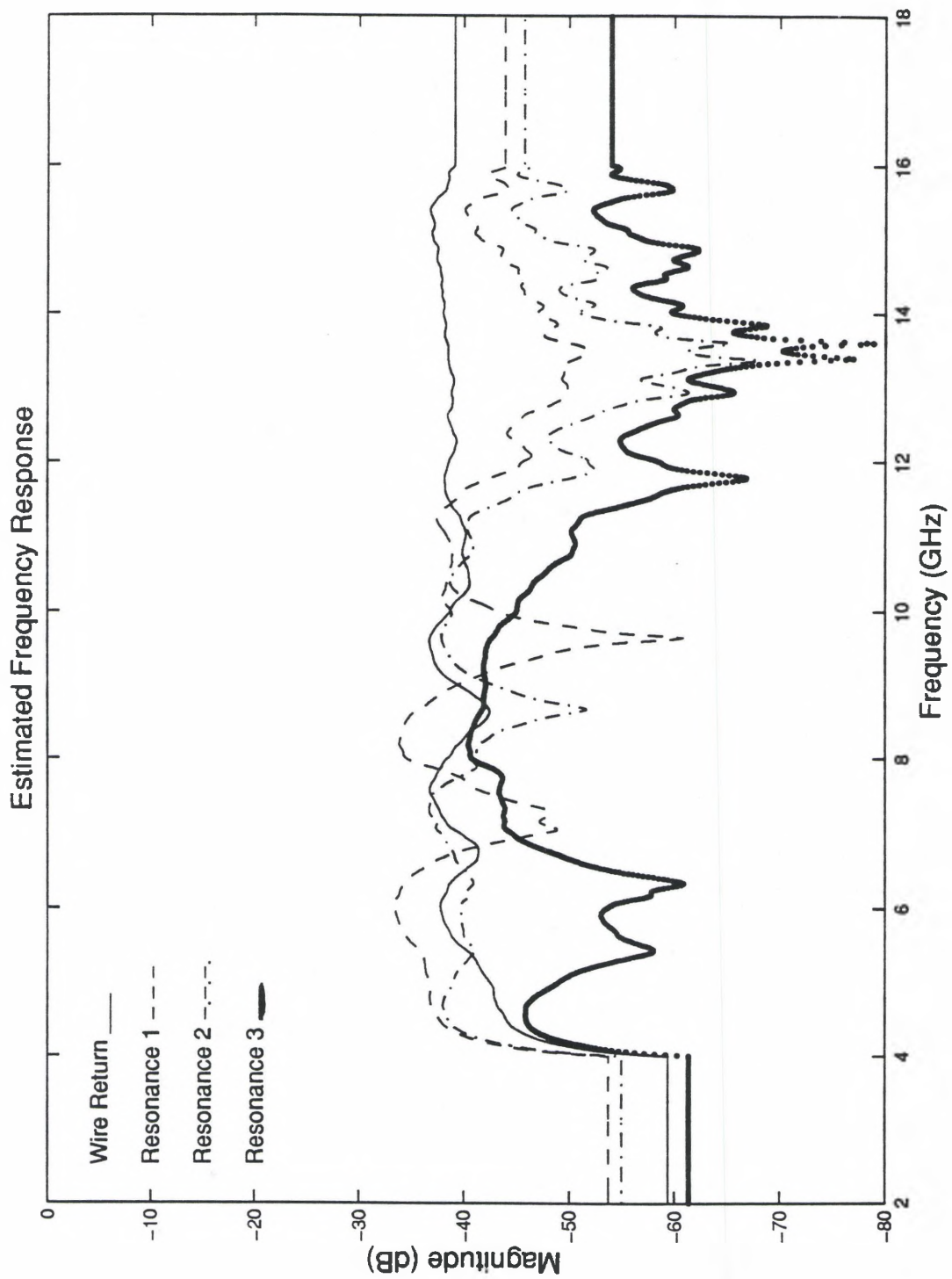


Figure 62. Estimated Frequency Response for Measured Case 3

3.3.4 Measured Case 4

The foam block with an embedded wooden rod represents a dielectric body with a strong inhomogeneity. The mounting configuration for this target is shown in Figure 63. The MUSIC spectrum had no trouble identifying the front and back of both the foam block and the wooden dowel rod (Figure 64). The length of the foam block was 14 13/16 inches. As such the time delay from the front to back faces of the foam should be 2.51 ns. The estimated MUSIC spectrum yields a total time of 2.608 ns, a difference of 3.9 %. In addition, the wooden dowel rod is one inch in diameter, or a corresponding diameter of 0.246 ns in time after adjusting for rod permittivity (plywood dielectric constant = 2.1). The MUSIC spectrum yielded a rod width of .2659 ns, a difference of .02 ns or 7.5%. This error can easily be attributed to the approximation in dielectric constant, which can only be greater than the one assumed - yielding a closer solution to that predicted. Each of the frequency responses shown in Figure 65 are well behaved and were easy to model.

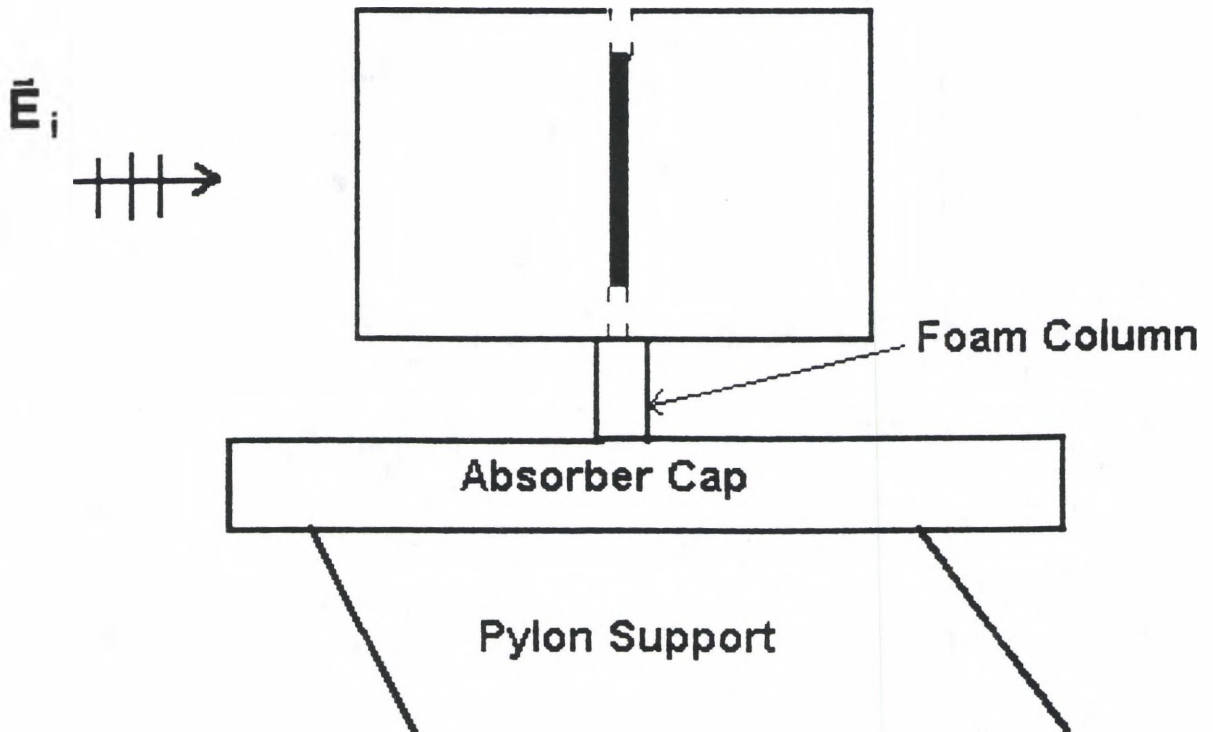


Figure 63. Measured Case 4 Geometry

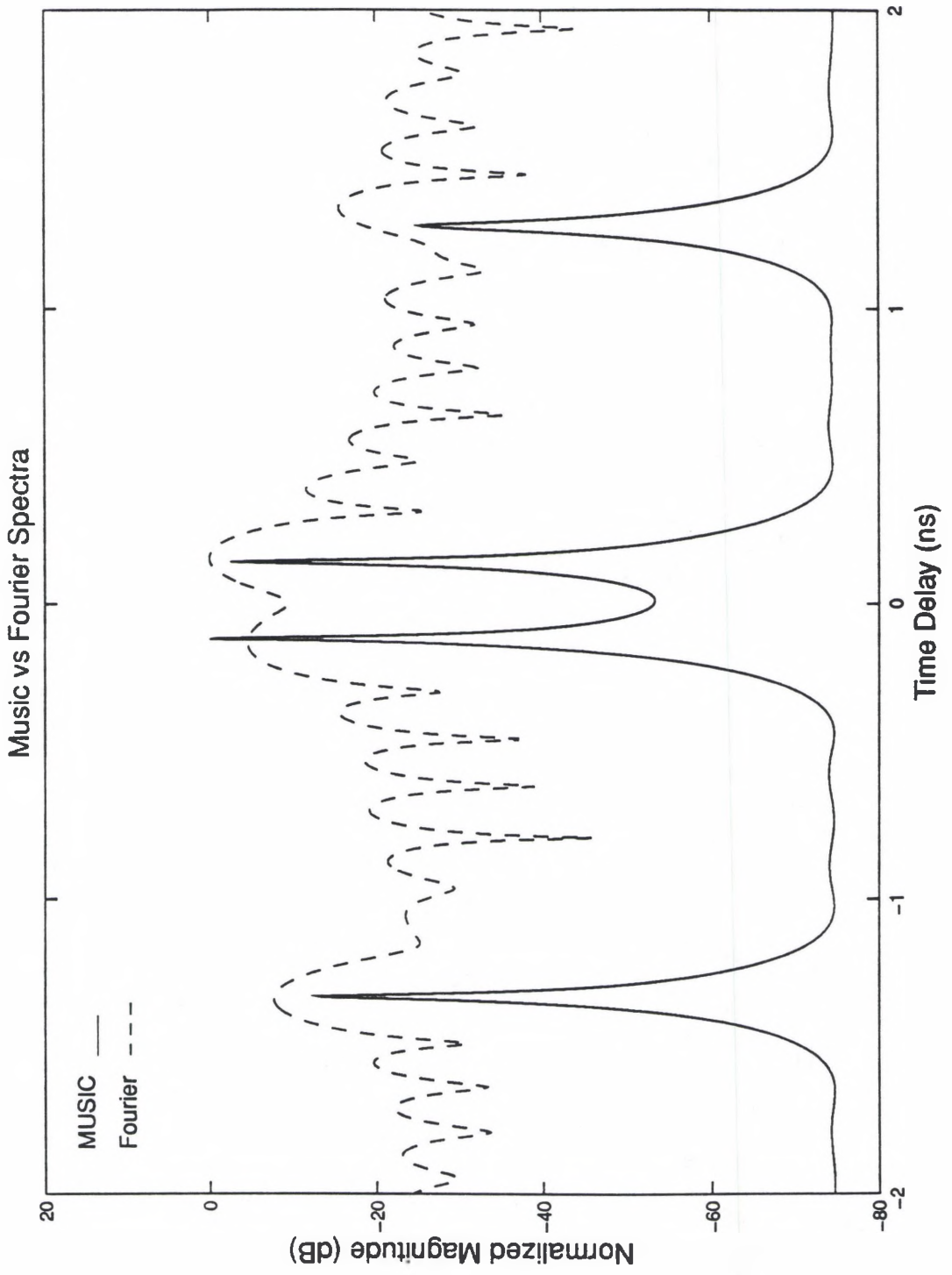


Figure 64. MUSIC and Fourier Spectra for Measured Case 4

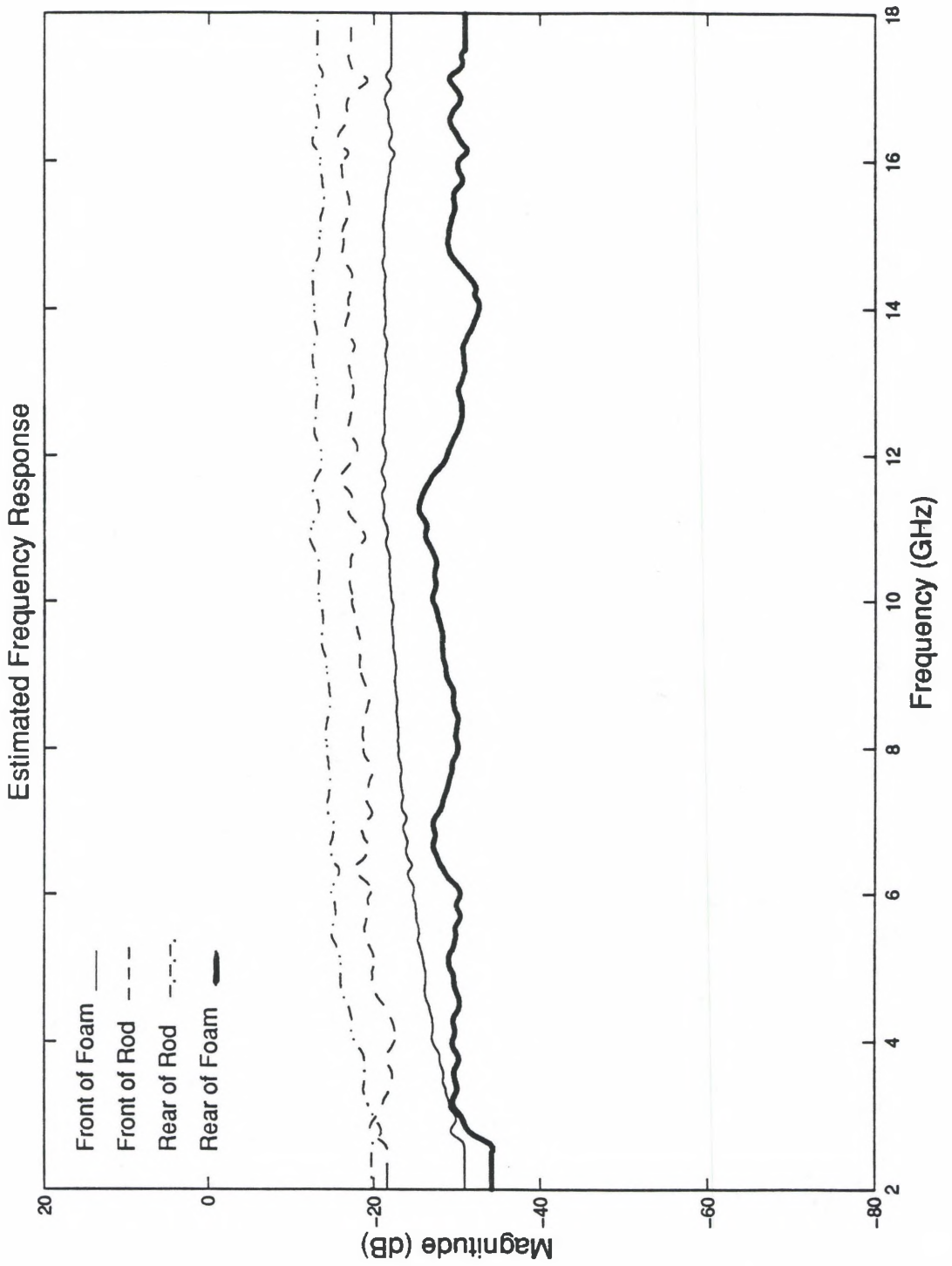



Figure 65. Estimated Frequency Response for Measured Case 4

3.3.5 Measured Case 5

This target represents a dielectric with a weak inhomogeneity, an often troublesome source to detect. The mounting configuration for this target is shown in Figure 66. Without the wooden dowel rod, the objective is to locate the dielectric hole in the midst of the two large dielectric faces. This not only presents a challenge to detect the hole proper, but it also presents a dynamic range problem. Since the majority of the energy scattering from the hole lies from 15-18 GHz, this region was chosen to resolve the hole. The MUSIC spectrum was able to determine the location of the foam faces and the front and back of the open hole. Although detected, the time delays corresponding to front and back of the hole are incorrect. The time delay corresponding to the front of the hole should be the same as the front of the wooden dowel rod, but, instead are shown to be at -.5494 and -.1232 ns respectively. The rear of the hole, since the dielectric constant of the hole itself is one, should have a time delay of 0.17 ns behind the front. However, this time delay of .1114 ns is actually .6608 ns behind the front of the hole. This time delay estimation error may be attributed to insufficient bandwidth and the dynamic range between the foam faces and the hole mechanisms. The local maximum in the rear face frequency response of Figure 68 is due to estimation error and not from the foam face itself.

Styrofoam Block Minus Wooden Dowel Rod

\vec{E}_i 

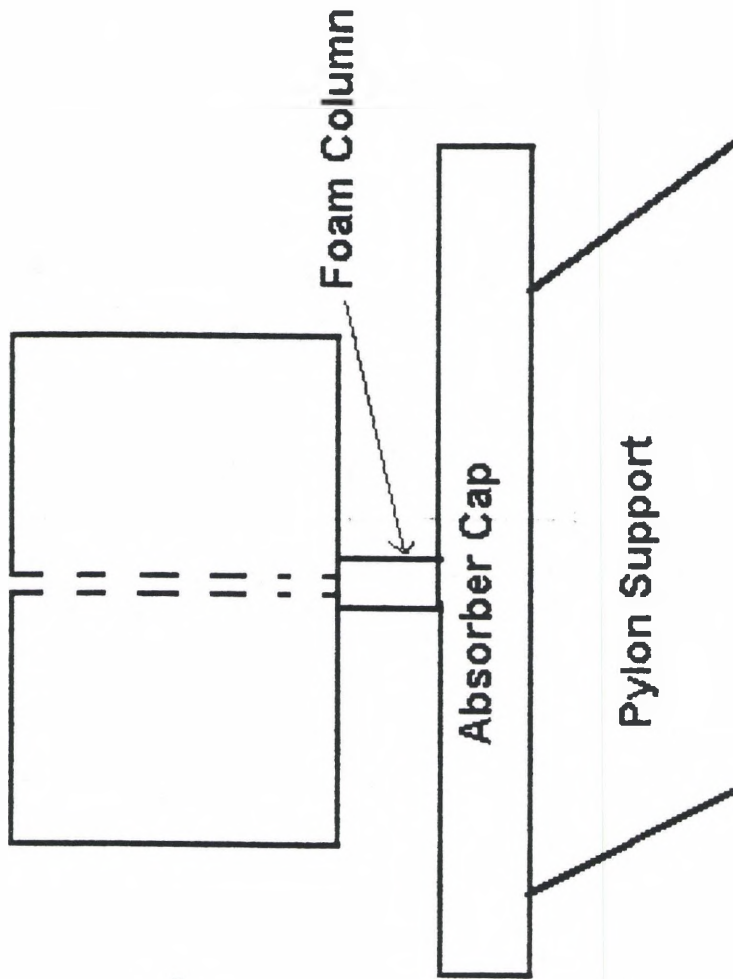


Figure 66. Measured Case 5 Geometry

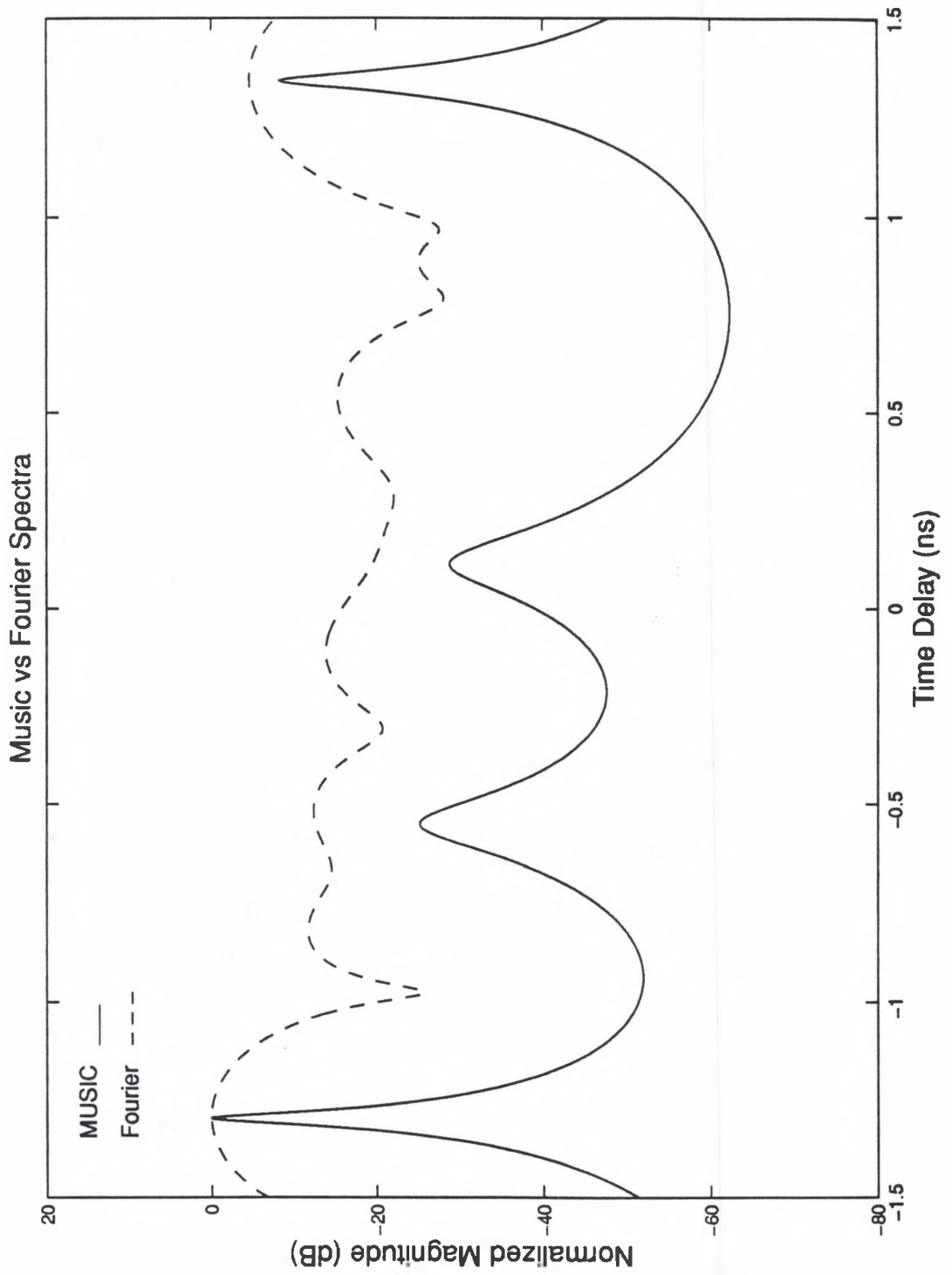


Figure 67. MUSIC and Fourier Spectra for Measured Case 5

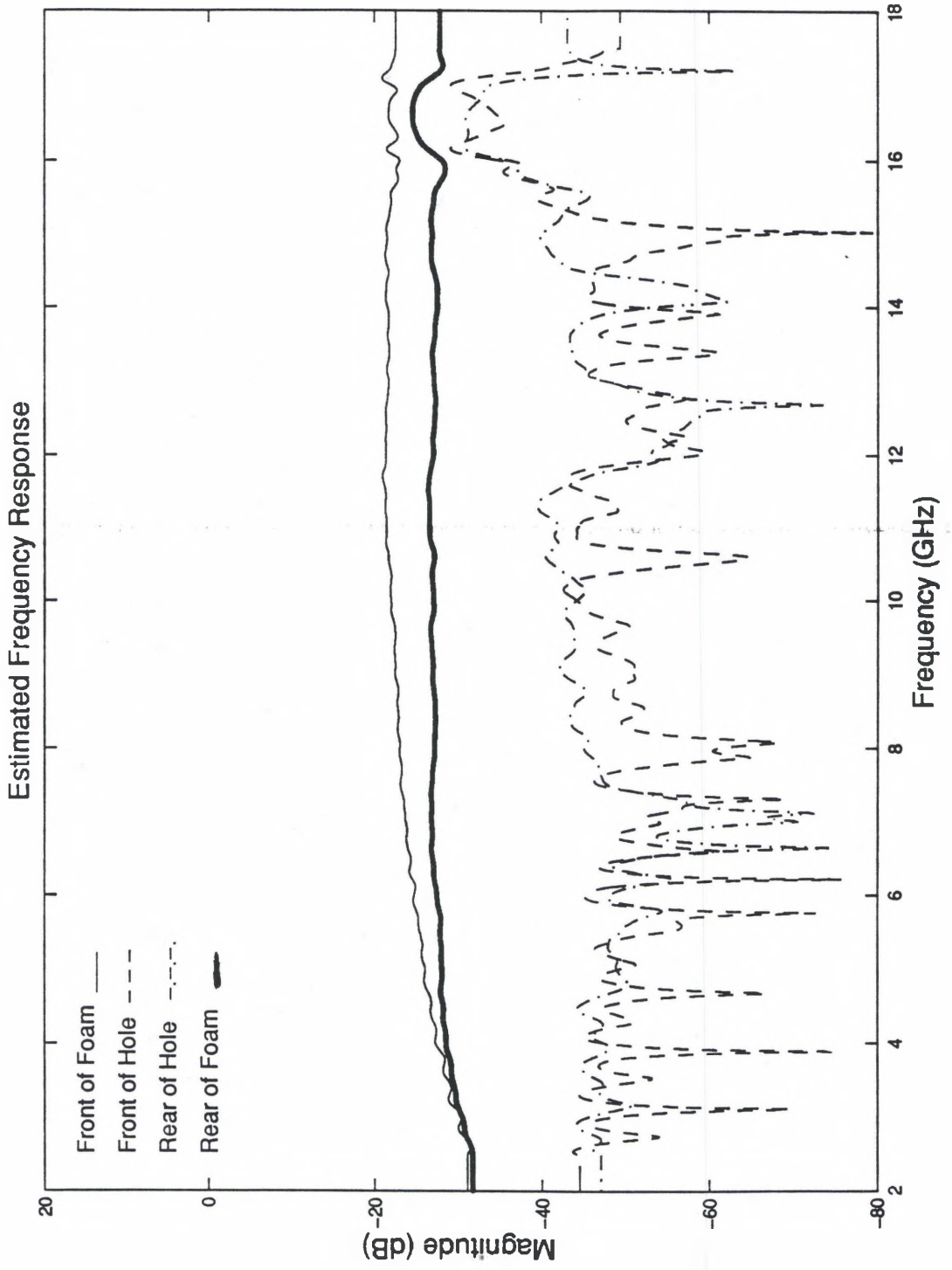


Figure 68. Estimated Frequency Response for Measured Case 5

CHAPTER IV

SUMMARY AND CONCLUSIONS

This study has demonstrated a method for determining the location and frequency response of a collection of closely-spaced scattering centers. The method begins by developing a signal model, from which a correlation matrix is obtained. The MUSIC algorithm uses an eigen-decomposition of this matrix to identify the location of the scattering centers. These locations are used, then, by a regression model to extract the frequency response of the scattering centers.

Traditionally, scattering centers have been identified via the Fourier transform. This approach works quite well if the scattering centers are sufficiently far from each other and non-resonant. These restrictions have led to the development of "super-resolution" techniques such as MUSIC, which are not bound by the Rayleigh resolution criterion nor subject to Gibb's phenomenon. Although computationally more expensive than the Fourier transform, the method reveals information which otherwise could not be uncovered. In addition, as computer speeds reach into the hundreds of megahertz, differences in computation times become less of a problem.

A formulation of the MUSIC algorithm and associated regression model has been presented. The MUSIC discussion starts with the development of the correlation matrix. An eigen-decomposition of this matrix reveals the number and location of the scattering centers. The eigenvectors of the matrix are separated into two orthogonal subspaces entitled the "signal-plus-noise" and "noise" spaces respectively. A scanning vector, comprised of basis functions taken from the signal model, is projected on to the noise space. When this vector becomes

orthogonal to the noise space a scattering center location has been found. The discussion of regression analysis begins with a model which takes into account frequency response estimation error and allows for frequency dependent signal parameters. The regression concept models each scattering center as a polynomial over a frequency band of interest. The model begins with an assumption that the polynomials are of zero order and then expands to include an arbitrary set of polynomial functions. Ultimately, the model leads to an "over-determined" set of linear algebraic equations which is solved by the method of least squares. The output of these equations is a set of complex coefficients representing the frequency response of the individual scattering centers.

A parametric study was performed on a two point-source scenario (20 dB SNR) to identify limitations in MUSIC resolution and accuracy. The study revealed that bandwidth and number of apertures were the primary factors in both. Once the data samples were sufficiently decorrelated, then bandwidth was the primary determinant of resolution and accuracy.

The method was then applied to a series of synthetic and measured data sets. The synthetic data was comprised of five combinations of point, "linear" and resonant scattering types. Each scenario was run under a "just resolved" and "fully resolved" parameter set. The "just resolved" conditions mean that only enough bandwidth was used to "just resolve" the required scattering centers. These locations were then used by the regression model to derive the frequency response of each source. The "just resolved" frequency response in all cases experienced degradation due to inexact location of the scattering centers. These errors manifest themselves in magnitude errors and, in the case of a resonant source, an incorrect resonant frequency. On the other hand, the "fully resolved" data were all accurately modeled. Even a multiple resonance data set was reconstructed with proper resonance frequencies and magnitudes of each.

The measured data set consisted of broadband backscatter information for five targets: an 8 inch sphere, 9.6 inch ogive, 0.7 inch wire, foam block with embedded 1 inch diameter wooden dowel rod, and the same foam block without the dowel rod leaving the 1 inch diameter

hole exposed. The 8 inch sphere was selected as a canonical target whose scattering properties are well understood. As the theory predicted, the method accurately found the sphere's specular and creeping wave returns. In addition, the method located a measurement error associated with the mounting structure. The MUSIC spectrum for the measured data was overlaid with the MUSIC spectrum obtained from the Mie series with excellent agreement. Then, the frequency response of both the measured and Mie data were overlaid. The agreement between the specular returns was excellent. However, the creeping wave tracked the Mie data until approximately 11 GHz, where chamber clutter begins to dominate.

The 9.6 inch ogive was selected as a canonical, but difficult target to measure. Its low broadband signature (low SNR) and traveling wave return from its mounting surface created a difficult measurement scenario above 9 GHz. The MUSIC spectrum resolved the front and rear tips of the ogive with great precision. In addition, the mounting support return was also evident at the boundaries where it met the surface of the ogive. The MUSIC spectrum is overlaid with the exact solution from the method of moments with excellent agreement. The frequency response of the front and rear tips are also overlaid with the calculated solution with general agreement until 10 GHz where chamber clutter begins to dominate.

The wire was selected as a canonical resonant source. Its MUSIC spectrum reveals a peak from the structure of the wire and three additional decaying returns. These additional returns are separated in time by the reciprocal of the resonant frequency. The frequency response of each of the mechanisms is also shown.

The two dielectric measurements were selected to demonstrate the utility of the method for dielectrics with both strong and weak inhomogeneities. The embedded dowel experiment easily resolved the front and back of the foam and rod respectively. The frequency response of each of these returns was well behaved and easy to model. The measurement of the foam with the exposed hole was also resolved but not as easily as the rod. The MUSIC spectrum, although identifying the hole's existence, did not accurately estimate its location. The estimated frequency response of the foam faces were accurately obtained. The frequency response of the

open hole accurately showed a maximum return at 16.5 GHz, which is not a part of the flat foam physics. Overall, the method was quite successful in estimating the frequency response of various scattering mechanisms in the presence of noise.

While it is demonstrated here quite definitively that it is possible to decompose the measured data to reveal the underlying scattering physics, this investigation is more a beginning than an end. A number of questions need further investigation:

- i) Not enough targets with resonances have been studied. It would be especially interesting to measure and study targets with multi-mode resonances.
- ii) The signal model used here presumes a well defined phase center associated with each scattering center. That may not always be the case. It is reasonable to inquire as to what the manifestations are of a scattering center whose phase center is a function of frequency. How does one include that in the signal model?
- iii) Another interesting target that deserves special mention is an antenna. Antenna scattering involves both the structural mode and the radiation mode. It is natural to wonder how these different modes manifest themselves in terms of optimal extraction? Is it possible to separate them?
- iv) The investigation reported here efficiently yields a time delay frequency diagram of the targets. Since wavelet theory¹⁹ is designed to provide such a time-frequency description, it is natural to seek to establish the relationship between the present technique and wavelet theory.

BIBLIOGRAPHY

- ¹ A.J. Poggio, M. L. Van Blaricum, E.K. Miller and R Mittra, "Evaluation of a Processing Technique for Transient Data," *IEEE Transactions on Antennas and Propagation*, vol. AP-26, p.165, January 1978.
- ² M. L. Van Blaricum and R. Mittra, "Problems and Solutions Associated with Prony's Method for Processing Transient Data," *IEEE Transactions on Antennas and Propagation*, vol. AP-26, p.174, January 1978.
- ³ V. F. Pisarenko, "On the Estimation of Spectra by Means of Non-linear Functions of the Covariance Matrix," *Geophys. J. R. Astr. Soc.*, vol. 28, pp. 511-531, 1972.
- ⁴ R. Schmidt, "Multiple Emitter Location and Signal Parameter Estimation," *RADC Spectrum Estimation Workshop*, pp. 243-258, 1979.
- ⁵ T. P. Delfeld and F.C. Delfeld, "Use of the MUSIC Algorithm in the analysis of Compact Range Field Probe Data," *Proceedings of the 11th Annual Symposium of AMTA*, Monterey, CA, October 1989.
- ⁶ I.J. Gupta, "Imaging the Compact Range Probe Data using MUSIC Algorithm," *Proceedings of International Conference on Millimeter Wave and Microwave*, Dehra Dun, India, December 1990.
- ⁷ J. Moore and H. Ling, "Super-resolved Time-Frequency Analysis of Wideband Backscattered Data," *IEEE Transactions on Antennas and Propagation*, vol. AP-43, p.623, June 1995.
- ⁸ J. Moore, L.C. Trintinalia, H. Ling and G. Xu, "Superresolved Time-Frequency Processing of Wideband Radar Echo Using ESPRIT," *Microwave and Optical Technology Letters*, vol. 9, p. 17, May 1995.
- ⁹ R. Roy, A. Paulraj, and T. Kailath, "ESPRIT -- A subspace rotation approach to estimation of parameters of cicoids in noise," *IEEE Transactions on Acoustics, Speech, and Signal Processing*, vol. ASSP-34, pp. 1340-1342, October 1986.
- ¹⁰ S. Haykin, *Adaptive Filter Theory, Second Edition*, Prentice Hall, 1991.
- ¹¹ Ibid.
- ¹² Ibid.
- ¹³ Ibid.
- ¹⁴ R. Bracewell, *The Fourier Transform and its Applications*, Mc Graw Hill, 1978.
- ¹⁵ C.W.I Pistorius, "New Main Reflector, Subreflector, and Dual Chamber Concepts for Compact Range Applications," Ph.D. Dissertation, The Ohio State University, 1986.

¹⁶ H. Kim, and H. Ling, "Wavelet Analysis of Radar Echo from Finite-Size Targets," *IEEE Transactions on Antennas and Propagation*, vol. AP-41, p.200, February 1993.

¹⁷ C. A. Balanis, *Advanced Engineering Electromagnetics*, John Wiley & Sons, 1989

¹⁸ J. M. Putnam and L. N. Medgyeshi-Mitschang, "Combined Field Integral Equation Formulation for Axially Inhomogeneous Bodies of Revolution (Combined Field Formulation of CICERO)," Report MDCQA003, December 1987, McDonnell Douglas Research Laboratories; prepared under Contract No. 33-4257 for Sandia National Laboratory.